SOLUBILITY OF CO2-PHILIC POLYHEDRAL OLIGOMERIC SILSESQUIOXANES IN SUPERCRITICAL CARBON DIOXIDE

A THESIS SUBMITTED TO
THE GRADUATE SCHOOL OF NATURAL AND APPLIED SCIENCES
OF
MIDDLE EAST TECHNICAL UNIVERSITY

BY

CANSU DEMIRTAŞ

IN PARTIAL FULFILLMENT OF THE REQUIREMENTS
FOR
THE DEGREE OF MASTER OF SCIENCE
IN
CHEMICAL ENGINEERING

JUNE 2019

Approval of the thesis:

SOLUBILITY OF CO2-PHILIC POLYHEDRAL OLIGOMERIC SILSESQUIOXANES IN SUPERCRITICAL CARBON DIOXIDE

submitted by **CANSU DEMIRTAŞ** in partial fulfillment of the requirements for the degree of **Master of Science in Chemical Engineering Department, Middle East Technical University** by,

Prof. Dr. Halil Kalıpçılar
Dean, Graduate School of **Natural and Applied Sciences** _____

Prof. Dr. Pınar Çalık
Head of Department, **Chemical Engineering** _____

Assoc. Prof. Dr. Çerağ Dilek Hacıhabiboğlu
Supervisor, **Chemical Engineering, METU** _____

Examining Committee Members:

Prof. Dr. Naime Aslı Sezgi
Chemical Engineering Dept., METU _____

Assoc. Prof. Dr. Çerağ Dilek Hacıhabiboğlu
Chemical Engineering, METU _____

Prof. Dr. Göknur Bayram
Chemical Engineering Dept., METU _____

Assoc. Prof. Dr. Özlem Güçlü Üstündağ
Food Engineering Dept., Yeditepe Uni _____

Assist. Prof. Dr. Harun Koku
Chemical Engineering Dept., METU _____

Date: 27.06.2019

I hereby declare that all information in this document has been obtained and presented in accordance with academic rules and ethical conduct. I also declare that, as required by these rules and conduct, I have fully cited and referenced all material and results that are not original to this work.

Name, Surname: Cansu Demirtaş

Signature:

ABSTRACT

SOLUBILITY OF CO2-PHILIC POLYHEDRAL OLIGOMERIC SILSESQUIOXANES IN SUPERCRITICAL CARBON DIOXIDE

Demirtaş, Cansu
Master of Science, Chemical Engineering
Supervisor: Assoc. Prof. Dr. Çerağ Dilek Hacıhabiboğlu

June 2019, 90 pages

Polyhedral oligomeric silsesquioxanes (POSS) modified with various functional groups and carbon dioxide (CO_2) binary systems' phase behavior have been studied in a high- pressure visible cell to contribute to the development of environmentally friendly processes of POSS with supercritical carbon dioxide. POSS can show different hybrid material properties due to its functional groups attached to its cage structure. Supercritical carbon dioxide, which is referred as an environmentally friendly solvent, can exhibit specific interactions such as Lewis acid-base interactions or weak hydrogen bonding due to its quadrupole moment, and form single phase solutions with various materials.

The studied POSS structures, which can form homogenous solutions with CO_2, include octatrimethylsiloxy, methacryl, isooctyl, octaisobutyl, and trifluoropropyl POSS. Octatrimethylsiloxy POSS-CO_2 system has been studied for the first time, while the other POSS-CO_2 phase behavior studies have been conducted at different temperature ranges than those studied previously. Experimental data have been correlated using semi-empirical density-based models which are Mendez-Santiago and Teja (MST), Chrastil, Bartle, Chrastil Modified Wang (C-W), del Valle and Aguilera (del Valle) and Kumar and Johnston (K-J).

The methacryl POSS-CO_2 and isooctyl POSS-CO_2 liquid-vapor equilibrium curves, and octaisobutyl POSS-CO_2, trifluoropropyl POSS-CO_2, and octatrimethylsiloxy POSS-CO_2 solid-vapor equilibrium curves have been constructed. Solubility versus CO_2 density isotherms were obtained at the cloud and dew points of the POSS-CO_2 systems. Among all the POSS types, octatrimethylsiloxy POSS has the highest measured solubility in supercritical carbon dioxide. The best solubility fits have been obtained with Chrastil Modified Wang model for all the binary systems.

Keywords: POSS, Supercritical Carbon Dioxide, Solubility, CO2 density, Density-based Models

ÖZ

KARBONDİOKSİT İLE ETKİLEŞEN POLİHEDRAL OLİGOMERİK SİLSESKUİOKSANLARIN SÜPERKRİTİK KARBONDİOKSİTTE ÇÖZÜNÜRLÜKLERİ

Demirtaş, Cansu
Yüksek Lisans, Kimya Mühendisliği
Tez Danışmanı: Doç. Dr. Çerağ Dilek Hacıhabiboğlu

Haziran 2019, 90 sayfa

Farklı fonksiyonel gruplara sahip polihedral oligomerik silseskuioksan (POSS) ve karbondioksit (CO_2) içeren ikili sistemlerinin faz davranışları, POSS'un süperkritik karbondioksit ile çevre dostu işlemlerinin geliştirilmesine katkıda bulunmak için yüksek basınca dayanıklı içi gözlenebilir bir hücrede incelenmiştir. POSS kafes yapısına bağlı fonksiyonel grupları nedeniyle farklı hibrit malzeme özellikleri gösterebilir. Çevre dostu bir çözücü olarak adlandırılan süperkritik karbondioksit, sergilediği kuadrupol momentinden dolayı Lewis asit-baz etkileşimleri veya zayıf hidrojen bağı gibi spesifik etkileşimler sergileyebilir ve çeşitli malzemelerle tek fazlı çözeltiler oluşturabilir.

Çalışmada kullanılan ve CO_2 ile homojen çözeltiler oluşturabilen POSS yapıları, oktatrimetilsiloksi, metakril, izoktil, oktaizobütil ve trifloropropil POSS'lardır. Octatrimetilsiloksi POSS-CO_2 sistemi ilk kez çalışılmış, diğer POSS-CO_2 faz çalışmaları ise daha önceki çalışmalardan farklı sıcaklık aralıklarında yapılmıştır. Deneysel veriler yarı deneysel yoğunluk temelli Mendez-Santiago ve Teja (MST), Chrastil, Bartle, Chrastil Modifiye Wang (CW), del Valle ve Aguilera (del Valle) ve Kumar ve Johnston (KJ) korelasyonları ile modellenmiştir.

Metakril POSS-CO_2 ve izoktil POSS-CO_2 sıvı-buhar dengesi eğrileri ve oktaizobütil POSS-CO_2, trifloropropil POSS-CO_2 ve oktatrimetilsiloksi POSS-CO_2 katı-buhar dengesi eğrileri oluşturulmuştur. Çözünürlük-CO_2 yoğunluğu izotermleri POSS-CO_2 sistemlerinin bulutlanma ve çiğlenme noktalarında elde edilmiştir. Tüm POSS tipleri arasında oktatrimetilsiloksi POSS süperkritik karbondioksit içerisinde en yüksek çözünürlüğe sahiptir. Tüm ikili sistemler için en iyi çözünürlük uyumu Chrastil Modified Wang modelinde elde edilmiştir

Anahtar Kelimeler: POSS, Süperkritik Karbondioksit, Çözünürlük, CO2 yoğunluğu, Yoğunluk Temelli Modeller

To Hanım & Rıfat Demirtaş

ACKNOWLEDGEMENTS

First of all, I would like to express my sincere appreciation to my supervisor Assoc. Prof. Dr. Çerağ Dilek Hacıhabiboğlu for her invaluable guidance, criticism and advices throughout the research.

I would also like to thank to Prof. Dr. Işik Önal and İlker Tezsevin for their invaluable support in DFT studies, guidance and helpful comments.

I also thank to my lab mates Novendra and Başak Kanya for helping me through my laboratory studies, for their suggestions and enjoyable friendship. And heartfelt thanks to my friends with whom I shared unforgettable memories in METU, Ankara and thanks for their understanding, patience and precious friendship.

I owe my aunt Özgül Kaymaz a great debt of gratitude for her endless love, support and encouragement through no matter what happens. I especially thank to my fiancé, Mehmet Orhan Şenses, for his supportive attitude, patience and for many things that I cannot put into words.

Above all, I would like to send my greatest gratitude to my dear mom and dad; Hanım Demirtaş and Rıfat Demirtaş for never giving up on me and always being supportive to the greatest extent possible. Without them this thesis would not have been possible.

TABLE OF CONTENTS

ABSTRACT v

ÖZ… vii

ACKNOWLEDGEMENTS x

TABLE OF CONTENTS xi

LIST OF TABLES xiv

LIST OF FIGURES xvi

CHAPTERS

1. INTRODUCTION 1

1.1. Polyhedral Oligomeric Silsesquioxane (POSS) 1

1.2. Supercritical Fluids (SCF) 2

1.2.1. Supercritical Carbon Dioxide 5

1.2.2. Solubility in Supercritical Carbon Dioxide 6

1.3. Solubility Modelling in Supercritical CO_2 8

1.3.1. Semi-empirical Density Based Methods 9

1.3.1.1. Chrastil Model 9

1.3.1.2. Chrastil Modified by Wang Model 10

1.3.1.3. Del Valle and Aguilera Model 11

1.3.1.4. Kumar and Johnston Model 11

1.3.1.5. Mendez-Santiago and Teja Model 11

1.3.1.6. Bartle Model 11

1.3.2. Solubility Data Correlation with Semi-Empirical Density Based Methods 12
1.4. The Objectives of this Study 12
2. LITERATURE SURVEY 15
2.1. Applications of POSS 15
2.2. POSS-scCO_2 Systems 16
2.2.1. Experimental studies on POSS – CO_2 Systems 16
2.2.2. Computational / Theoretical studies on POSS – CO_2 Systems 18
2.2.3. Applications of POSS – CO_2 Systems 18
3. EXPERIMENTAL METHODS 21
3.1. Materials 21
3.2. Solubility Experiments 22
3.2.1. Experimental Set-Up 22
3.2.2. Cloud and Dew Point Measurements 23
4. RESULTS AND DISCUSSION 27
4.1. S-V Equilibria of Octatrimethyl Siloxy POSS-CO_2 Binary System 27
4.1.1. Comparison of Octatrimethyl Siloxy POSS-CO_2 Systems with other CO_2-philic Materials – CO_2 Systems 31
4.1.1.1. Comparison of Octatrimethyl Siloxy POSS-CO_2 Systems with Sugar Acetate – CO_2 Systems 31
4.1.1.2. Comparison of Octatrimethyl Siloxy POSS-CO_2 Systems with Naphthalene -CO_2 Systems 34
4.2. S-V Equilibria of Trifluoropropyl POSS-CO_2 Binary System 37
4.3. S-V Equilibria of Octaisobutyl POSS-CO_2 Binary System 39
4.4. L-V Equilibria of Methacryl POSS-CO_2 Binary System 41

4.5. L-V Equilibria of Isooctyl POSS-CO_2 Binary System 44
4.6. Effects of Temperature and Pressure on CO_2 Density at Phase Separation 46
4.7. Modeling of Solubility 59
4.7.1. Octatrimethyl Siloxy POSS Solubility Modelling.....59
4.7.2. Trifluoropropyl POSS Solubility Modelling 65
4.7.3. Octaisobutyl POSS Solubility Modelling.....69
4.7.4. Methacryl POSS Solubility Modelling.....72
4.7.5. Isooctyl POSS Solubility Modelling 75
5. CONCLUSIONS 79
REFERENCES.....81

LIST OF TABLES

TABLES

Table 1.1. Properties of gas, liquid and SCF Phases [17]..... 5
Table 1.2. Critical properties and safety data of some SCFs [15]. 6
Table 4.1. The cloud point pressures of SPOSS-CO_2 binary system at 308 K, 313 K, 318 K, 323 K, and 328 K, and the corresponding carbon dioxide densities. 27
Table 4.2. The cloud point pressures of TFPOSS-CO_2 binary system at 318 K, and 328 K and the corresponding carbon dioxide densities. 37
Table 4.3. The cloud point pressures of OIPOSS-CO_2 binary system at 318 K, and 328 K, and the corresponding carbon dioxide densities. 39
Table 4.4. The dew point pressures of MPOSS-CO_2 binary system at 318 K, and 328 K, and the corresponding carbon dioxide densities. 42
Table 4.5. The dew point pressures of IOPOSS-CO_2 binary system at 318 K, and 328 K, and the corresponding carbon dioxide densities. 44
Table 4.6. The estimated solubility mol fractions of SPOSS-CO_2 binary systems. .. 62
Table 4.7. The empirical parameters of the density-based models and the AARD (%) values obtained for the SPOSS solubility in $scCO_2$..... 65
Table 4.8. The estimated solubility mol fractions of TFPOSS-CO_2 binary systems. 67
Table 4.9. The empirical parameters of the density-based models and the AARD (%) values obtained for the TFPOSS solubility in $scCO_2$. 68
Table 4.10. The estimated solubility mol fractions of OIPOSS-CO_2 binary systems. 70
Table 4.11. The empirical parameters of the density-based models and the AARD (%) values obtained for the OIPOSS solubility in $scCO_2$..... 71
Table 4.12. The estimated solubility mol fractions of MPOSS-CO_2 binary systems. 73

Table 4.13. The empirical parameters of the density-based models and the AARD (%) values obtained for the MPOSS solubility in $scCO_2$. 74
Table 4.14. The estimated solubility mol fractions of IOPOSS-CO_2 binary systems. 76
Table 4.15. The empirical parameters of the density-based models and the AARD (%) values obtained for the IOPOSS solubility in $scCO_2$. 77

LIST OF FIGURES

FIGURES

Figure 1.1. POSS Cage Structures [1]. 1
Figure 1.2. Pressure – Temperature Phase Diagram [12]. 3
Figure 1.3. Carbon dioxide density variance with pressure under constant temperatures [15]. 4
Figure 1.4. Solubility isotherms of phenanthrene – CO_2 binary system at 313K, 323K and 333 K [34]. 8
Figure 3.1. Chemical structures of a) octatrimethyl siloxy POSS, b) trifluoropropyl POSS, c) octaisobutyl POSS, d) methacryl POSS, e) isooctyl POSS. 22
Figure 3.2. The experimental set-up used in the POSS-CO_2 cloud and dew point measurements. 23
Figure 4.1. Cloud point isotherms of the octatrimethylsiloxy POSS–CO_2 binary system; 308 K (■), 313 K (○), 318 K (◊), 323 K (□) and 328 K (Δ). The estimated error bars are comparable to the size of the symbols. 30
Figure 4.2. Solubility of octatrimethylsiloxy POSS (■) and sugar acetate (●) [69] in $scCO_2$ plotted against the cloud and dew points of the binary system at 308 K, respectively. 31
Figure 4.3. Solubility of octatrimethylsiloxy POSS (■) and sugar acetate (●) [69] in $scCO_2$ plotted against the cloud and dew points of the binary system at 313 K, respectively. 32
Figure 4.4. Solubility of octatrimethylsiloxy POSS (■) and sugar acetate (●) [69] in $scCO_2$ plotted against the cloud and dew points of the binary system at 318 K, respectively. 33
Figure 4.5. Solubility of octatrimethylsiloxy POSS (■) and sugar acetate (●) [69] in $scCO_2$ plotted against the cloud and dew points of the binary system at 323 K, respectively. 34

Figure 4.6. Solubility of octatrimethylsiloxy POSS (■) and naphthalene (●) [73] in $scCO_2$ plotted against the cloud points of the binary system at 308 K. 35
Figure 4.7. Solubility of octatrimethylsiloxy POSS (■) and naphthalene (●) [73] in $scCO_2$ plotted against the cloud points of the binary system at 328 K. 36
Figure 4.8. Cloud point isotherms of the trifluoropropyl POSS–CO_2 binary system; 318 K (◊), and 328 K (Δ). The estimated error bars are comparable to the size of the symbols. 38
Figure 4.9. Cloud point isotherms of the octaisobutyl POSS–CO_2 binary system; 318 K (◊), and 328 K (Δ). The estimated error bars are comparable to the size of the symbols. 41
Figure 4.10. Dew point isotherms of the methacryl POSS–CO_2 binary system; 318 K (◊), and 328 K (Δ). The estimated error bars are comparable to the size of the symbols. 43
Figure 4.11. Dew point isotherms of the isooctyl POSS–CO_2 binary system; 318 K (◊), and 328 K (Δ). The estimated error bars are comparable to the size of the symbols. 45
Figure 4.12. Solubility of octatrimethylsiloxy POSS in $scCO_2$ plotted against CO_2 densities at the cloud points of the binary system at (-) 308 K, (●) 313 K, (♦) 318 K, (■) 323 K and (▲) 328 K. 47
Figure 4.13. Solubility of octaisobutyl POSS in $scCO_2$ plotted against CO_2 densities at the cloud points of the binary system at (♦) 318 K and (▲) 328 K. 48
Figure 4.14. Solubility of trifluoropropyl POSS in $scCO_2$ plotted against CO_2 densities at the cloud points of the binary system at (♦) 318 K and (▲) 328 K. 49
Figure 4.15. Solubility of methacryl POSS in $scCO_2$ plotted against CO_2 densities at the cloud points of the binary system at (♦) 318 K and (▲) 328 K. 50
Figure 4.16. Solubility of isooctyl POSS in $scCO_2$ plotted against CO_2 densities at the cloud points of the binary system at (♦) 318 K and (▲) 328 K. 51
Figure 4.17. Solubility of POSS with various functional groups in $scCO_2$ plotted against the CO_2 densities at the cloud or dew points at 308 K; (■)

octatrimethylsiloxy POSS-CO_2, (○) trifluoropropyl POSS-CO_2 [2] (●) octaisobutyl POSS-CO_2 [3], (♦) isooctyl POSS-CO_2 [3] (▲) methacryl POSS-CO_2 [3]. 52
Figure 4.18. Solubility of POSS with various functional groups in scCO_2 plotted against the CO_2 densities at the cloud or dew points at 323 K; (■) octatrimethylsiloxy POSS-CO_2, (○) trifluoropropyl POSS-CO_2 [2] (●) octaisobutyl POSS-CO_2 [3], (♦) isooctyl POSS-CO_2 [3] (▲) methacryl POSS-CO_2 [3]. 53
Figure 4.19. Solubility of POSS with various functional groups in scCO_2 plotted against the CO_2 densities at the cloud or dew points at 318 K; (■) octatrimethylsiloxy POSS-CO_2, (○) trifluoropropyl POSS-CO_2, (●) octaisobutyl POSS-CO_2, (♦) isooctyl POSS-CO_2, (▲) methacryl POSS-CO_2. 54
Figure 4.20. Solubility of POSS with various functional groups in scCO_2 plotted against the CO_2 densities at the cloud or dew points at 328 K; (■) octatrimethylsiloxy POSS-CO_2, (○) trifluoropropyl POSS-CO_2, (●) octaisobutyl POSS-CO_2, (♦) isooctyl POSS-CO_2, (▲) methacryl POSS-CO_2. 55
Figure 4.21. Solubility of POSS with various functional groups in scCO_2 plotted against the cloud or dew point pressures at 308 K; (■) octatrimethylsiloxy POSS-CO_2, (○) trifluoropropyl POSS-CO_2 [2] (●) octaisobutyl POSS-CO_2 [3], (♦) isooctyl POSS-CO_2 [3] (▲) methacryl POSS-CO_2 [3]. 56
Figure 4.22. Solubility of POSS with various functional groups in scCO_2 plotted against the cloud or dew point pressures at 318 K; (■) octatrimethylsiloxy POSS-CO_2, (○) trifluoropropyl POSS-CO_2 (●) octaisobutyl POSS-CO_2, (♦) isooctyl POSS-CO_2 (▲) methacryl POSS-CO_2. 57
Figure 4.23. Solubility of POSS with various functional groups in scCO_2 plotted against the cloud or dew point pressures at 323 K; (■) octatrimethylsiloxy POSS-CO_2, (○) trifluoropropyl POSS-CO_2 [2] (●) octaisobutyl POSS-CO_2 [3], (♦) isooctyl POSS-CO_2 [3] (▲) methacryl POSS [3]. 58
Figure 4.24. Solubility of POSS with various functional groups in scCO_2 plotted against the cloud or dew point pressures at 328 K; (■) octatrimethylsiloxy POSS-

CO_2, (○) trifluoropropyl POSS-CO_2 (●) octaisobutyl POSS-CO_2, (♦) isooctyl POSS-CO_2 (▲) methacryl POSS-CO_2. 59
Figure 4.25. The density based correlations, (——) C-W, (·····) Chrastil, (– – –) D-A, (- - -) K-J, (– · –) MST, (— —) Bartle, and the experimental solubility data of SPOSS in scCO_2 (□) plotted against the CO_2 densities at the cloud points at a) 308 K, b) 313K, c) 318 K, d) 323 K, and e) 328 K.....62
Figure 4.26. The density based correlations, (——) C-W, (·····) Chrastil, (– – –) D-A, (- - -) K-J, (– · –) MST, (— —) Bartle, and the experimental solubility data of TFPOSS in scCO_2 (○) plotted against the CO_2 densities at the cloud points at a) 318 K, and b) 328 K.....67
Figure 4.27. The density based correlations, (——) C-W, (·····) Chrastil, (– – –) D-A, (- - -) K-J, (– · –) MST, (— —) Bartle, and the experimental solubility data of OIPOSS in scCO_2 (□) plotted against the CO_2 densities at the cloud points at a) 318 K, and b) 328 K.....70
Figure 4.28. The density based correlations, (——) C-W, (·····) Chrastil, (– – –) D-A, (- - -) K-J, (– · –) MST, (— —) Bartle, and the experimental solubility data of MPOSS in scCO_2 (□) plotted against the CO_2 densities at the cloud points at a) 318 K, and b) 328 K.....73
Figure 4.29. The density based correlations, (——) C-W, (·····) Chrastil, (– – –) D-A, (- - -) K-J, (– · –) MST, (— —) Bartle, and the experimental solubility data of IOPOSS in scCO_2 (□) plotted against the CO_2 densities at the cloud points at a) 318 K, and b) 328 K.....76

CHAPTER 1

INTRODUCTION

1.1. Polyhedral Oligomeric Silsesquioxane (POSS)

Silsesquioxane molecule chemical formula is $R_nSi_nO_{1.5n,}$ where R represents hydrogen or groups including alkyl, acrylate, amine, hydroxyl, etc. [1]. Silsesquioxane molecules can be categorized as random, ladder, cage and partial cage structures. Polyhedral Oligomeric Silsesquioxane (POSS) has inorganic-organic hybrid cage structures which can have T8-eight, T10-ten or T12-twelve Si atoms, as shown in Figure 1.1.

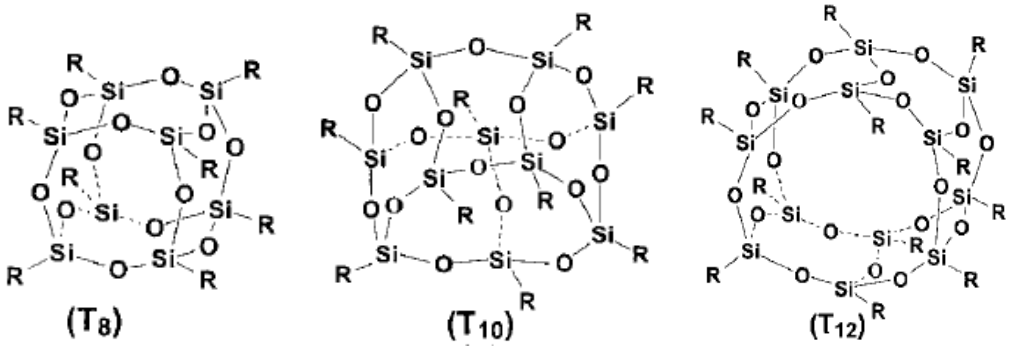

Figure 1.1. POSS Cage Structures [1].

Phase behavior studies of supercritical fluid systems with new-generation materials aid the design of environmentally friendly material processes using supercritical carbon dioxide and development of new supercritical fluid technologies. Recently, polyhedral oligomeric silsesquioxanes (POSS) with functional groups such as trifluoropropyl, isobutyl, isooctyl or methacryl have been found to be soluble in supercritical carbon dioxide [2-3]. Not all types are soluble though, like those with

methyl or phenyl groups. The fact that not all the POSS components are soluble in supercritical carbon dioxide ($scCO_2$) [3] shows that POSS is required to be functionalized with groups which can either exhibit Lewis acid-base interactions and weak hydrogen bonding with CO_2 [4], or branched alkyl groups that may provide entropic contribution. Among the studied POSS, the highest solubility in $scCO_2$ was exhibited by octatrimethlysiloxy POSS [5], whereas POSS with methacrylate groups had the lowest solubility [3].

POSS have widespread polymer applications as nanofillers improving various properties of polymers such as thermal resistance, fire retardancy, oxidation resistance, electric insulation capacity, and mechanical properties [6-8]. POSS molecules generally have no odor, low vapor pressure and are environmentally friendly. Their functional organic groups allow them to interact with polymer chains, which increase their compatibility with the polymer matrix, providing a better distribution of POSS within the polymer. These functional groups are diversified to enable the reactivity of POSS so that they can be used for polymerization [9]. Polymers containing POSS have wide application areas such as packaging, biopharmaceutical, catalyst support, coating, membrane materials, electronic, optical, and magnetic nano devices [10-11]. The use of POSS as biomedical and imaging reagents has also gained importance in recent years since most of them are biocompatible.

1.2. Supercritical Fluids (SCF)

Substances exist in nature as solid, liquid and gas phases as shown in Figure 1.2 where phases are divided by boundaries. Supercritical fluid (SCF) exists above the fluid's critical points; temperature (T_c) and pressure (P_c). Although, liquid and gas phases have different properties in standard conditions, at critical temperature and pressure point; liquid, gas and SCF co-exist and SCF demonstrates features from both gaseous and liquid states [12].

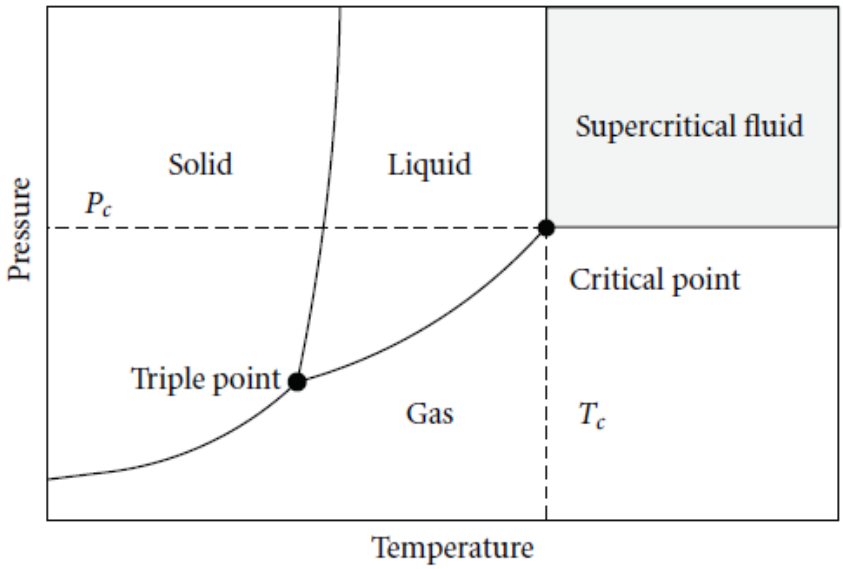

Figure 1.2. Pressure – Temperature Phase Diagram [12].

SCF has tunable density [13] Supercritical carbon dioxide density is illustrated in Figure 1.3 where density variation is represented as a function of pressure under constant temperature. Close to the SCF critical temperature or pressure values, a deviation in the temperature of pressure of the system leads to a large density change, exhibiting a large compressibility. At the critical point the isothermal compressibility is infinite [14].

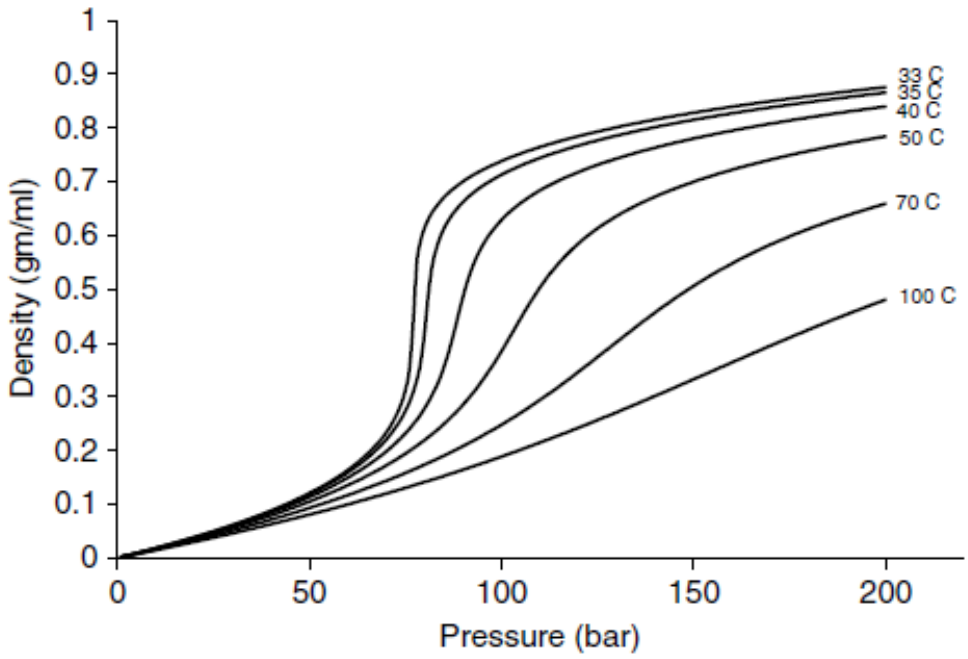

Figure 1.3. Carbon dioxide density variance with pressure under constant temperatures [15].

Properties of gas, liquid and SCF have been listed in Table 1.1. SCF density is lower than the liquid and higher than the gas phases. There is a proportionality between solvation power and density [16]. At constant temperature, SCF density can be increased with pressure rise so solvation power of SCF will be also increased and demonstrate liquid like density. The supercritical state provides better mass transfer properties such as has lower dynamic viscosity, lower surface tension and higher diffusion coefficient when compared with the liquid state. By depending on system pressure and temperature adjustments, SCF's diffusivity, viscosity, polarity, and solvent strength properties can be tuned.

Table 1.1. Properties of gas, liquid and SCF Phases [17].

State	Density (g/ml)	Dynamic viscosity (g/cm.s)	Diffusion Coefficient (cm^2/s)
Gas	0.0006- 0.0020	0.0001- 0.0030	0.1- 0.4
Supercritical fluid (T_c,P_c)	0.2- 0.5	0.0001- 0.0003	0.0007
Liquid	0.6- 1.6	0.002- 0.030	0.000002- 0.000020

Supercritical fluids have started to be used for material processing due to higher rates of mass and heat transfer, and environmentally safer properties when compared with organic solvents [18]. Organic solvents are usually harmful to environment and human health due to the release of volatile organic compounds [19-20]. Therefore, with the improvement and increment of SCF processing there will be an opportunity to reduce the usage of organic solvents.

1.2.1. Supercritical Carbon Dioxide

Carbon dioxide is a highly preferred solvent in SCF technologies. Some of the SCFs used in the industry has been listed in Table 1.2 where carbon dioxide has special properties that are more advantageous compared to the other supercritical fluids such as non-toxicity, non-flammability, abundancy and lower cost. Supercritical carbon dioxide ($scCO_2$) has relatively low critical temperature and pressure (T_c = 304.2K, P_c = 7.3MPa) which also provides process applicability with thermal sensitive materials [21-23]. Supercritical carbon dioxide is used as an alternative solvent in different applications like decaffeination of tea and coffee [24], cleaning and drying processes of microelectromechanical systems [19], polymer production and processing [25], semi-conductor processing [26], chemical reactions, separation processing, waste treatment and plastic recycling, and nanoparticles synthesis [27].

Table 1.2. Critical properties and safety data of some SCFs [15].

Supercritical Fluid	**T_c (K)**	**P_c (bar)**	**Safety Hazard**
Ethylene	282.2	50.4	Flammable Gas
Carbon Dioxide	304.1	73.8	-
Ethane	305.4	48.8	Flammable Gas
Propane	369.8	42.5	Extremely Flammable
Ammonia	405.4	113.0	Flammable and Toxic
Toluene	591.8	41.0	Highly Flammable
Water	647.3	221.2	-

Carbon dioxide exhibits charge separation due to positively charged C atom and negatively charged O atoms [16], [28]. It has molecular symmetry and zero dipole moment. While CO_2 is a nonpolar solvent, it has a quadrupole moment, and through its electron deficient carbon, it can undergo Lewis acid (LA) (electron acceptor) and Lewis base (LB) (electron donor) interactions [29]. Thus, when molecules can exhibit such interactions, they can dissolve in liquid and supercritical CO_2 [30], [31].

1.2.2. Solubility in Supercritical Carbon Dioxide

As mentioned in part 1.2 and 1.2.1, $scCO_2$ has started to be used in industry due to being environmentally friendly, non-toxic, non-flammable and inexpensive solvent. Solubility and phase behavior data of materials, especially for unique ones like POSS, in supercritical carbon dioxide is important to be known before being used in industrial applications. By determining the solubility data, system's necessary design features can be adjusted which is important for application effectiveness. The solubility of solute is defined generally in terms of mole fraction or weight fraction dissolved in the supercritical solvent phase.

The vapor pressure, molecular structure and weight, and polarity of the solute are the properties which determine the solubility of solutes in supercritical carbon dioxide [32]. As also highlighted in part 1.2, there is a correlation between solvation power and solvent density which can be changed with small changes in the temperature or pressures of SCF. With these changes, enthalpy, entropy or diffusivity which are density-dependent parameters, can be also affected directly. Therefore, the solubility of solute in supercritical carbon dioxide can be varied. By increasing the supercritical carbon dioxide density, by increasing the pressure, the solubility of the solute can also be increased [15].

The vapor pressure of the solute and the density of supercritical carbon dioxide depend on temperature which directly affects the solubility of solute. Although solvent density or solvation power decreases; vapor pressure increases with temperature increment. When temperature of the system increases, chemical potential thus vapor pressure increases which also increases the solubility of the system in high-pressure region. On the other hand, in low-pressure region, instead of vapor pressure, supercritical carbon dioxide density is more dominant so with the increment of temperature, solvent density and solubility decrease [33]. For example, in Figure 1.4, crossover pressure can be seen where three isothermal lines are crossing at 165 bar. Below the crossover point, at isobaric conditions, at 333 K, phenanthrene has lower solubility than at 313 K in supercritical carbon dioxide because of low solvent density effect. On the other hand, above the crossover point at isobaric conditions, 333 K phenanthrene has higher solubility than at 313 K due to the vapor pressure effect in the solubility [15].

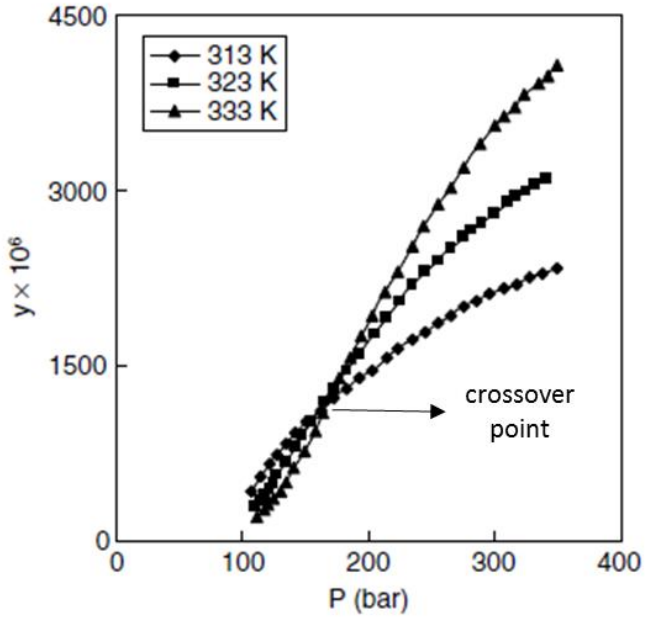

Figure 1.4. Solubility isotherms of phenanthrene – CO_2 binary system at 313K, 323K and 333 K [34].

1.3. Solubility Modelling in Supercritical CO_2

In the literature, there are limited solute solubility data in supercritical carbon dioxide, due to the experiments' high temperature and pressure requirement, which are generally difficult to conduct and time consuming [35], [36]. For this reason, mathematical modelling, equation of state (EOS) and semi-empirical density-based models, provide an opportunity to correlate the solubility data.

EOS models are theoretical models which require critical pressure and temperature, vapor pressure and acentric factor parameters [37], [38]. These thermodynamic parameters are mainly not readily available for hybrid materials. In order to estimate the critical properties, group contribution techniques can be useful. However, hybrid materials are complex structures, and group estimation techniques for hybrid-caged structures are not well-developed yet. There are various estimations to apply the

group contribution techniques for the prediction of thermodynamic parameters; however, they are usually not reliable and accurate [39]. Consequently, EOS Models give high errors due to inaccurate parameter prediction estimations [40], [41]. This problem also occurred in our previous studies in the critical parameter estimations of systems involving hybrid caged structures like POSS.

Semi-empirical density-based models are mainly used to correlate the solubility of solutes in supercritical fluids for which only experimental temperature, pressure and the density of the supercritical fluid are required to be known. Generally semi-empirical density-based models give successful results in 10-30 MPa pressure range but fail at higher pressure and density regions [42].

1.3.1. Semi-empirical Density Based Methods

Some of the most commonly applied correlations are Chrastil, Chrastil modified by Wang (C-W), del Valle and Aguilerra (d-A), Kumar and Johnston (K-J), Mendez-Santiago and Teja (MST), and Bartle models. The effects of temperature, pressure and solvent density.are considered in correlation of the measured solubility data.

1.3.1.1. Chrastil Model

The Chrastil equation [43] is,

$$\ln(S_j) = a\, ln(\rho_1) + \frac{b}{T} + c \qquad [1]$$

where 1 denotes the supercritical solvent and j denotes the solute, T is temperature, ρ is the density of the solvent, a is an association number representing the number of the molecules in the solvato complex, b is dependent on the heats of solvation and vaporization of the solute, and c is dependent on the molecular weights of the solute and supercritical solvent. $S_j$is the solubility of the solute in the supercritical solvent (g/L).

1.3.1.2. Chrastil Modified by Wang Model

The Chrastil model modified by Wang [38], developed from the phase equilibrium rules, the solvation concept and the high-pressure reaction equilibrium constant with four adjustable parameters are given as:

$$\ln(S_j) = a + \frac{b}{T} + c\,\rho_1 + d\,\ln(P) \quad [2]$$

where;

a depends on the solvation entropy (ΔS^0) and the solute vapor pressure (P^{sat}) with relation,

$$a = \frac{\Delta S^0}{R} + \ln(P^{sat}) \quad [3]$$

b depends on the solvation enthalpy (ΔH^0), the molar volume (V_s^s) and the solute vapor pressure (P^{sat}) with relation,

$$b = \frac{-(\Delta H^0 + V_s^s\,P^{sat})}{R} \quad [4]$$

c is related to the second virial coefficient of the solute (B_{22}), the mixed second virial coefficient (B_{12}), the molar volume, and the association number (k) with relation,

$$c = -[2\,(B_{12} - kB_{22}) + (k-1)\,B_{11}] + V_s^s \quad [5]$$

$$d = k - 1 \quad [6]$$

S_j is the solubility of the solute in the supercritical solvent (g/L).

1.3.1.3. Del Valle and Aguilera Model

Del Valle and Aguilera model is another modification of the Chrastil's equation which was proposed to compensate the variation of enthalpy of vaporization ΔH_{vap} with temperature and used for the correlation of vegetable oil solubility in high-pressure CO_2 [31]. The equation is:

$$\ln(S_j) = a\, ln(\rho_1) + \frac{b}{T} + \frac{c}{T^2} + d. \quad [7]$$

1.3.1.4. Kumar and Johnston Model

Kumar and Johnston proposed a model [45] based on the linear relationship between ln y_j and ρ_1 which is expressed as:

$$\ln(y_j) = a + \frac{b}{T} + c\rho_1. \quad [8]$$

1.3.1.5. Mendez-Santiago and Teja Model

The density-based model proposed by Mendez-Santiago and Teja [46] is based on the theory of dilute solutions. However, the requirement of the solute sublimation pressure data can cause a problem since this data is not available for many compounds. For the solute sublimation pressure, Antoine equation was used, and the model was expressed as:

$$Tln(y_j P) = a + b\rho_1 + cT. \quad [9]$$

1.3.1.6. Bartle Model

The semi-empirical model proposed by Bartle et al. [47] is given as

$$\ln\left(\frac{y_j P}{P_{ref}}\right) = a + \frac{b}{T} + c(\rho_1 - \rho_{ref}) \quad [10]$$

where the reference pressure (P_{ref}) is 0.1 MPa, the reference density (ρ_{ref}) is 700 kg/m^3, and the parameter b is related to the vaporization enthalpy of the solute (ΔH_{vap}) .

1.3.2. Solubility Data Correlation with Semi-Empirical Density Based Methods

The solubility data of each POSS were correlated with each model using MATLAB where the objective function, absolute average relative deviation (AARD), expressed as

$$AARD\ (\%) = \frac{100}{N}\sum_{i}^{N}\left|\frac{y_i^p - y_i^e}{y_i^e}\right| \qquad [11]$$

was minimized. Here N is the number of data points, y_i^p is the calculated solubility and y_i^e is the experimental solubility data.

1.4. The Objectives of this Study

The aim of this study is to investigate the phase behavior of the binary systems containing CO_2 and polyhedral oligomeric silsesquioxanes (POSS) which can show different hybrid material properties due to their functional groups attached to its cage structure. Supercritical carbon dioxide ($scCO_2$), which is referred as an environmentally friendly solvent, can exhibit specific interactions such as weak hydrogen bonding or Lewis acid-base interactions due to its quadrupole moment and form single phase solutions with various materials [4]. In the previous POSS - $scCO_2$ solubility studies at 308 K and 323 K, trifluoropropyl, methacryl, isooctyl, and octaisobutyl POSS were found to be soluble in $scCO_2$ [2,3]. In this study to see

the effects of temperature and pressure on the solubilities of POSS's; methacryl, isooctyl, octaisobutyl and trifluoropropyl POSS were studied at 318 K and 328 K. It is known that due to their segmental mobilities and high free volumes, silicone-based compounds can be highly CO_2-philic and exhibit significant solubility in $scCO_2$ [48-60]. The affinity of components to CO_2 can be improved through incorporation of siloxane functionalization [61]. Increasing the CO_2-philicity of components with such modification can decrease the pressure and temperature requirements of the supercritical fluid technologies that they are applied in. Therefore, in this work, with the aim of finding a novel POSS with higher CO_2 affinity, the phase behavior of the siloxy-modified POSS-CO_2 binary system was studied to observe the effect of siloxane groups. To observe the effect of siloxane groups which can increase the CO_2-philicity of POSS components and decrease the pressure and temperature requirements of the supercritical fluid applications, the phase behavior of the siloxy-modified POSS-CO_2 binary system was also studied to observe at 313K-328K range [5]. The methacryl POSS-CO_2 and isooctyl POSS-CO_2 liquid-vapor equilibrium curves, and octaisobutyl POSS-CO_2, trifluoropropyl POSS-CO_2, and octatrimethylsiloxy POSS-CO_2 solid-vapor equilibrium curves have been constructed. Solubility versus CO_2 density isotherms were obtained at the cloud and dew points of the POSS-CO_2 systems to predict which functional group modified POSS is more soluble in $scCO_2$ at the studied conditions Mendez-Santiago and Teja (MST), Chrastil, Bartle, Chrastil Modified Wang (C-W), del Valle and Aguilera (del Valle) and Kumar and Johnston (K-J) semi-empirical density-based models have been used to correlate the experimental data due to lack of information on the critical properties and group contribution constants of POSS in literature, which prevented the estimation of the phase behavior of the binary systems with equation of states and their critical properties. The density-based equations were evaluated to examine how well they would fit the solubility data of the POSS-CO_2 binary system. This study is expected to be beneficial for the prediction of the solubility of POSS's at conditions around the vicinity of the studied temperature and pressure range, to be

used in the design and optimization of various supercritical fluid processes using carbon dioxide.

CHAPTER 2

LITERATURE SURVEY

2.1. Applications of POSS

Currently polyhedral oligomeric silsesquioxanes (POSS) are being used in a plethora of applications including composites, polymer processing, coatings, catalysis, drug delivery, and other biomedical applications. In the following paragraphs, some examples from the literature are given.

Alkyl chain length effect on morphological properties of polypropylene (PP) based nanocomposites have been studied by Fina et al. [62] by using octamethyl, octaisobutyl and octaisooctyl POSS, which have different functional group chain lengths. Melt blending technique was used to mix PP and POSS types. SEM analyses indicated that octaisobutyl POSS diffused into the PP structure better than the octamethyl POSS due to its long chain length which improves the compatibility of POSS with PP matrix and diffusion capability of POSS inside the polymer. Even though octaisooctyl POSS has longer chain length than octaisobutyl POSS, its dispersion was not better because crystallization behavior could be affected from octamethyl POSS, acting as a nucleating agent, and octaisobutyl POSS, initiating polymer polymorphism.

There is an impact of alkyl group length of POSS to the mechanical properties of the polymer composites. Baldi et al. [63] worked on this effect with isooctyl, octaisobutly and octamethyl POSS which have different alkyl group lengths. Each POSS blended with Polypropylene (PP) and created different functionalized POSS-PP blends. The measurements of the composites' mechanical properties showed that octamethyl-POSS composite had higher Young's modulus and lower yield strength

than pure PP. It was also proved that with the increment of isooctyl and octaisobutly POSS amount, yield strength was increased, and Young's modulus was decreased. Octamethyl POSS–PP composite was also found to be more efficient to eliminate the fracture instability when compared with pure PP.

Moist and saltwater are affecting the performance of polymer composites. For this reason, carbon fiber was coated with octaisobutyl POSS in H Mahfuz et al. [64] study to improve the mechanical features of the fiber matrix and strengthen the carbon/vinyl ester composites. By coating the carbon fibers with POSS, it was observed that while retaining the attained properties of the composites, water absorption was decreased, and the interlaminar shear strength and velocity impact were developed enhanced.

S.R. Jin et al. [65] worked with octaisobutyl methacryl and octasilane POSS to prepare poly(methyl methacrylate) (PMMA) nanocomposites with 50 and 660 nm film thicknesses. Glass transition and relaxation enthalpy decreased with the thickness. Due to the physical ageing property of methacryl POSS, MPOSS/PMMA nanocomposites exhibited reduction in glass transition temperature and relaxation enthalpy.

2.2. POSS-scCO$_2$ Systems

2.2.1. Experimental studies on POSS – CO$_2$ Systems

Recently, the phase behavior of the binary systems which consist of CO_2 and polyhedral oligomeric silsesquioxanes (POSS) modified with various functional groups have been studied to contribute to the development of environmentally friendly processes of POSS with supercritical carbon dioxide ($scCO_2$). [2,3]

In the study of Dilek [2], trifluoropropyl POSS thermodynamic phase behavior in supercritical carbon dioxide was investigated. Trifluoropropyl POSS, which has

CO_2-philic fluoroalkyl structure, dissolves in supercritical carbon dioxide at 308-323 K temperature and 8.3-14.8 MPa pressure ranges and exhibits maximum of 4.4% by weight and 0.17% by mole solubility fractions. Solid-vapor phase equilibrium curves were constructed with the obtained cloud points and solubility data. The solubility of trifluoropropyl POSS in scCO_2 decreases with an isobaric temperature increase; therefore, the decreasing CO_2 density is dominant on the phase behavior of the systems, compared to the increasing POSS vapor pressure. Using the obtained solubility data, the process conditions for supercritical fluid coating of PMMA bars have been determined and the coating was conducted with supercritical carbon dioxide.

A similar study was conducted by Kanya [3] with methacryl, isooctyl, octaisobutyl POSS, all of which formed homogenous solutions with supercritical carbon dioxide. On the other hand, octamethyl POSS was found insoluble in supercritical carbon dioxide. Methacryl and isooctyl POSS dew-points and octaisobutyl POSS cloud points were measured at 308-323 K, up to 30 MPa. Methacryl and isooctyl POSS liquid-vapor and octaisobutyl POSS solid-vapor equilibrium curves were constructed. Like trifluoropropyl POSS, methacryl and isooctyl POSS solubility decreases with an isobaric temperature increase, which leads to decreasing supercritical carbon dioxide density, and thus its solvation power. Isooctyl POSS was found to be more soluble than methacryl POSS at 308 and 323 K. The crossover point has been identified in octaisobutyl POSS-CO_2 binary system above which the increase in the vapor pressure with increasing temperature is dominant on POSS dissolution in supercritical carbon dioxide, compared to the solvent density effect. These results prove that the solubility of POSS in supercritical carbon dioxide, and the phase behavior of the binary systems are directly affected by the POSS functional groups.

2.2.2. Computational / Theoretical studies on POSS – CO_2 Systems

Tezsevin et al. [4] conducted a theoretical study to explore the interactions between CO_2 and functionalized POSS structures by using Gaussian 09 software, first time in the literature. Density Functional Theory (DFT) principles were applied in the study. For the investigation, octatrifluoromethyl, octatrifluoropropyl POSS [2] (for which the solubility in supercritical carbon dioxide was studied experimentally), and insoluble octamethyl POSS [2] were selected to the determine interactions between carbon dioxide and the functional groups. Results showed that there were dipole-quadrupole charge interactions between the fluorinated POSS and CO_2. While in the CO_2-octamethyl POSS system weak O-H interaction was observed, in the CO_2-octatrifluoromethyl POSS system, only C-F interaction was observed. On the other hand, CO_2-octatrifluoropropyl POSS system exhibited both interaction types, i.e., weak hydrogen bonding between the oxygen atom of carbon dioxide and the hydrogen atom of the functionalized POSS structure and Lewis acid-base interaction between the carbon atom of carbon dioxide and the fluorine atom of the POSS functional group. Among the three POSS-CO_2 systems, the strongest intermolecular interactions were observed with this binary system, exhibiting both types of interactions.

2.2.3. Applications of POSS – CO_2 Systems

After the solubility of fluoroalkyl POSS in supercritical CO_2 was discovered, CO_2-philic POSS has been started to be used in material processes applying supercritical CO_2. Eris et al. for example created microchannels in a silica aerogel for optofluidic applications by extracting trifluoropropyl POSS fine rods from the aerogel [66]. Initially, trifluoropropyl POSS was melted in a U-Shape mold and then solidified. For gelation, the mold was put into the silica solution, aging process was applied, then silica alcogels were prepared. Due to the solubility of fluoro POSS in supercritical carbon dioxide, the POSS fine rods were extracted from the alcogels

during the supercritical drying process. After the extraction, hollow U-shape gel structure channels were generated. The aerogel surface, where silanol groups were located, reacted with hexamethyldisilazane in the presence of $scCO_2$. In this way, the aerogel channels gained hydrophobic feature. Finally, by passing light through the water-filled channel, optofluidic waveguides were created.

Methacryl POSS was used by Costeux and Zhu [67] to obtain nanoporous polymer foams with increased cell nucleation density to be used for thermal insulation. Supercritical carbon dioxide was applied to thermoplastic polymers as the foaming agent and high-pore volume and uniform nanocellular foams were produced. Methacryl POSS and silica nanoparticles were added to poly(methyl methacrylate) (PMMA) and styrene acrylonitrile (SAN) copolymers to improve the polymer cell nucleation density, and it was proved that the cell density was increased three orders of magnitude after carbon dioxide foaming.

Trifluoropropyl POSS was used by Novendra et al. [68] as a pore inducer in a highly crystalline poly($_L$-lactic acid) (P_LLA) (around 40%) to significantly decrease the supercritical foaming temperature of P_LLA at the CO_2-processing pressure of 20 MPa. The PLLA-POSS composite films were prepared by solvent casting, which were then processed with supercritical carbon dioxide. Supersaturation of the polymer has been reached by rapid depressurization of supercritical carbon dioxide, which provides nucleation and growth of the pores in the polymer matrix. Semi-crystalline polymers with high crystallinity can only be foamed with carbon dioxide when the saturation temperature is closer to the melting point of the polymer, which is about 443 K for PLLA. In this work, even though the supercritical CO_2 processing of PLLA with crystallinity greater than 30% was conducted at a low temperature as 313 K, by using the CO_2-philic POSS, a porous PLLA was obtained with porosity up to 40% the first time in the literature. Under the same process conditions, pore formation was not observed in P_LLA when no cell nucleators were added to the polymer. Similarly, when a non-CO_2-philic POSS was used as a cell nucleator, pore

formation was also not seen in P_LLA, which shows that such decrease in the process temperature can only be achieved when a CO_2-philic cell nucleator is used.

CHAPTER 3

EXPERIMENTAL METHODS

3.1. Materials

Octatrimethylsiloxy POSS (97%), methacryl POSS (97.2%), isooctyl POSS (99.0%), octaisobutyl POSS (99.4%) and trifluoropropyl POSS (96.8 %), Figure 3.1, were obtained from Hybridplastics (Hattiesburg, MS, USA). Molecular formulas of the structures are $C_{24}H_{72}O_{20}Si_{16}$, $(C_7H_{11}O_2)_8(SiO_{1.5})_8$, $(C_8H_{17})_8(SiO_{1.5})_8$, $(C_4H_9)_8(SiO_{1.5})_8$, and $(C_3H_4F_3)_{12}(SiO_{1.5})_{12}$, respectively. The samples were stored at room temperature and used without further purification. Octatrimethylsiloxy POSS, octaisobutyl POSS and trifluoropropyl POSS were obtained in powder form with bulk densities of 0.66 g/cm^3, 0.63 g/cm^3 and 1.5 g/cm^3, respectively and isooctyl POSS and methacryl POSS were obtained in liquid form with viscosities of 19 and 18 Poise at 298K and densities of 1.01 g/cm^3 and 1.2 g/cm^3, respectively. Carbon dioxide (99.9%) was obtained from Linde Gas (Ankara, Turkey).

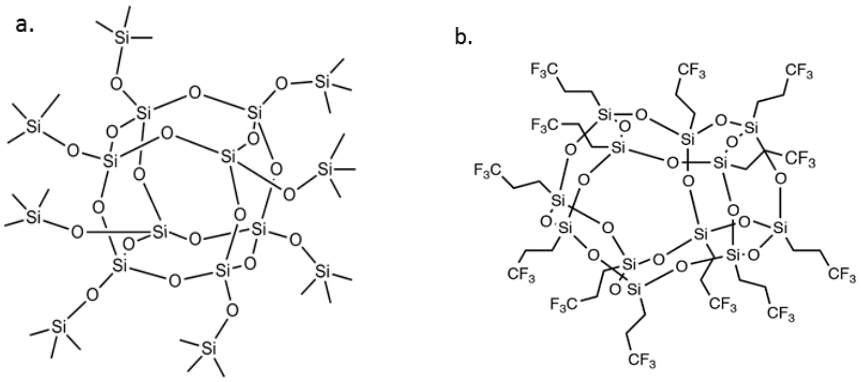

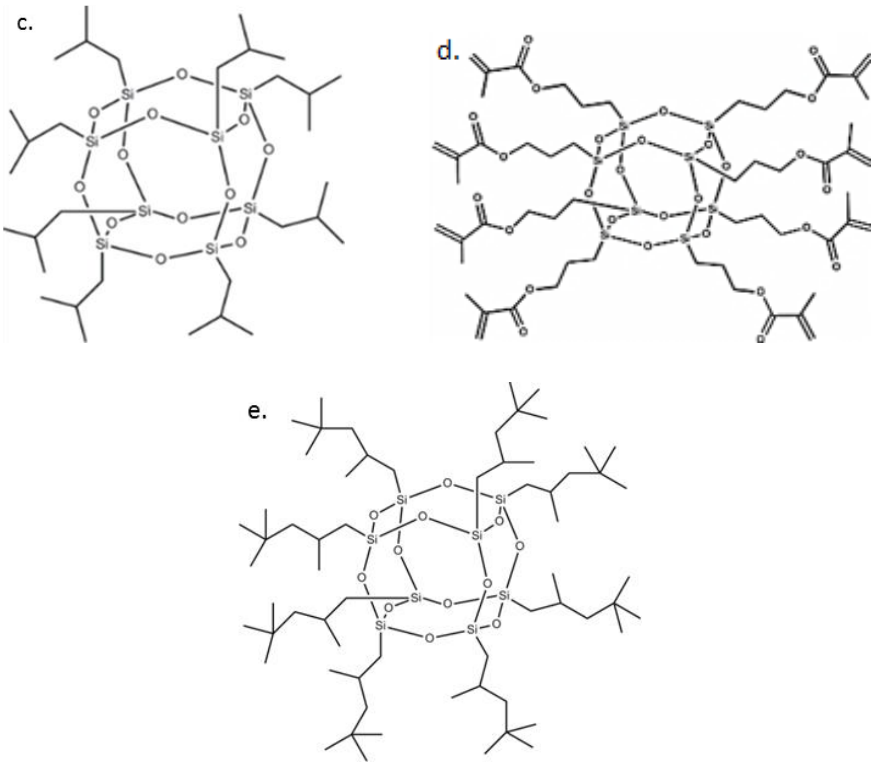

Figure 3.1. Chemical structures of a) octatrimethyl siloxy POSS, b) trifluoropropyl POSS, c) octaisobutyl POSS, d) methacryl POSS, e) isooctyl POSS.

3.2. Solubility Experiments

3.2.1. Experimental Set-Up

The cloud and dew points of the POSS–CO_2, binary systems were detected in a high-pressure set up represented schematically in Figure 3.2. The system contains a custom-made jacketed stainless-steel high-pressure vessel with windows and an inner cylindrical volume of 46.15±0.07 cm^3. The temperature of the contents of the vessel is measured with a thermocouple (Omega Engineering, KMQXL-IM150U-150) with the tip located inside the vessel. The vessel is also coupled with a pressure transducer (Omega Engineering, PX419), inlet and outlet valves, and a rupture disc. Accuracies of the thermocouple and pressure transducer are ±0.5 K and ±0.03 MPa,

respectively. A high-pressure syringe pump (Teledyne ISCO-260D) with ±0.05 MPa pressure accuracy is used to charge dense CO_2 into the vessel. The high-pressure tubing connecting the vessel and the syringe pump is coupled with a check valve to avoid reverse flow. The temperature of the high-pressure system is controlled with a water circulating heater (Polyscience, 9112) within a range of ±0.01 K. A magnetic stir plate is used to mix the solution continuously.

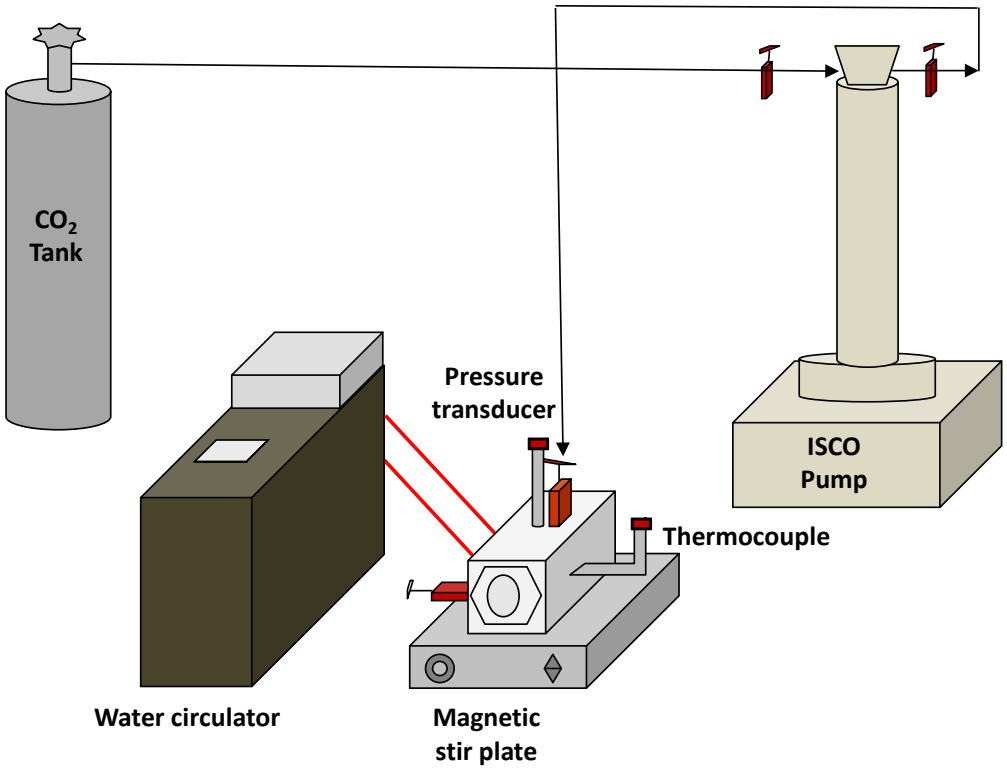

Figure 3.2. The experimental set-up used in the POSS-CO_2 cloud and dew point measurements.

3.2.2. Cloud and Dew Point Measurements

The solubilities of liquid and solid POSS's have been measured at the dew and cloud point, respectively. Apart from phase of solute which segregated from POSS-CO_2

homogenous mixture, experiment application process is the same for both POSS's [2, 3, 5].

Initially, the high-pressure vessel was loaded with a desired amount of POSS, which was weighed to an accuracy of ±0.0001 g. The temperature of the vessel was increased to the set temperature using the water circulating heater. After setting the temperature and pressure of the ISCO pump to the desired values, CO_2 was introduced from the syringe pump working at the constant-pressure mode, into the tubing between the vessel and the syringe pump. The volume of the pump reservoir filled with CO_2 was recorded, and CO_2 was introduced into the vessel slowly through the vessel inlet valve. When the pressure of the vessel reached that of the syringe pump, and the pump ceased delivering, the inlet valve was closed, and the volume of the pump reservoir was recorded. The weight of CO_2 in the vessel was calculated from the density of CO_2 at the constant loading temperature and pressure, which was obtained from the NIST Chemistry Web-Book [68] and the volume of the CO_2 loaded into the vessel, which was equal to the difference between the two recorded volume data. The POSS weight fraction in the POSS-CO_2 solution was determined from the weights of the loaded POSS and CO_2. The error in the calculated weight concentrations of POSS is within ±0.8% due to the pressure and temperature accuracies of the syringe pump, and the accuracy of the balance. The system pressure was high enough that the loaded solute was completely dissolved in CO_2 and a homogenous solution was obtained while the contents of the vessel were vigorously and continuously stirred. As the mixing continued, the exit valve of the vessel was slightly opened, and the system was depressurized very slowly (≈ 0.007 MPa/s) and isothermally to maintain the solution homogenous with constant composition. The cloud or dew point pressure was recorded immediately as soon as the cloudiness became visually detectable due to the precipitation of POSS from the single-phase solution. The cloud points of the Octatrimethylsiloxy POSS – CO_2 binary system were measured with this procedure at temperatures of 308, 313, 318, 323, and 328 K. At each temperature ten measurements were performed. The cloud

points of the Octaisobutyl POSS – CO_2 and Trifluoropropyl POSS–CO_2 binary systems were measured at temperatures of 318 and 328 K. At each temperature seven and six measurements were performed, respectively. The dew points of the Methacryl POSS – CO_2 and Isooctyl POSS–CO_2 binary systems were measured at temperatures of 318 and 328 K. At each temperature eight and six measurements were performed, respectively. The repeatability of the measurements was determined by performing at least three of the experiments at each temperature, which were selected randomly and carried out on different days with the same procedure described above. As a result, the relative errors between the successive runs were less than 0.9% for cloud or dew pressure. The reliability of the experimental procedure was verified in the previous solubility studies by reproducing the literature data of the extensively studied ethanol-CO_2 binary system liquid–vapor equilibria [2].

CHAPTER 4

RESULTS AND DISCUSSION

4.1. S-V Equilibria of Octatrimethyl Siloxy POSS-CO_2 Binary System

POSS molecules with different functionalities such as fluoroalkyl, methacrylate, isobutyl, and isooctyl have recently been found to be soluble in $scCO_2$ at a CO_2 density range of 0.5-0.95 g/cm^3 [2,3]. Among all these POSS types, trifluoropropyl POSS exhibits the highest CO_2 affinity with a solubility of about 4.4 % by wt. corresponding to 0.17×10^{-2} mol fr. at the CO_2 density of 0.74 g/cm^3 at 308 K.

In this study, the investigation of the functional group contribution on the solubility of POSS in $scCO_2$ is continued with the siloxy functionality. The phase behavior studies of SPOSS with trimethylsiloxy groups attached to the Si atoms of the cage structure were carried out with the cloud point measurements. The solubility data of octatrimethlysiloxy POSS (SPOSS) in $scCO_2$ are given in Table 4.1.

Table 4.1. The cloud point pressures of SPOSS-CO_2 binary system at 308 K, 313 K, 318 K, 323 K, and 328 K, and the corresponding carbon dioxide densities.

SPOSS weight fraction	**SPOSS mol fraction**	**P_{cloud} (MPa)**	**CO_2 Density (g/cm^3)**
308 K			
0.0104	0.0004	7.99	0.413
0.0155	0.0006	8.03	0.442
0.0258	0.0010	8.09	0.482
0.0353	0.0014	8.16	0.527
0.0498	0.0020	8.36	0.587

0.0709	0.0030	8.60	0.625
0.0918	0.0039	8.92	0.656
0.1038	0.0045	9.16	0.673
0.1296	0.0058	9.49	0.691
0.1521	0.0069	10.38	0.726
313 K			
0.0118	0.0005	8.93	0.466
0.0350	0.0014	9.29	0.550
0.0388	0.0016	9.47	0.577
0.0553	0.0023	9.68	0.601
0.0750	0.0032	9.88	0.619
0.0816	0.0035	9.96	0.625
0.0943	0.0040	10.06	0.633
0.1081	0.0047	10.19	0.642
0.1292	0.0057	10.31	0.650
0.1534	0.0070	10.60	0.665
318 K			
0.0121	0.0005	9.86	0.476
0.0306	0.0012	10.19	0.525
0.0429	0.0017	10.44	0.554
0.0601	0.0025	10.67	0.577
0.0744	0.0031	10.79	0.587
0.0886	0.0038	10.94	0.598
0.1023	0.0044	11.01	0.604
0.1168	0.0051	11.08	0.609
0.1431	0.0065	11.23	0.618
0.1678	0.0078	11.47	0.632
323 K			
0.0125	0.0005	10.75	0.475

0.0334	0.0013	11.07	0.509
0.0423	0.0017	11.24	0.526
0.0598	0.0025	11.46	0.545
0.0744	0.0031	11.77	0.569
0.0885	0.0038	11.81	0.572
0.1013	0.0044	11.89	0.577
0.1144	0.0050	11.94	0.581
0.1396	0.0063	12.07	0.589
0.1670	0.0077	12.14	0.593
328 K			
0.0137	0.0005	11.85	0.492
0.0341	0.0014	12.11	0.513
0.0468	0.0019	12.41	0.537
0.0655	0.0027	12.57	0.545
0.0805	0.0034	12.65	0.550
0.0948	0.0041	12.74	0.556
0.1091	0.0048	12.82	0.561
0.1229	0.0054	13.00	0.572
0.1500	0.0068	13.18	0.581
0.1762	0.0083	13.36	0.590

The solid-vapor equilibrium isotherms of the SPOSS-CO_2 binary system are plotted in Figure 4.1 as the solubility mole fr. vs the cloud point pressures. The higher-pressure region corresponding to the right-hand side of each isotherm represents the conditions where SPOSS is completely dissolved in the supercritical fluid and the binary system forms a homogeneous phase. The solubility of SPOSS increases with isothermally increased pressure due to the increased CO_2 density. On the other hand, SPOSS solubility in scCO_2 decreases considerably with the isobaric increase in temperature due to the dominant negative effect of the decreasing CO_2 density on the

solubility, which overcomes the positive contribution of the increase in the solute vapor pressure [33]. A 5 K increase in temperature can lead to a solubility decrease as low as 7 folds. The 308 K solubility isotherm converges with the 313 K solubility isotherm at about 10.6 MPa, exhibiting a possible crossover pressure. Below the crossover pressure, decreasing CO_2 density with temperature has a more prominent influence on solubility compared to that of increasing vapor pressure of the solid. This influence of density becomes less pronounced at higher concentrations as the isotherms approach the crossover pressure.

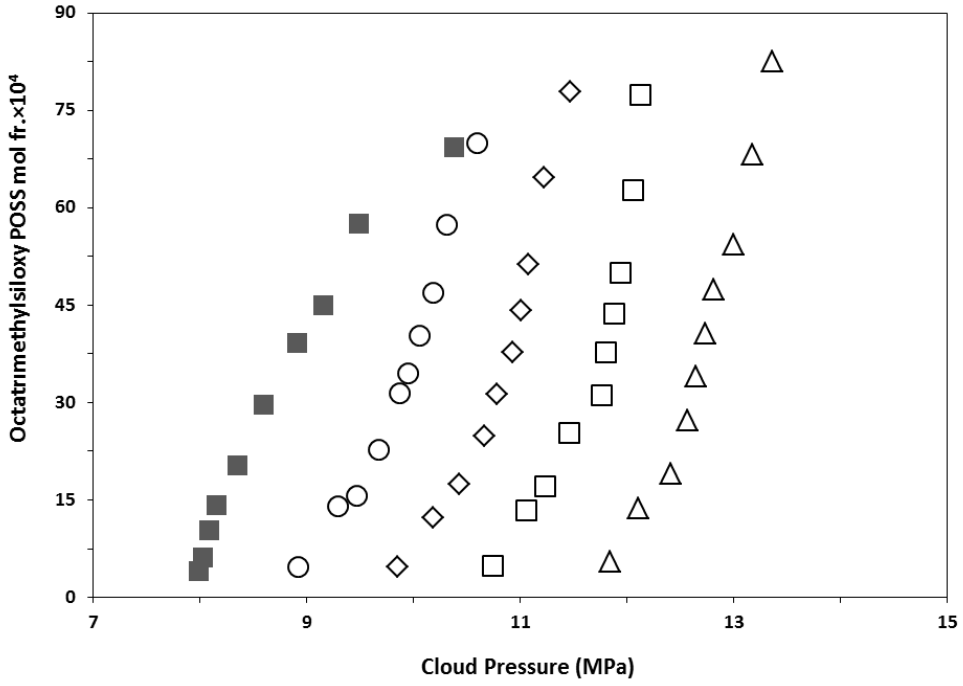

Figure 4.1. Cloud point isotherms of the octatrimethylsiloxy POSS–CO_2 binary system; 308 K (■), 313 K (○), 318 K (◊), 323 K (□) and 328 K (Δ). The estimated error bars are comparable to the size of the symbols.

4.1.1. Comparison of Octatrimethyl Siloxy POSS-CO_2 Systems with other CO_2-philic Materials – CO_2 Systems

4.1.1.1. Comparison of Octatrimethyl Siloxy POSS-CO_2 Systems with Sugar Acetate – CO_2 Systems

Compared to a highly CO_2-philic acetylated sugar, β-D-galactose pentaacetate [69], SPOSS exhibits a comparable solubility, which can allow its application in a plethora of supercritical fluid processes like supercritical debinding [70-72].With SPOSS, at 308 K, 10.4 MPa pressure is required for the dissolution of the solute in CO_2 at a weight fr. of 0.15, while this pressure is about 10.2 MPa for the sugar acetate, as showed in Figure 4.2.

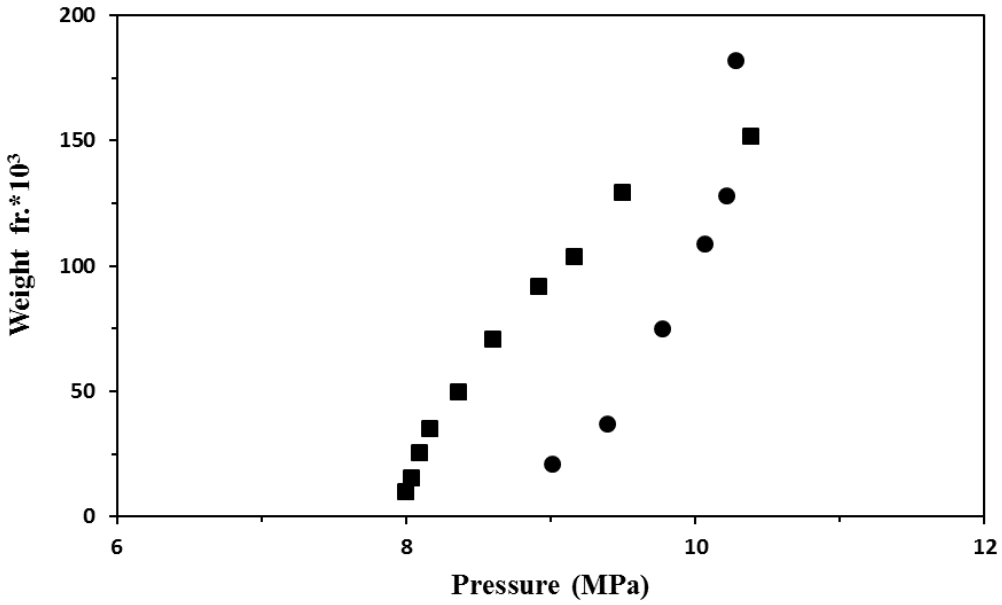

Figure 4.2. Solubility of octatrimethylsiloxy POSS (■) and sugar acetate (●) [69] in $scCO_2$ plotted against the cloud and dew points of the binary system at 308 K, respectively.

While with both components the dissolution pressure increases with temperature, this increase is less pronounced for SPOSS compared to the sugar acetate. To attain 0.15 solubility weight fr., the required pressures at 313 K, 318 K and 323 K are 12.0, 13.7 and 15.5 MPa, whereas these are 10.6, 11.3 and 12.1 MPa for SPOSS, as presented in Figure 4.3, Figure 4.4, and Figure 4.5, respectively.

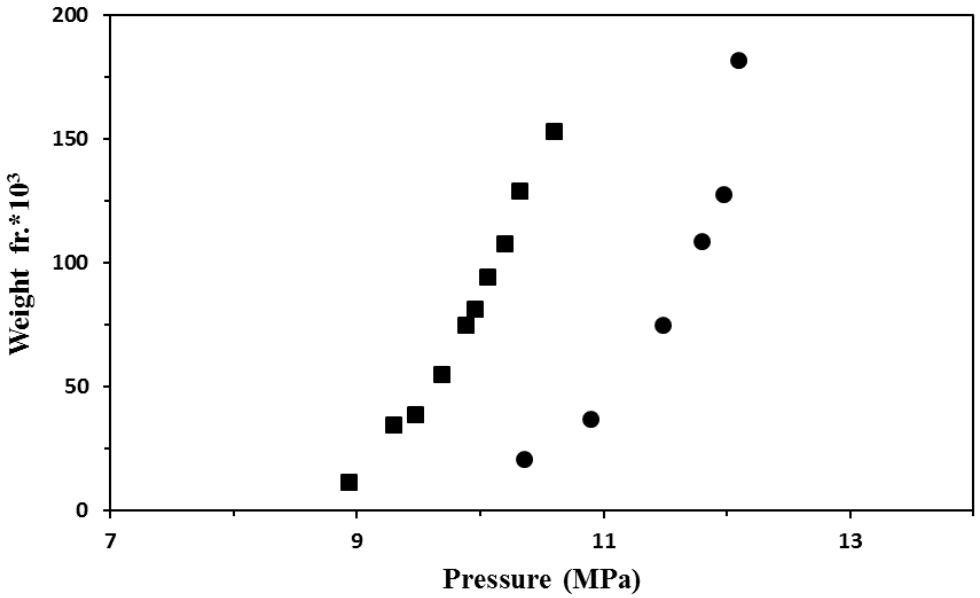

Figure 4.3. Solubility of octatrimethylsiloxy POSS (■) and sugar acetate (●) [69] in $scCO_2$ plotted against the cloud and dew points of the binary system at 313 K, respectively.

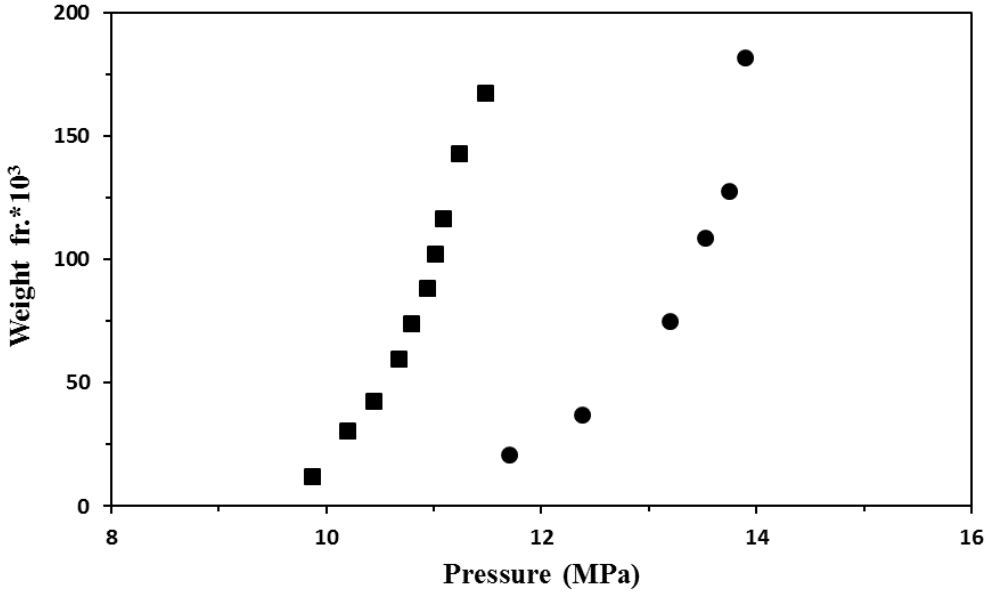

Figure 4.4. Solubility of octatrimethylsiloxy POSS (■) and sugar acetate (●) [69] in $scCO_2$ plotted against the cloud and dew points of the binary system at 318 K, respectively.

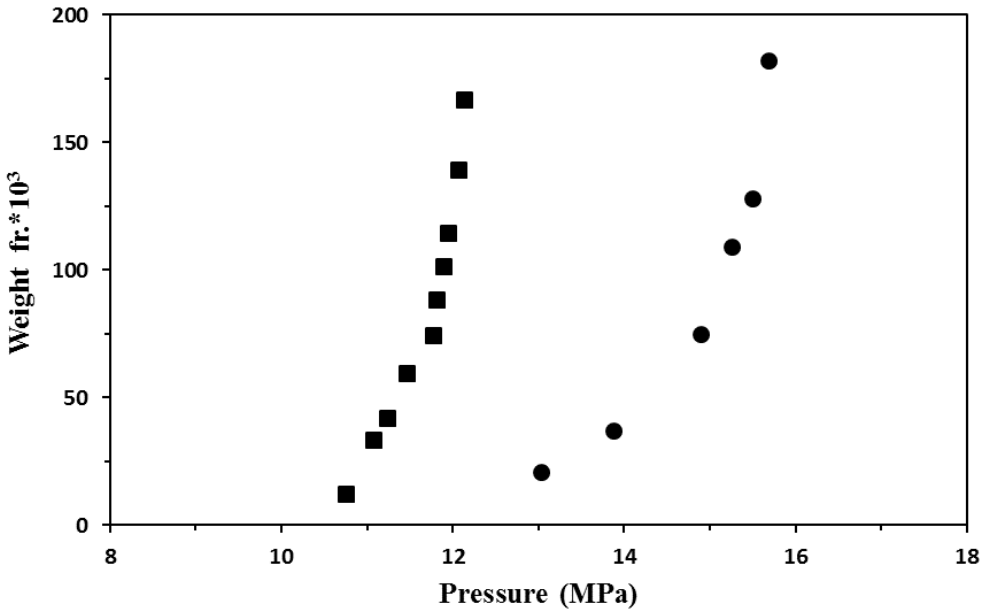

Figure 4.5. Solubility of octatrimethylsiloxy POSS (■) and sugar acetate (●) [69] in $scCO_2$ plotted against the cloud and dew points of the binary system at 323 K, respectively.

Although both solutes require comparable CO_2 density at the lower temperature, with temperature increase, SPOSS requires considerably lower CO_2 density than the sugar acetate for complete dissolution. The relatively increased solubility of SPOSS compared to the sugar acetate at the higher temperature can be attributed to the possible entropic contribution due to the rotational flexibility of the siloxane groups on the nanocage, and presumably less favorable solute-solute interactions of SPOSS.

4.1.1.2. Comparison of Octatrimethyl Siloxy POSS-CO_2 Systems with Naphthalene -CO_2 Systems

Naphthalene is a well-known CO_2-soluble solid material in literature. McHugh studied the naphthalene solubility in supercritical carbon dioxide at 308, 328, 335

and 338 K [73]. Compared to the solubility of naphthalene, SPOSS is less soluble in supercritical carbon dioxide. For example, at 308 K, in order to attain a solubility of 0.007 mole fr., SPOSS requires 10.4 MPa pressure, while naphthalene requires 8.6 MPa. When the temperature was increased to 328 K, 0.006 mole fr. of solubility was observed at 13.1 and 11 MPa for SPOSS and naphthaline, respectively as plotted in Figures 4.6 and 4.7. With the increment of temperature of the system, both components dissolution pressure increases, while this increase is more pronounced for SPOSS when compared to naphthalene.

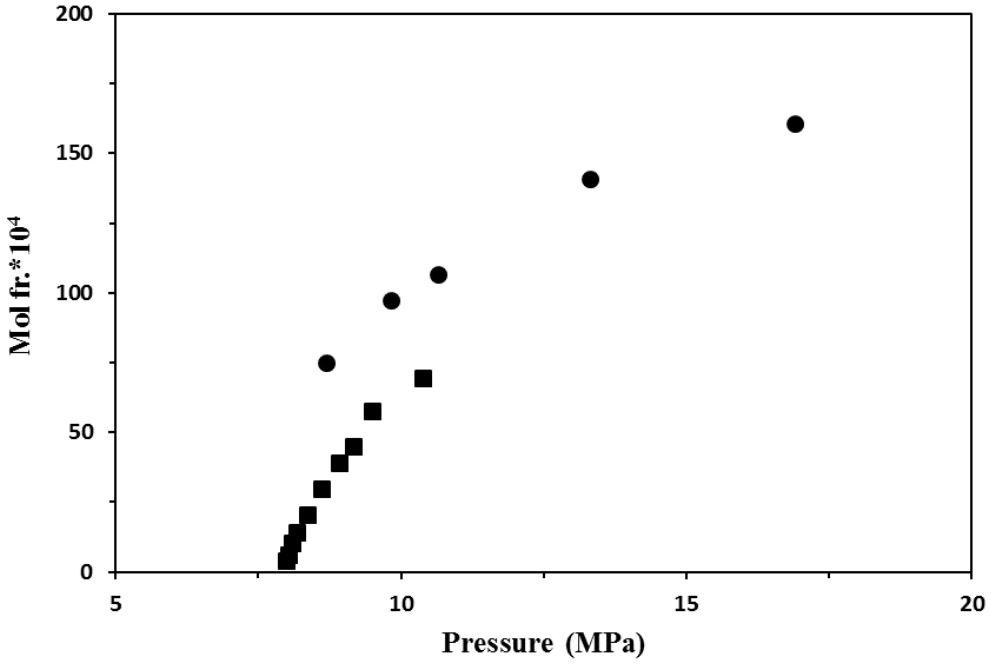

Figure 4.6. Solubility of octatrimethylsiloxy POSS (■) and naphthalene (●) [73] in $scCO_2$ plotted against the cloud points of the binary system at 308 K.

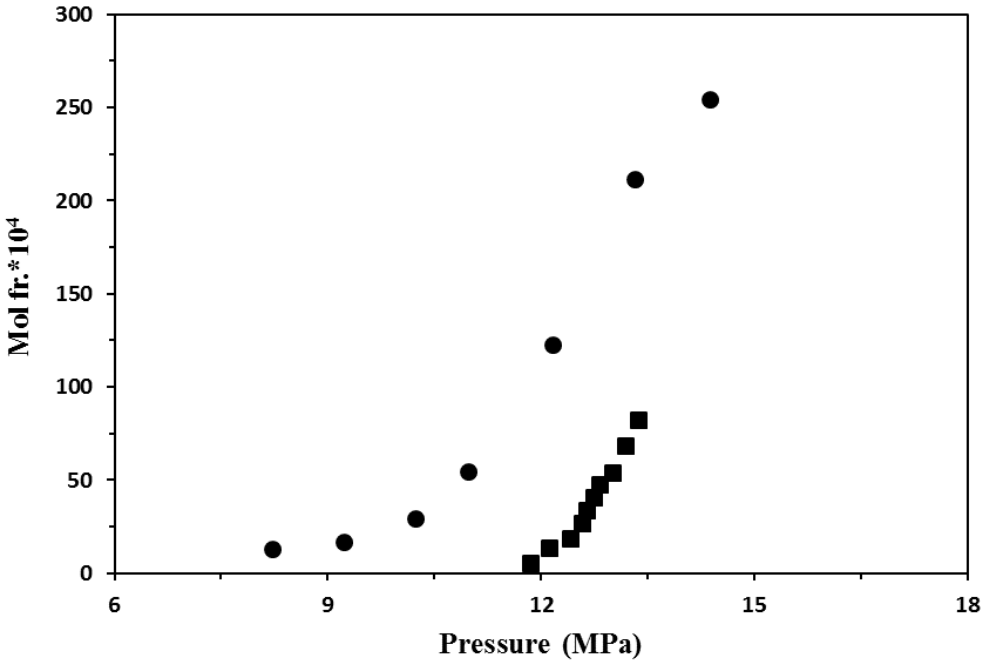

Figure 4.7. Solubility of octatrimethylsiloxy POSS (■) and naphthalene (●) [73] in $scCO_2$ plotted against the cloud points of the binary system at 328 K.

The solubility of SPOSS measured as 0.003 mol fr. at 308 K and 8.6 MPa in supercritical carbon dioxide binary system while naphthalene has 0.008 mole fr. which is 2.6 times higher. Under the isothermal conditions, with the increment of pressure to 10.4 MPa, solubility increased to 0.007 and 0.010 mol fr. for SPOSS and naphthalene, respectively. At this condition, naphthalene solubility was 1.5 times higher than SPOSS. Although naphthalene can dissolve in carbon dioxide more than SPOSS, pressure effect on the SPOSS solubility is more dominant at 308 K, in the 8.6-10.4 MPa pressure range. On the other hand, at 328 K, among the measured values, at the minimum pressure, which was approximately 12 MPa, 0.0005 mole fr. solubility was measured for SPOSS, while naphthalene solubility was 0.012 mole fr. which is 24 folds than SPOSS solubility. Moreover, at the same temperature and 13.4 MPa, the observed solubility of POSS was 0.008 mole fr. while naphthalene

solubility was 0.021 mole fr. at the same conditions which is 2.5 folds than SPOSS. Therefore, SPOSS solubility sensitivity to the system pressure increment in isothermal conditions is greater than the naphthalene at 328 K.

4.2. S-V Equilibria of Trifluoropropyl POSS-CO_2 Binary System

Trifluoropropyl POSS solubilities in supercritical carbon dioxide were studied at 308K and 323 K up to 15 MPa [2]. In this study, the solubility of trifluoropropyl POSS was measured at 318 K and 328 K up to 18 MPa to see the effects of different temperatures and pressures on the POSS's solubility. The cloud point pressures of POSS-CO_2 binary systems at 318 and 328 K, the corresponding CO_2 densities, and POSS's weight and mol fractions are given in Table 4.2.

Table 4.2. The cloud point pressures of TFPOSS-CO_2 binary system at 318 K, and 328 K and the corresponding carbon dioxide densities.

TFPOSS weight fraction	**TFPOSS mol fraction**	**P_{cloud} (MPa)**	**CO_2 Density (g/cm^3)**
318 K			
0.0016	0.00004	11.14	0.612
0.0079	0.00019	12.00	0.658
0.0156	0.00039	12.41	0.674
0.0286	0.00072	13.32	0.703
0.0421	0.00108	14.36	0.729
0.0541	0.00140	14.80	0.738
328 K			
0.0019	0.00005	12.74	0.556
0.0079	0.00020	14.90	0.650
0.0162	0.00040	15.51	0.668

0.0322	0.00082	16.26	0.687
0.0429	0.00110	17.17	0.707
0.0565	0.00147	17.97	0.723

In Figure 4.8, the solubility of trifluoropropyl POSS-CO_2 binary system at 318 and 328 K are plotted. Solid–vapor phase equilibrium curves were constructed by using the experimental mole fractions and system cloud point pressures. At constant temperature, solubility increases with pressure, which is because of the increasing density of carbon dioxide, in other words power of solvation. While at constant pressure, solubility is decreasing with temperature rise.

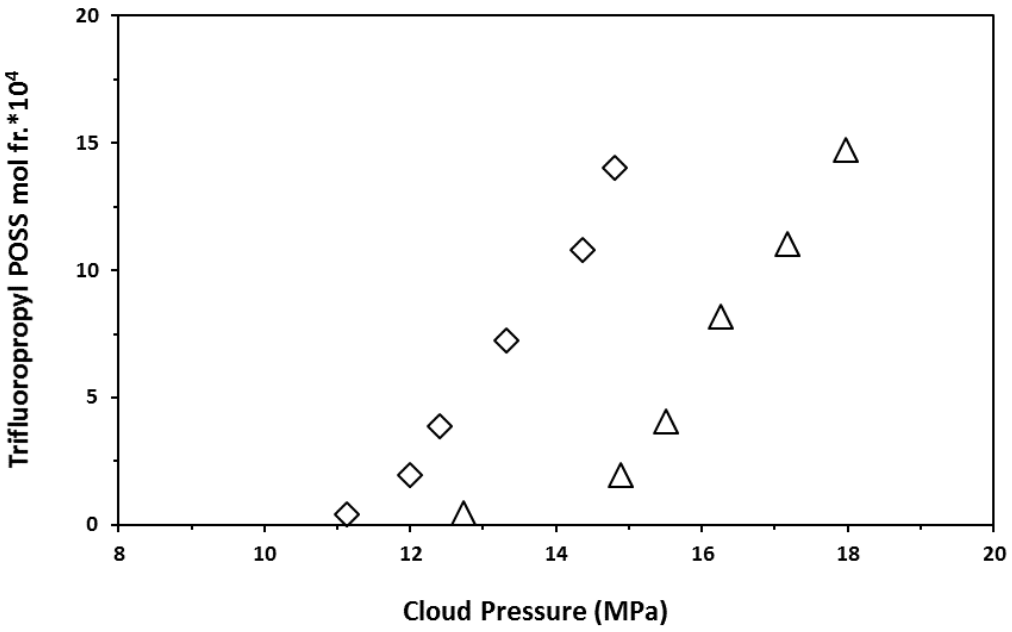

Figure 4.8. Cloud point isotherms of the trifluoropropyl POSS–CO_2 binary system; 318 K (◊), and 328 K (Δ). The estimated error bars are comparable to the size of the symbols.

4.3. S-V Equilibria of Octaisobutyl POSS-CO_2 Binary System

Octaisobutyl POSS solubilities in supercritical carbon dioxide were studied at 308K and 323 K up to 15 MPa [3]. In this study, the solubility of octaisobutyl POSS in $scCO_2$was studied at 318 K and 328 K up to 17 MPa to see the effects of different temperatures and pressures on the POSS's solubility. The cloud point pressures of POSS-CO_2 binary systems at 318 and 328 K, the corresponding CO_2 densities, and POSS's weight and mol fractions are given in Table 4.3.

Table 4.3. The cloud point pressures of OIPOSS-CO_2 binary system at 318 K, and 328 K, and the corresponding carbon dioxide densities.

OIPOSS weight fraction	**OIPOSS mol fraction**	**P_{cloud} (MPa)**	**CO_2 Density (g/cm^3)**
318 K			
0.0016	0.00008	11.41	0.629
0.0022	0.00011	11.69	0.643
0.0029	0.00015	12.31	0.670
0.0036	0.00018	13.29	0.702
0.0043	0.00022	13.83	0.716
0.0050	0.00025	13.94	0.719
0.0058	0.00029	14.31	0.728
328 K			
0.0015	0.00007	12.54	0.543
0.0021	0.00011	13.53	0.598
0.0028	0.00014	14.02	0.619
0.0036	0.00018	14.65	0.642
0.0043	0.00022	15.64	0.672
0.0050	0.00025	16.47	0.692

0.0058	0.00029	16.81	0.700

Figure 4.9 shows the solubility of octaisobutyl POSS in supercritical CO_2 at 318 and 328 K are plotted as mol. fr against dew-point pressures. The curves represent the solid–vapor phase equilibrium isotherms. At isothermal conditions, solubility increases with pressure, while at isobaric conditions solubility decreases with temperature decrease due to the density decrease of CO_2.

Trifluoropropyl POSS solubility at 14 MPa and 318 K was 0.04 while this value is 0.005 wt. fr. for octaisobutyl POSS. In other words, trifluoropropyl POSS has 8 folds solubility by weight than octaisobutyl POSS at 318K. On the other and, at 328 K trifluoropropyl POSS solubility at 14 MPa is 0.006 wt. fr. while it is 0.003 wt. fr. is for octaisobutyl POSS, which is 2 folds solubility by weight than octaisobutly POSS. Therefore, the temperature effect on the solubility in trifluoropropyl POSS is more pronounced.

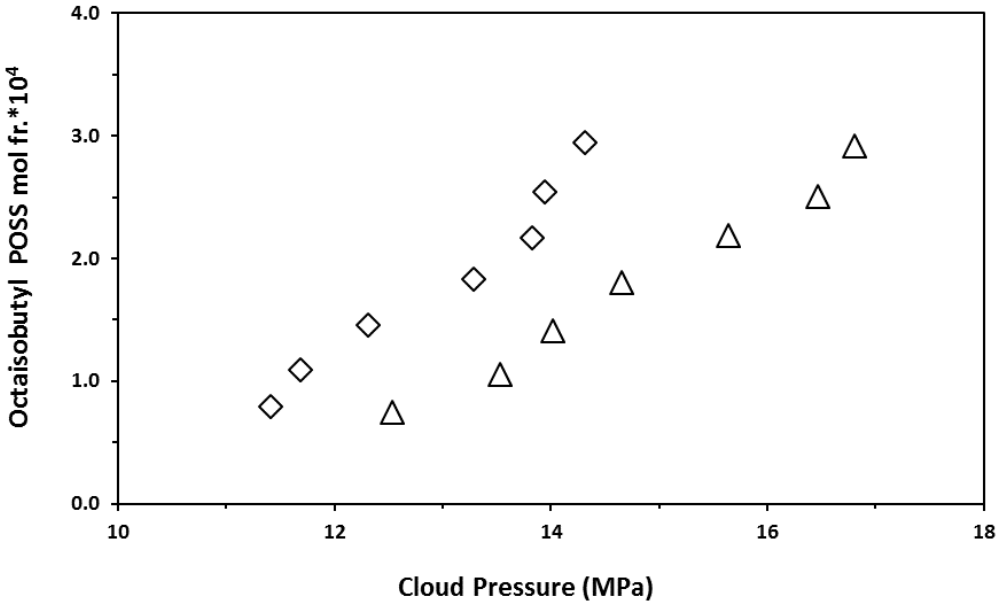

Figure 4.9. Cloud point isotherms of the octaisobutyl POSS–CO_2 binary system; 318 K (◊), and 328 K (Δ). The estimated error bars are comparable to the size of the symbols.

4.4. L-V Equilibria of Methacryl POSS-CO_2 Binary System

Methacryl POSS solubility in supercritical carbon dioxide was studied at 308K and 323 K up to 30 MPa [3]. In this study the solubility of methacryl POSS in supercritical carbon dioxide was carried out at 318 K and 328 K up to 30 MPa to observe the effects of different temperatures and pressures on the POSS's solubility. The dew point pressures of POSS-CO_2 binary systems at 318 and 328 K, the corresponding CO_2 densities, and POSS's weight and mol fractions are given in Table 4.4.

Table 4.4. The dew point pressures of MPOSS-CO_2 binary system at 318 K, and 328 K, and the corresponding carbon dioxide densities.

MPOSS weight fraction	**MPOSS mol fraction**	**P_{dew} (MPa)**	**CO_2 Density (g/cm^3)**
318 K			
0.0005	0.00002	16.00	0.760
0.0010	0.00003	18.31	0.793
0.0016	0.00005	19.81	0.811
0.0021	0.00006	21.22	0.825
0.0026	0.00008	22.91	0.840
0.0031	0.00010	25.94	0.864
0.0037	0.00012	28.52	0.881
0.0040	0.00012	29.11	0.885
328 K			
0.0006	0.00002	19.42	0.746
0.0009	0.00003	21.67	0.776
0.0013	0.00004	22.68	0.788
0.0019	0.00006	23.48	0.796
0.0025	0.00008	25.30	0.813
0.0031	0.00010	26.87	0.827
0.0039	0.00012	29.55	0.847
0.0041	0.00013	30.32	0.852

In Figure 4.10, the solubility of methacryl POSS in $scCO_2$ at 318 and 328 K are plotted as mol. fr versus dew-point pressures, representing the liquid–vapor phase equilibrium curves up-to 30 MPa. When the pressure increases at constant temperature, the density of CO_2 increases, and so the solubility of methacryl POSS

in $scCO_2$ also increases. On the other hand, when the pressure is kept constant and temperature increases, due to the reduction of solvent power, the solubility of methacryl POSS decreases. At the higher pressure region, about 30 MPa, two isotherms converge with each other. On the other hand, at lower pressure region, both isotherms are clearly separated. This shows that at the lower pressure region, with isobaric temperature increment, the decreasing CO_2 density is the dominant factor on the phase behavior of the system, compared to the increasing POSS vapor pressure. In contrast, at the higher-pressure region, the 328 K solubility isotherm approached to the 318 K isotherm, indicating that the increase in the POSS vapor pressure with increasing temperature and the decreasing CO_2 density have comparable effects on the solubility of POSS in $scCO_2$.

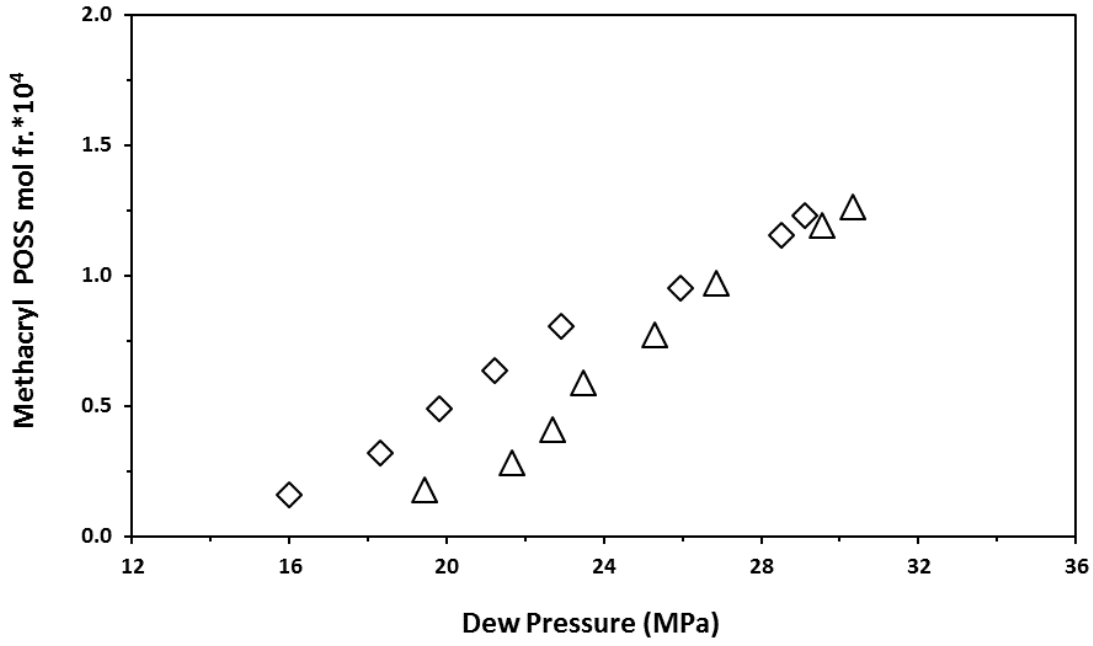

Figure 4.10. Dew point isotherms of the methacryl POSS–CO_2 binary system; 318 K (◊), and 328 K (Δ). The estimated error bars are comparable to the size of the symbols.

4.5. L-V Equilibria of Isooctyl POSS-CO_2 Binary System

Isooctyl POSS solubility in supercritical carbon dioxide was studied at 308K and 323 K up to 20 MPa [3]. In this study the solubility of isooctyl POSS in supercritical carbon dioxide was studied at 318 K and 328 K up to 22 MPa to see the effects of different temperatures and pressures on the POSS's solubility. The dew point pressures of POSS-CO_2 binary systems at 318 and 328 K, the corresponding CO_2 densities, and POSS's weight and mol fractions are given in Table 4.5.

Table 4.5. The dew point pressures of IOPOSS-CO_2 binary system at 318 K, and 328 K, and the corresponding carbon dioxide densities.

IOPOSS weight fraction	**IOPOSS mol fraction**	**P_{dew} (MPa)**	**CO_2 Density (g/cm^3)**
318 K			
0.0049	0.00016	14.69	0.736
0.0092	0.00031	16.55	0.769
0.0136	0.00046	17.51	0.783
0.0170	0.00058	18.34	0.794
0.0210	0.00071	19.53	0.808
0.0248	0.00084	20.33	0.816
328 K			
0.0067	0.00023	18.09	0.725
0.0089	0.00030	18.69	0.735
0.0135	0.00046	19.80	0.752
0.0179	0.00061	20.93	0.767
0.0216	0.00073	21.54	0.775
0.0244	0.00083	22.28	0.783

In Figure 4.11, the solubility of isooctyl POSS in $scCO_2$ at 318 and 328 K are plotted as mol. fr against dew-point pressures, which represent the liquid–vapor phase equilibrium up to 20 MPa. At constant temperature, the isooctyl POSS solubility in $scCO_2$ increases with pressure and at constant pressure, solubility decreases with temperature similar to the previously explained POSS types. When the solubility of isooctyl POSS in $scCO_2$ is compared with that of methacryl POSS at the 22 MPa and 328 K, it is observed that the solubility of isooctyl POSS is about twenty folds (wt. fr.) greater than that of the methacryl POSS. When all the POSS types are compared at the same temperature and pressure conditions, octatrimethly siloxy POSS is found to exhibit the highest solubility in $scCO_2$ while methacryl POSS is at the least soluble one.

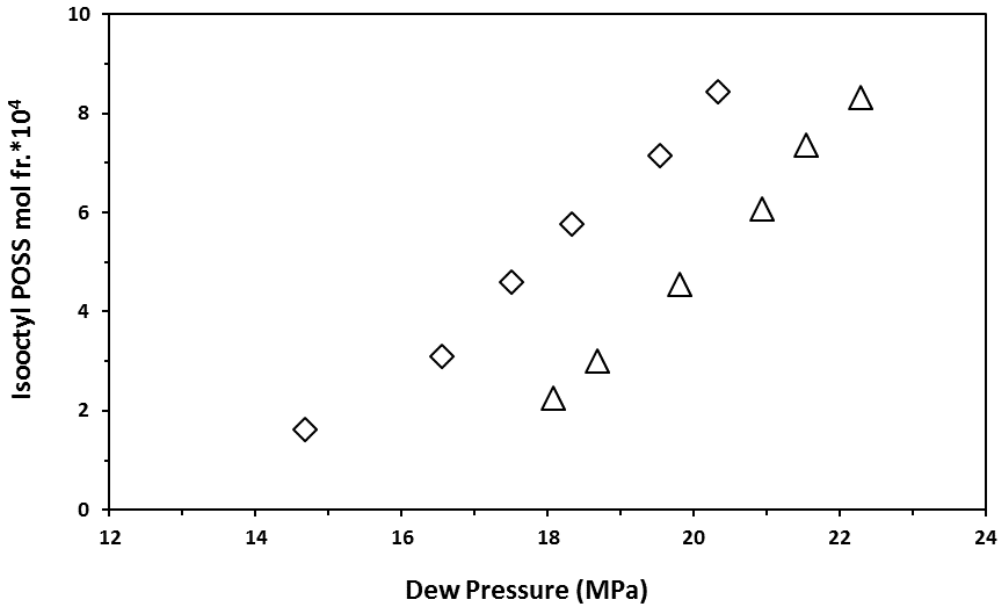

Figure 4.11. Dew point isotherms of the isooctyl POSS–CO_2 binary system; 318 K (◊), and 328 K (Δ). The estimated error bars are comparable to the size of the symbols.

4.6. Effects of Temperature and Pressure on CO_2 Density at Phase Separation

The solubility isotherms of SPOSS plotted against the CO_2 density at the cloud points of the binary system are given in Figure 4.12. The significance of the positive effect of temperature on the solubility of SPOSS in $scCO_2$ is observed at SPOSS concentrations greater than around 2×10^{-3} mol fr. A 20 K increase in the temperature from 308 K to 328 K leads to an increase in the solubility of SPOSS up to about 3.5 folds (wt. fr.) measured at a constant CO_2 density of 0.59 g/cm^3. Increased solubility of the solute with increasing temperature at constant solvent density is associated with the chemical potential of SPOSS and thus its increasing vapor pressure. The solubility increase with CO_2 density becomes more profound at higher temperatures. Increasing the CO_2 density from 0.53 g/cm^3 to 0.59 g/cm^3 at 323 K results in an increase in the solubility of about 4.6×10^{-3} mol fr., while at 308 K the same density increases results in only about $0.6\text{x}10^{-3}$ mol fr.

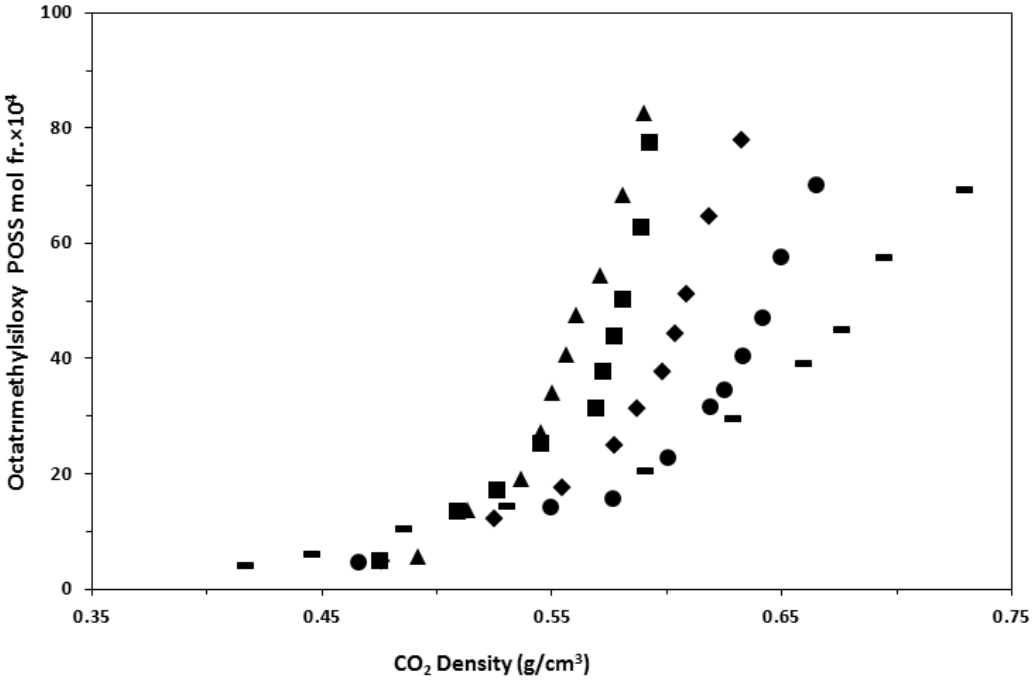

Figure 4.12. Solubility of octatrimethylsiloxy POSS in $scCO_2$ plotted against CO_2 densities at the cloud points of the binary system at (-) 308 K, (●) 313 K, (♦) 318 K, (■) 323 K and (▲) 328 K.

In Figure 4.13, the solubility mole fr. of octaisobutyl POSS versus the CO_2 density at the cloud points of the binary system were plotted. With 10 K temperature increase, from 318 K to 328 K, octaisobutyl POSS solubility increased approximately 1.6 folds (wt. fr.) measured at a constant CO_2 density of 0.70 g/cm^3. At constant solvent density, temperature increase causes an increase in the vapor pressure of the solute, leading to an increase in its solubility.

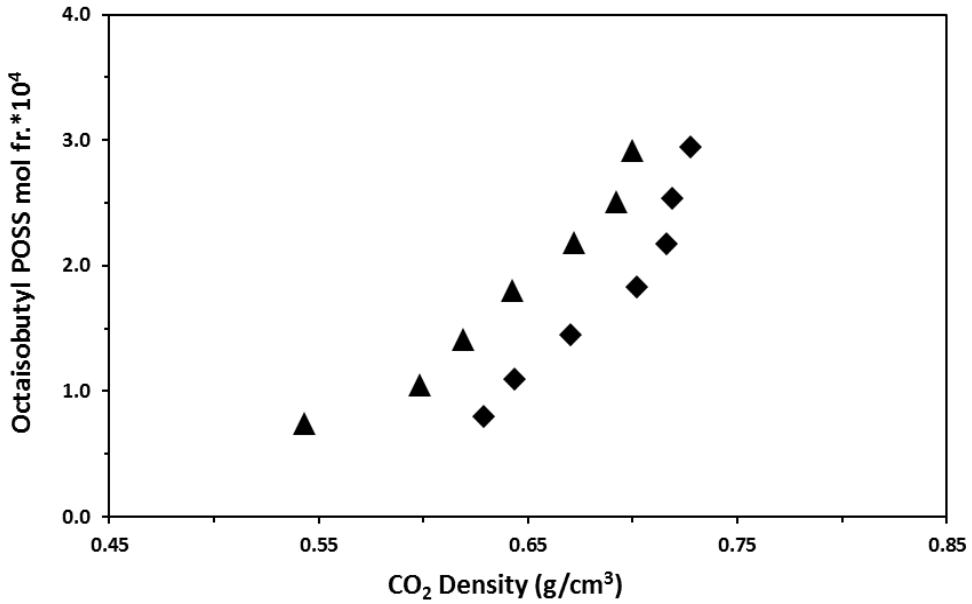

Figure 4.13. Solubility of octaisobutyl POSS in $scCO_2$ plotted against CO_2 densities at the cloud points of the binary system at (♦) 318 K and (▲) 328 K.

In Figure 4.14, solubility mole fraction of trifluoropropyl POSS is plotted against the CO_2 density at the cloud points of the binary system. At a constant CO_2 density of 0.72 g/cm^3, TFPOSS solubility increased approximately 1.3 folds (wt. fr.) with 10 K temperature increase, from 318 K to 328 K. At constant solvent density, corresponding to constant solvent power, the increase in solubility with increasing temperature is attributed to the increasing vapor pressure of the solute similar to the previously explained systems.

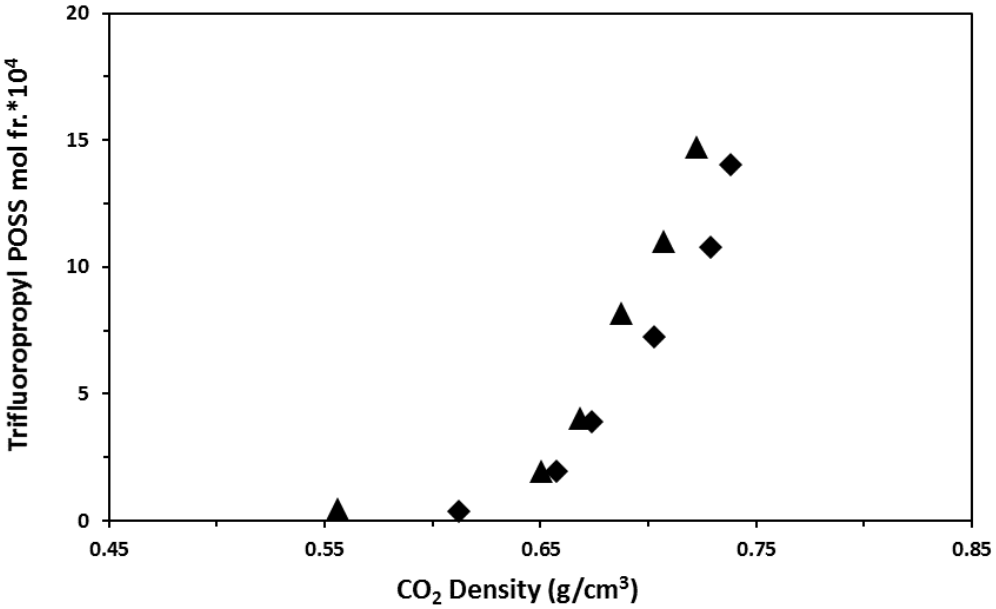

Figure 4.14. Solubility of trifluoropropyl POSS in $scCO_2$ plotted against CO_2 densities at the cloud points of the binary system at (♦) 318 K and (▲) 328 K.

In Figure 4.15, solubility mole fraction of methacryl POSS versus the CO_2 density at the cloud points of the binary system were plotted. Methacryl POSS solubility increased approximately 1.5 folds (wt. fr.) measured at a constant CO_2 density of 0.85 g/cm^3 with 10 K temperature increase, from 318 K to 328 K. At constant solvent density, the temperature increase leading to the solute's vapor pressure increase is the reason to the increase in the solubility of POSS, as explained earlier.

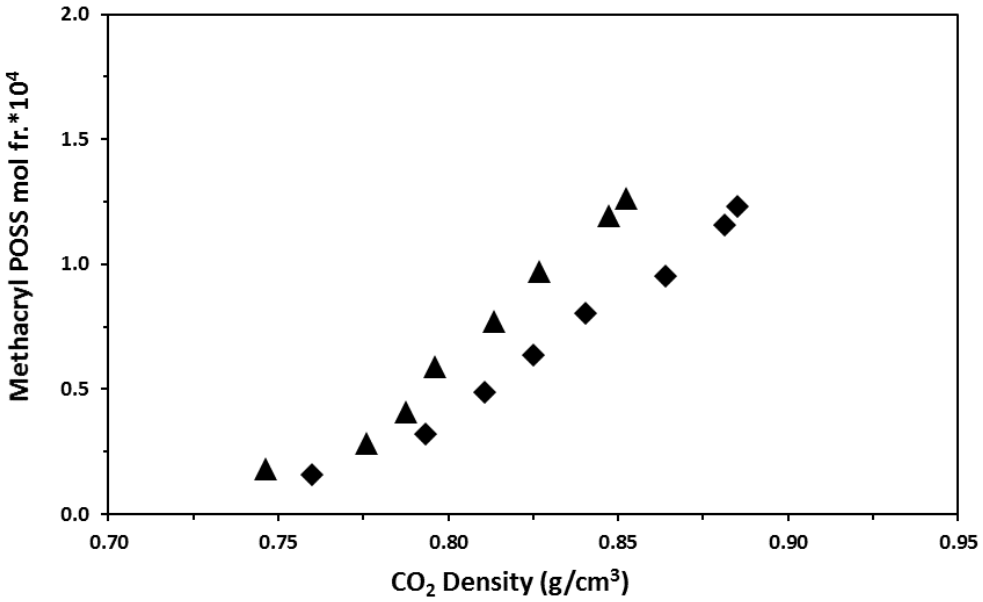

Figure 4.15. Solubility of methacryl POSS in $scCO_2$ plotted against CO_2 densities at the cloud points of the binary system at (♦) 318 K and (▲) 328 K.

In Figure 4.16, the solubility mole fraction of isooctyl POSS versus the CO_2 density at the cloud points of the binary system were plotted. Isooctyl POSS solubility increased approximately 1.8 folds (wt. fr.) with 10 K temperature increase, from 318 K to 328 K, at a constant CO_2 density of 0.78 g/cm^3. At constant solvent density, similar to the above systems, the increase in solubility of POSS with increasing temperature can be attributed to its increasing vapor pressure. Comparing the all types of POSS, the increase in the solubility due to temperature increase is most pronounced in SPOSS-CO_2 systems corresponding to an about 10 wt. % increase with 10 K increase from 318K to 328 K.

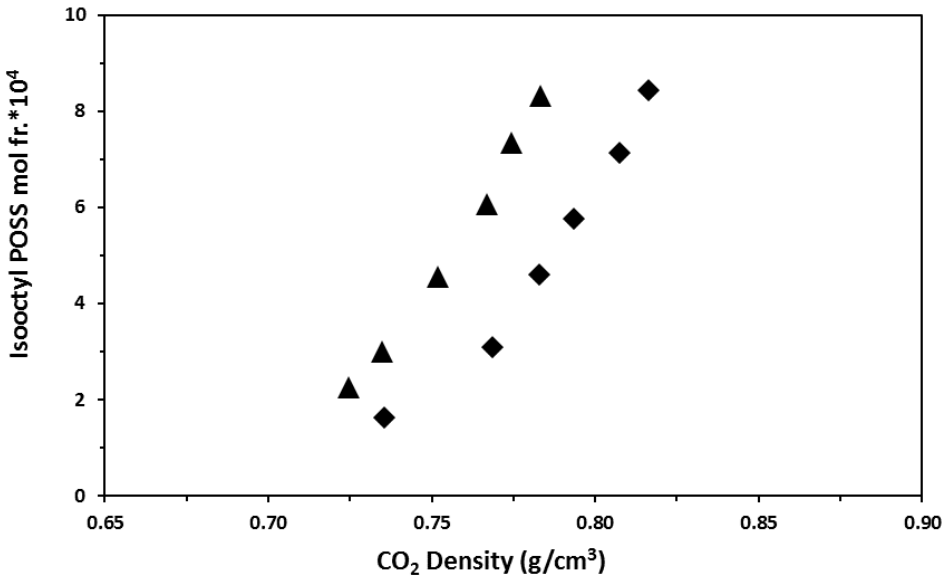

Figure 4.16. Solubility of isooctyl POSS in $scCO_2$ plotted against CO_2 densities at the cloud points of the binary system at (♦) 318 K and (▲) 328 K.

In Figures 4.17 and Figure 4.18, which represent the temperatures 308K and 323 K, respectively, the solubility isotherms of the previously studied $scCO_2$-soluble POSSs which are trifluoropropyl POSS, isooctyl POSS, octaisobutyl POSS, methacryl POSS [2,3], along with SPOSS versus the CO_2 density at the cloud or dew points of the binary systems were plotted. Among all the POSSs, SPOSS exhibits the highest solubility. Although silicones are less CO_2-philic compared to the fluorinated counterparts [51], here it is found that the trimethylsiloxane groups lead to more soluble SPOSS compared to the fluoroalkyl functionalized POSS. At 308 K and about 0.69 g/cm^3 CO_2 density, the solubility of SPOSS is 0.58×10^{-2} mol fr. while that of trifluoropropyl POSS is 0.93×10^{-3}. The lower solubility of the fluorinated alkyl-functionalized counterpart might be because of the longer alkyl chains of the fluorinated POSS.

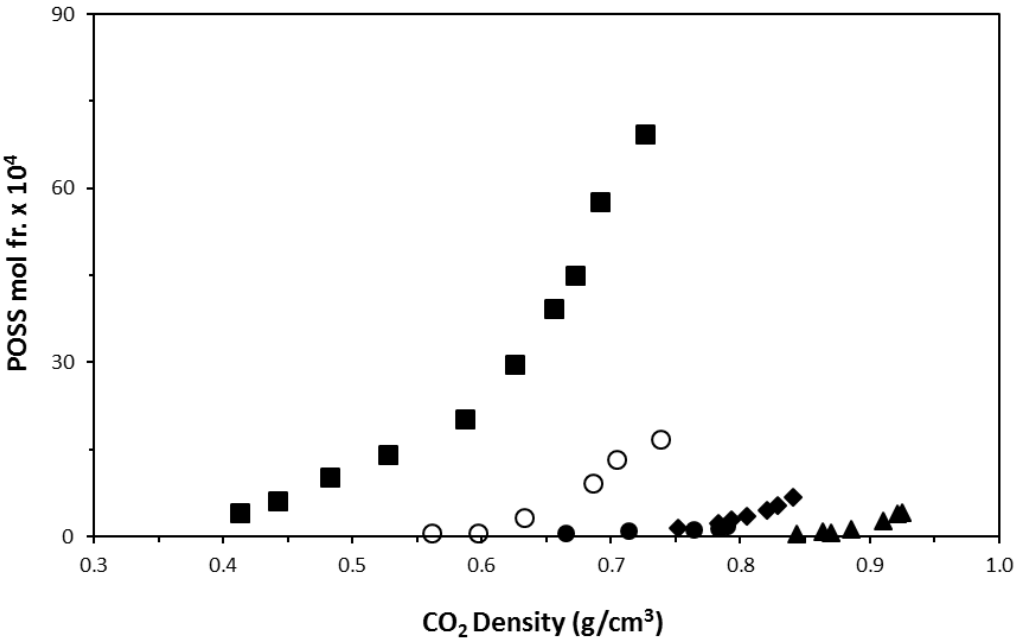

Figure 4.17. Solubility of POSS with various functional groups in $scCO_2$ plotted against the CO_2 densities at the cloud or dew points at 308 K; (■) octatrimethylsiloxy POSS-CO_2, (○) trifluoropropyl POSS-CO_2 [2] (●) octaisobutyl POSS-CO_2 [3], (♦) isooctyl POSS-CO_2 [3] (▲) methacryl POSS-CO_2 [3].

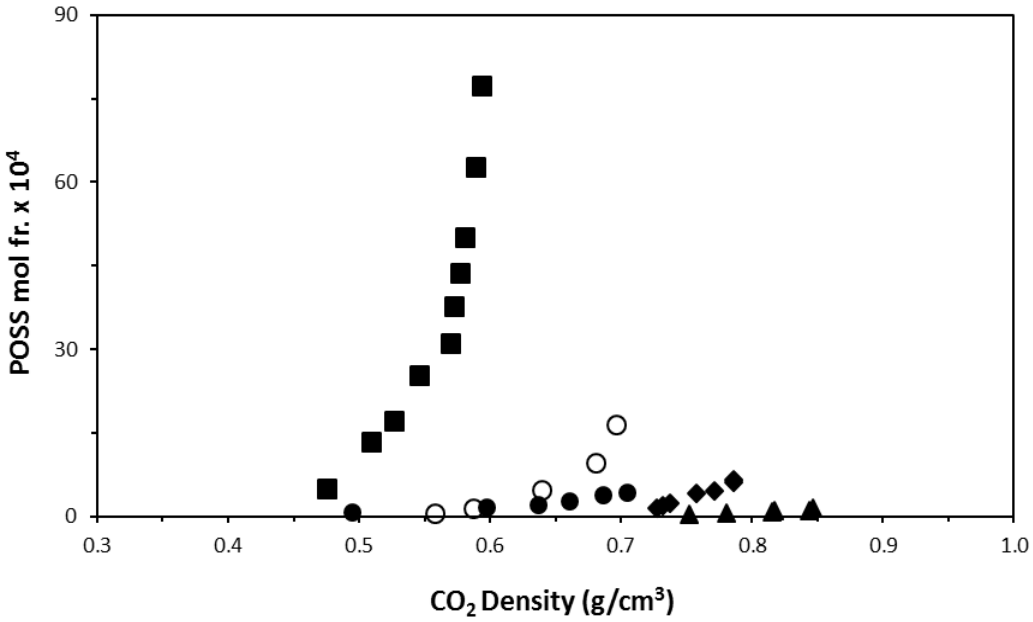

Figure 4.18. Solubility of POSS with various functional groups in $scCO_2$ plotted against the CO_2 densities at the cloud or dew points at 323 K; (■) octatrimethylsiloxy POSS-CO_2, (○) trifluoropropyl POSS-CO_2 [2] (●) octaisobutyl POSS-CO_2 [3], (♦) isooctyl POSS-CO_2 [3] (▲) methacryl POSS-CO_2 [3].

Solubility isotherms of trifluoropropyl, isooctyl, octaisobutyl, methacryl and octatrimethlysiloxy POSS in supercritical carbon dioxide are plotted against the CO_2 density at the cloud or dew points of the binary systems at 318 K and 328 K, Figure 4.19 and 4.20, respectively. Like Figure 4.17 and 4.18, octatrimethlysiloxy POSS exhibits the highest solubility among all POSSs at these temperatures. In order to exhibit the same solubility, octatrimethlysiloxy POSS requires the lowest solvation power or solvent density while methacryl POSS requires the highest solvation power, in other words density of $scCO_2$.

At 318K and 14 MPa, trifluoropropyl POSS, octaisobutyl POSS and isooctyl POSS solubilities are 10.8×10^{-4}, 2.9×10^{-4}, 1.6×10^{-4} mol fr., respectively, while the highest

solubility of methacryl POSS is only 1.2 × 10^{-4} mol fr. at 29 MPa. Octatrimethlysiloxy POSS has the highest solubility among all the POSS types also at this temperature as expected from the 308 and 323 K studies. Its solubility at 318 K is 78×10^{-4} mole fr. at 318 K just at 11MPa. This trend continues also at 328 K, octatrimethlysiloxy POSS has the highest solubility, while methacryl POSS is the least soluble POSS. In order to reach a solubility of about 3 × 10^{-4} by mole, the system pressure is required to be around 11, 15, 17 and 19 MPa for octatrimethlysiloxy, trifluoroproyl, octaisobutyl and isooctyl POSS respectively, while even up to 30 MPa, methacryl POSS cannot reach this level of solubility.

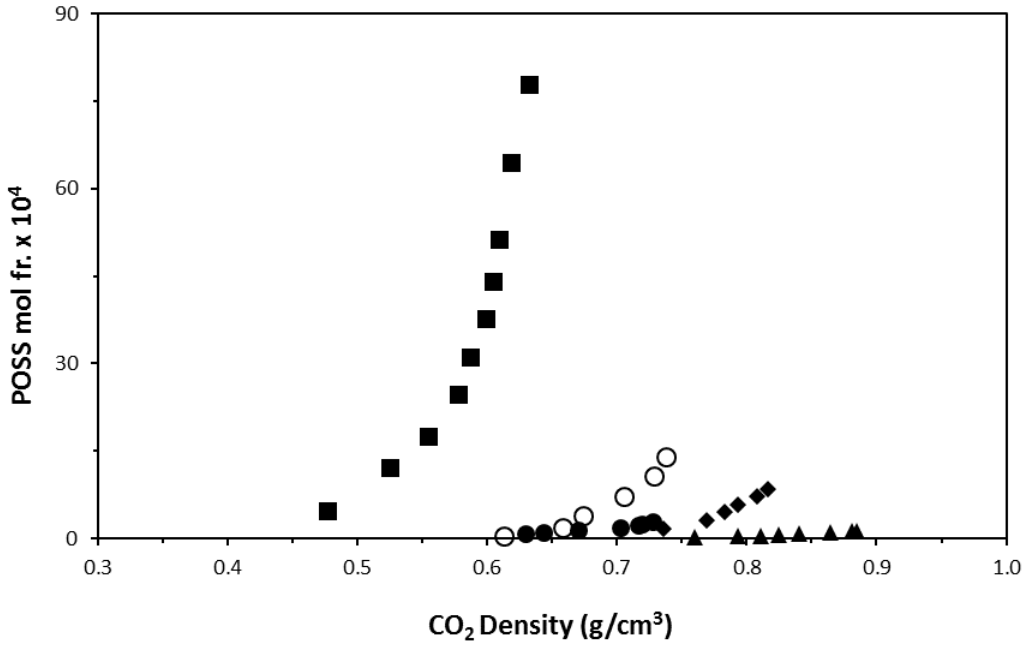

Figure 4.19. Solubility of POSS with various functional groups in $scCO_2$ plotted against the CO_2 densities at the cloud or dew points at 318 K; (■) octatrimethylsiloxy POSS-CO_2, (○) trifluoropropyl POSS-CO_2, (●) octaisobutyl POSS-CO_2, (♦) isooctyl POSS-CO_2, (▲) methacryl POSS-CO_2.

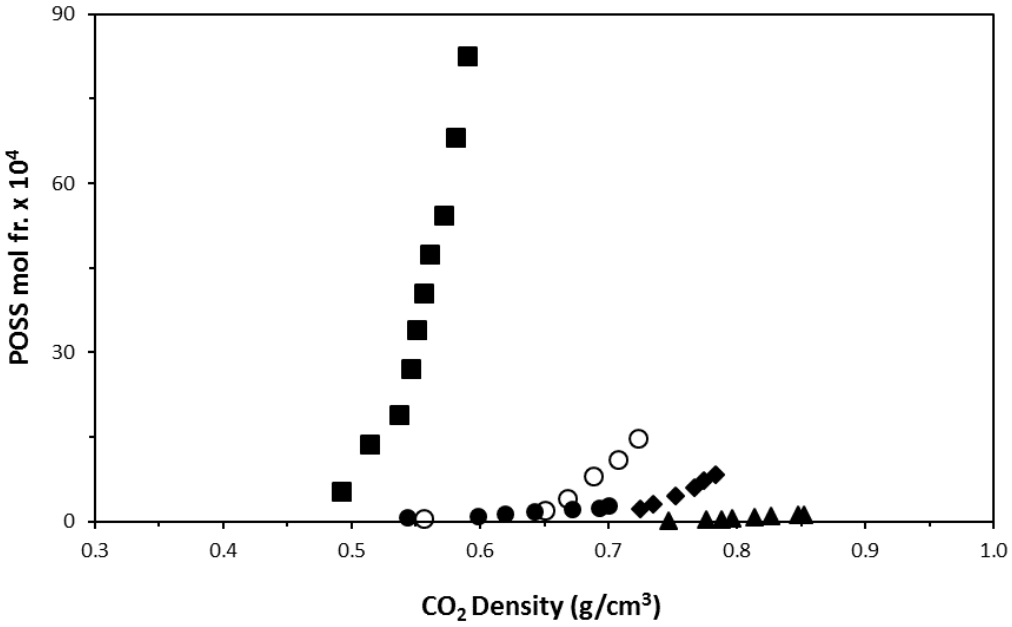

Figure 4.20. Solubility of POSS with various functional groups in $scCO_2$ plotted against the CO_2 densities at the cloud or dew points at 328 K; (■) octatrimethylsiloxy POSS-CO_2, (○) trifluoropropyl POSS-CO_2, (●) octaisobutyl POSS-CO_2, (♦) isooctyl POSS-CO_2, (▲) methacryl POSS-CO_2.

Solubility isotherms of trifluoropropyl, isooctyl, octaisobutyl, methacryl and octatrimethlysiloxy POSS in supercritical carbon dioxide are plotted as mol. fr. against cloud or dew point pressures at 308 K, 318 K, 323K and 328 K, in Figure 4.21, 4.22, 4.23 and 4.24, respectively. Like Figure 4.17, 4.18, 4.19 and 4.20 octatrimethlysiloxy POSS exhibits the highest solubility among all POSSs at these temperatures.

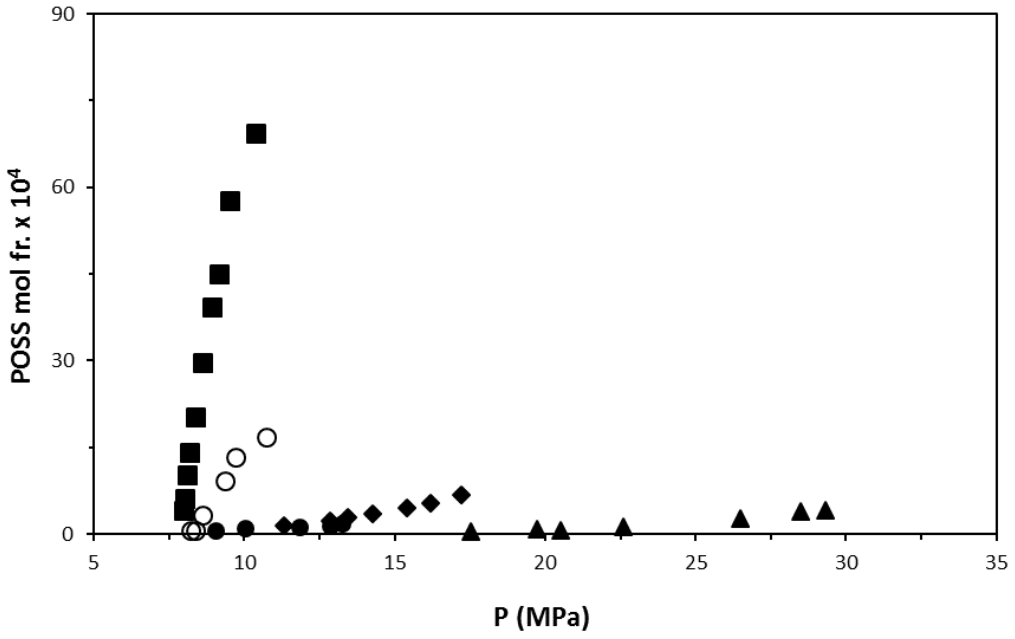

Figure 4.21. Solubility of POSS with various functional groups in $scCO_2$ plotted against the cloud or dew point pressures at 308 K; (■) octatrimethylsiloxy POSS-CO_2, (○) trifluoropropyl POSS-CO_2 [2] (●) octaisobutyl POSS-CO_2 [3], (♦) isooctyl POSS-CO_2 [3] (▲) methacryl POSS-CO_2 [3].

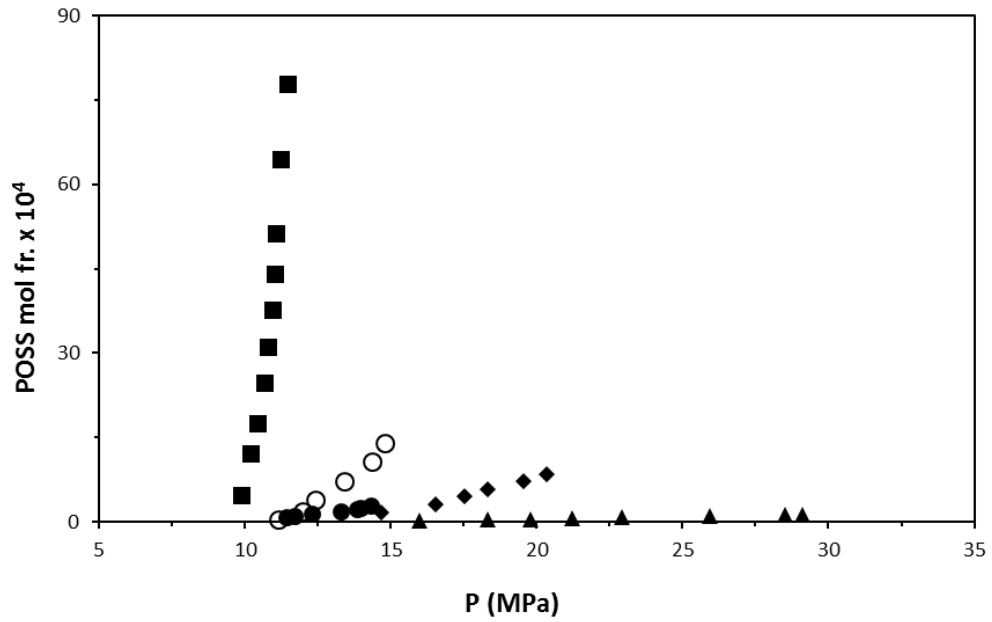

Figure 4.22. Solubility of POSS with various functional groups in $scCO_2$ plotted against the cloud or dew point pressures at 318 K; (■) octatrimethylsiloxy POSS-CO_2, (○) trifluoropropyl POSS-CO_2 (●) octaisobutyl POSS-CO_2, (♦) isooctyl POSS-CO_2 (▲) methacryl POSS-CO_2.

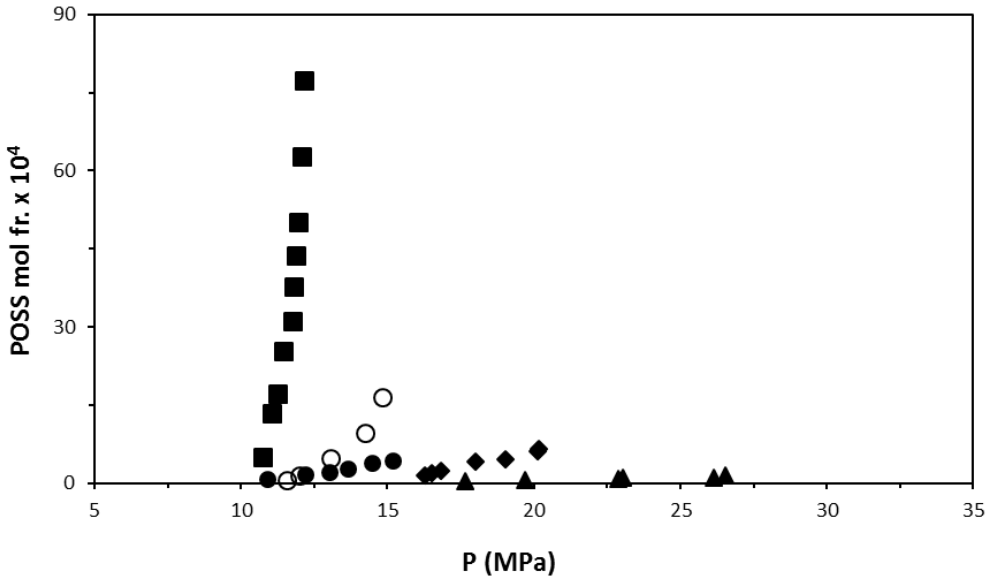

Figure 4.23. Solubility of POSS with various functional groups in $scCO_2$ plotted against the cloud or dew point pressures at 323 K; (■) octatrimethylsiloxy POSS-CO_2, (○) trifluoropropyl POSS-CO_2 [2] (●) octaisobutyl POSS-CO_2 [3], (♦) isooctyl POSS-CO_2 [3] (▲) methacryl POSS [3].

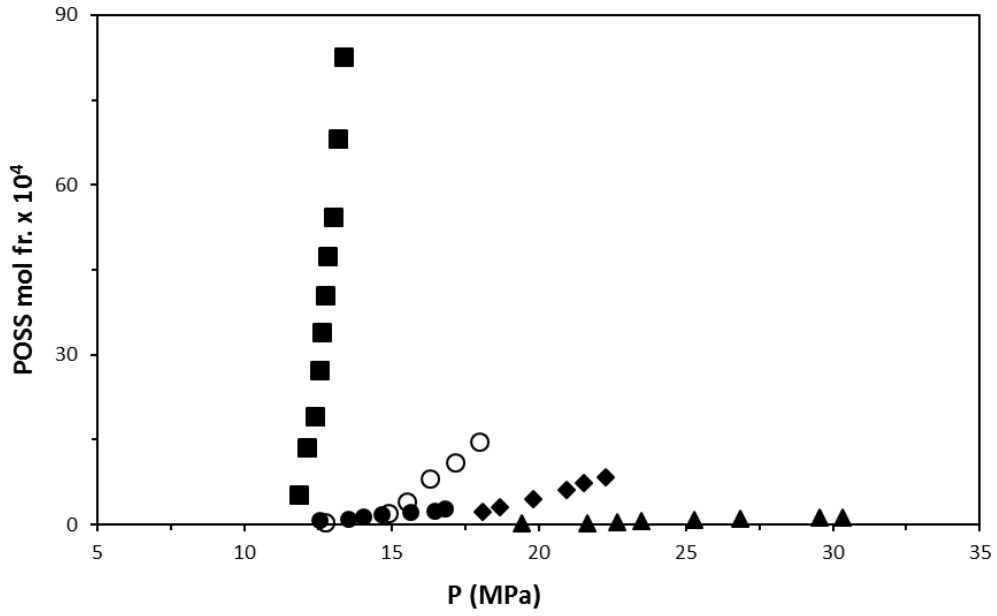

Figure 4.24. Solubility of POSS with various functional groups in $scCO_2$ plotted against the cloud or dew point pressures at 328 K; (■) octatrimethylsiloxy POSS-CO_2, (○) trifluoropropyl POSS-CO_2 (●) octaisobutyl POSS-CO_2, (♦) isooctyl POSS-CO_2 (▲) methacryl POSS-CO_2.

4.7. Modeling of Solubility

4.7.1. Octatrimethyl Siloxy POSS Solubility Modelling

The solubility data of octatrimethlysiloxy POSS in $scCO_2$ at 308,313,318,323 and 328 K have been correlated by various density-based semi-empirical models which are Chrastil [43], Chrastil modified by Wang (C-W) [38], del Valle and Aguilerra (d-A) [44], Kumar and Johnston (K-J) [45], Mendez-Santiago and Teja (MST) [46] ,and Bartle models [47]. The solubility values obtained with the correlations are listed in Table 4.6. The calculated and experimental mole fractions plotted against the experimental solvent density data at each temperature are given in Figure 4.25.

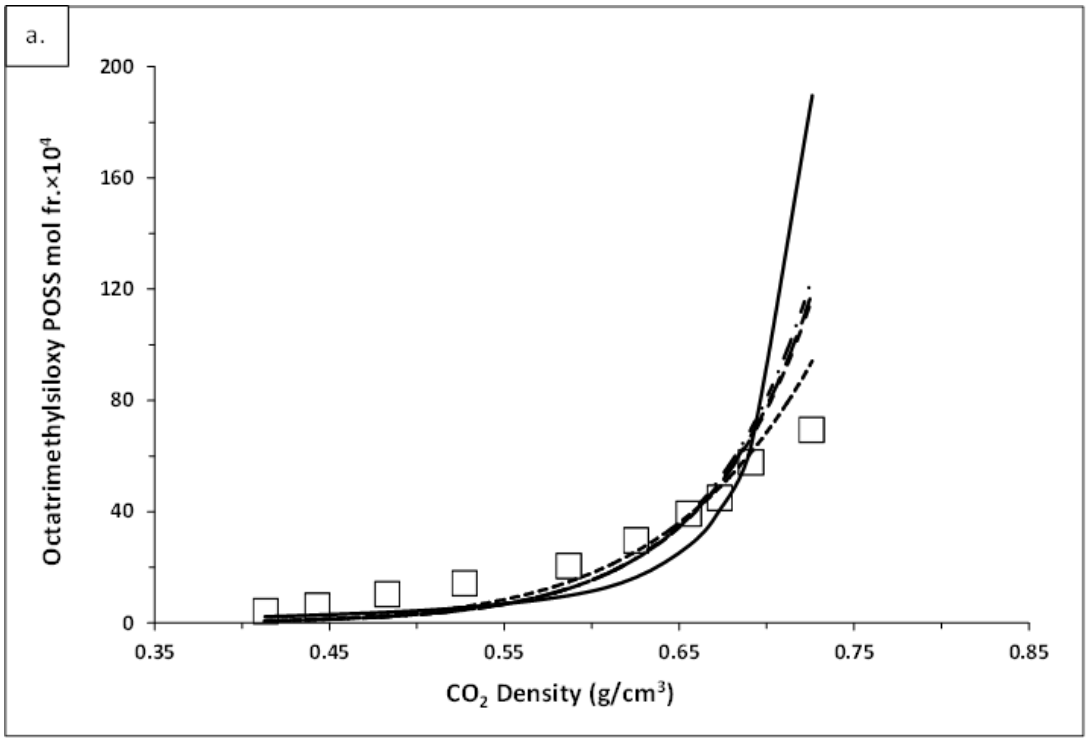
a.
Octatrimethylsiloxy POSS mol fr.×10⁴
200
160
120
80
40
0
0.35
0.45
0.55
0.65
0.75
0.85
CO2 Density (g/cm3)

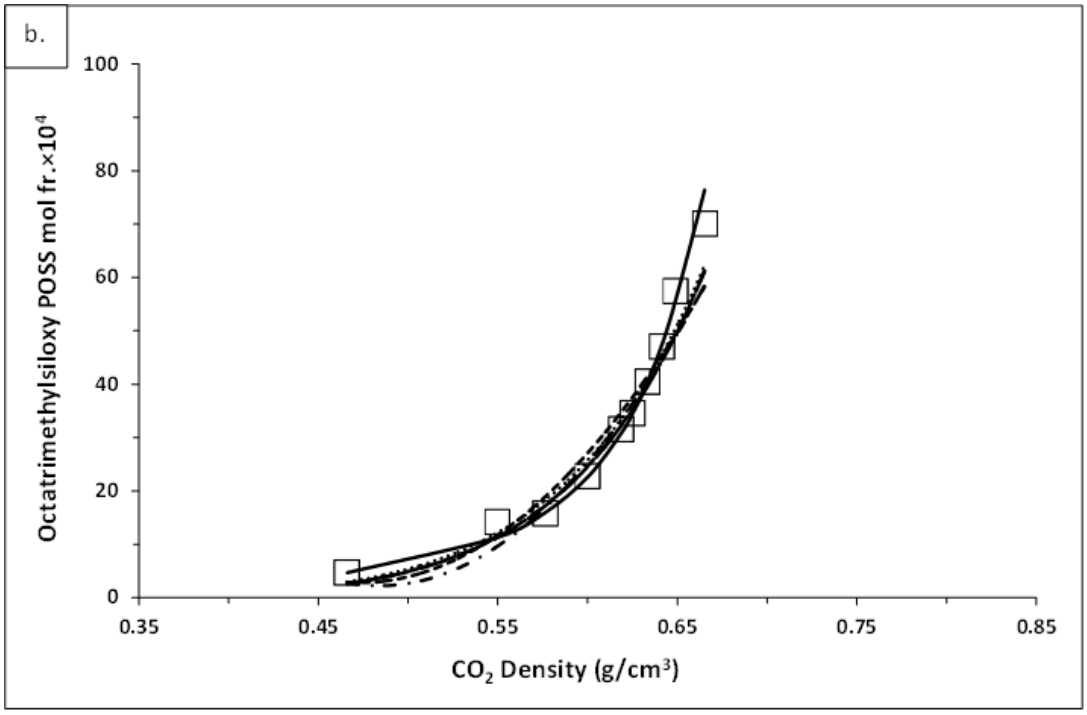
b.
Octatrimethylsiloxy POSS mol fr.×10⁴
100
80
60
40
20
0
0.35
0.45
0.55
0.65
0.75
0.85
CO2 Density (g/cm3)

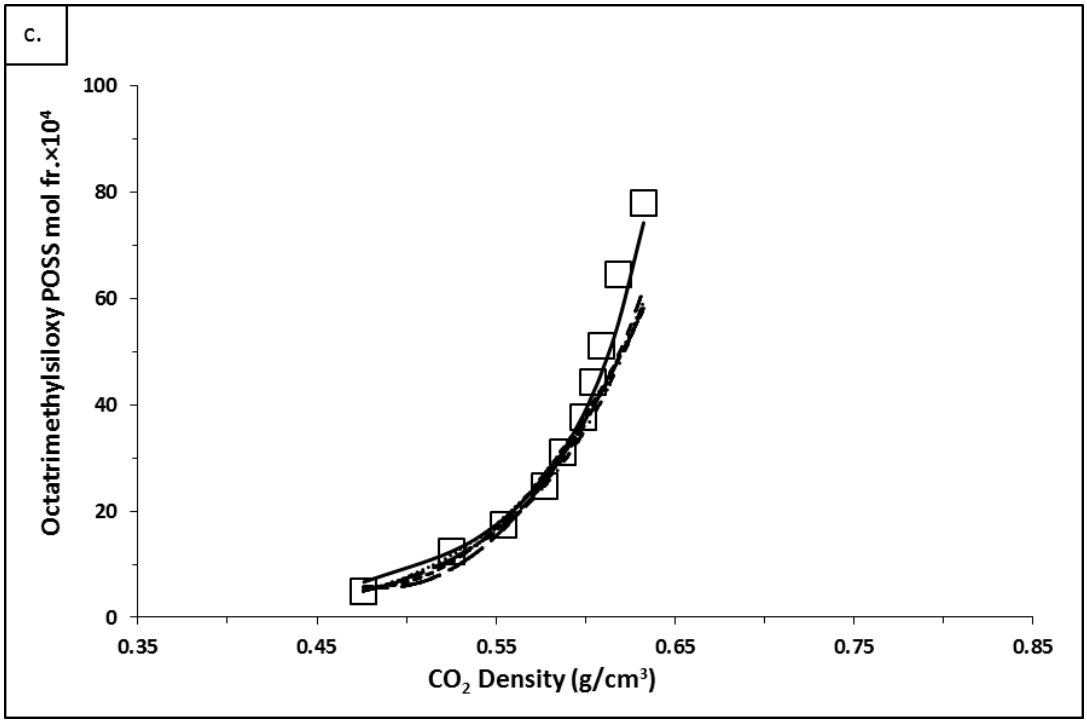
c.
Octatrimethylsiloxy POSS mol fr.×10⁴
100
80
60
40
20
0
0.35
0.45
0.55
0.65
0.75
0.85
CO2 Density (g/cm3)

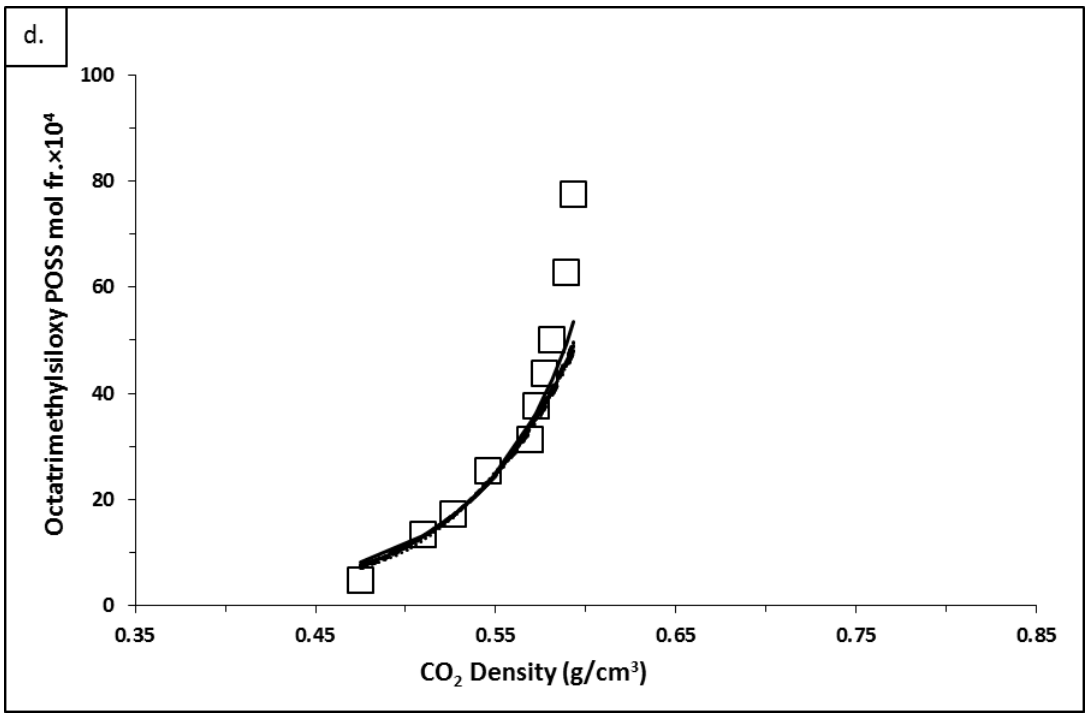
d.
Octatrimethylsiloxy POSS mol fr.×10⁴
100
80
60
40
20
0
0.35
0.45
0.55
0.65
0.75
0.85
CO2 Density (g/cm3)

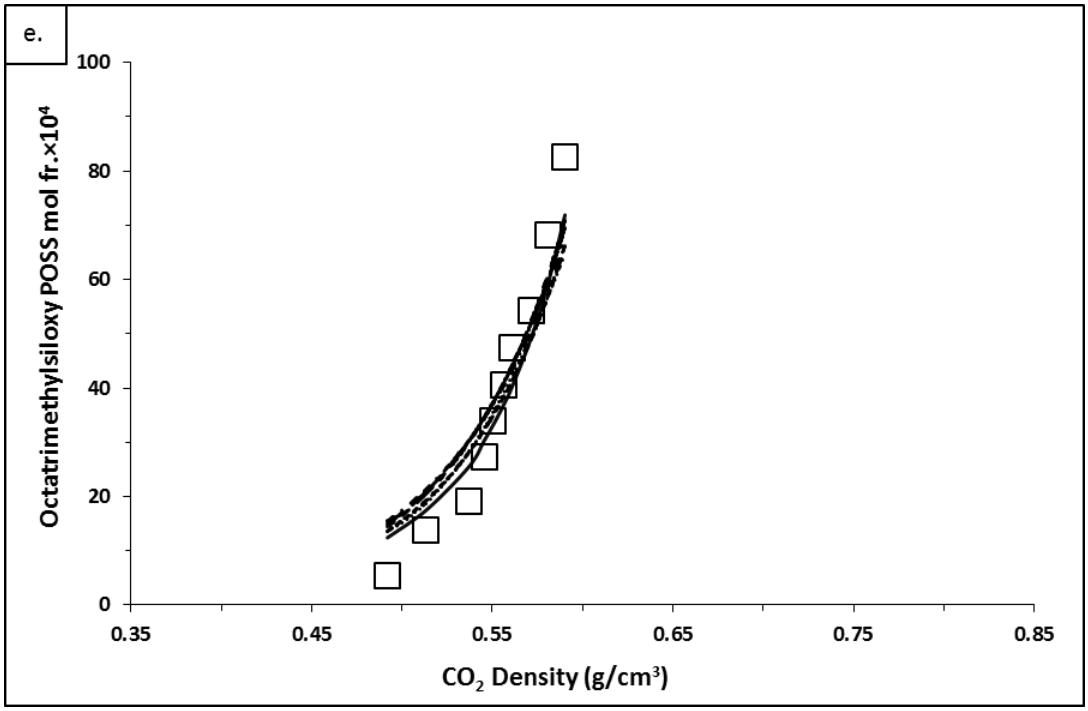

Figure 4.25. The density based correlations, (——) C-W, (·····) Chrastil, (– – –) D-A, (- - -) K-J, (– · –) MST, (— —) Bartle, and the experimental solubility data of SPOSS in $scCO_2$ (□) plotted against the CO_2 densities at the cloud points at a) 308 K, b) 313K, c) 318 K, d) 323 K, and e) 328 K.

Table 4.6. The estimated solubility mol fractions of SPOSS-CO_2 binary systems.

308 K						
Octatrimethylsiloxy POSS Mole Fractions						
Experimental	**Chrastil**	**C-W**	**d-A**	**K-J**	**MST**	**Bartle**
0.0004	0.0001	0.0002	0.0001	0.0001	0.0001	0.0001
0.0006	0.0001	0.0003	0.0001	0.0001	0.0001	0.0001
0.0010	0.0003	0.0004	0.0003	0.0002	0.0002	0.0002
0.0014	0.0006	0.0006	0.0006	0.0005	0.0005	0.0005
0.0020	0.0015	0.001	0.0015	0.0013	0.0013	0.0013

0.0030	0.0026	0.0016	0.0026	0.0023	0.0024	0.0024
0.0039	0.0039	0.0028	0.0039	0.0038	0.0040	0.0039
0.0045	0.0048	0.0040	0.0049	0.0050	0.0052	0.0051
0.0058	0.0061	0.0064	0.0061	0.0067	0.0069	0.0067
0.0069	0.0094	0.0190	0.0094	0.0117	0.0116	0.0110
313 K						
Octatrimethylsiloxy POSS Mole Fractions						
Experimental	**Chrastil**	**C-W**	**d-A**	**K-J**	**MST**	**Bartle**
0.0005	0.0003	0.0005	0.0003	0.0003	0.0003	0.0003
0.0014	0.0012	0.0011	0.0012	0.0011	0.0011	0.0011
0.0016	0.0018	0.0016	0.0019	0.0016	0.0017	0.0017
0.0023	0.0026	0.0023	0.0026	0.0024	0.0024	0.0024
0.0032	0.0034	0.0031	0.0034	0.0033	0.0033	0.0033
0.0035	0.0037	0.0035	0.0037	0.0036	0.0036	0.0036
0.0040	0.0042	0.0040	0.0042	0.0041	0.0041	0.0041
0.0047	0.0047	0.0048	0.0047	0.0047	0.0047	0.0047
0.0057	0.0052	0.0057	0.0052	0.0053	0.0052	0.0053
0.0070	0.0056	0.0076	0.0056	0.0058	0.0056	0.0056
318 K						
Octatrimethylsiloxy POSS Mole Fractions						
Experimental	**Chrastil**	**C-W**	**d-A**	**K-J**	**MST**	**Bartle**
0.0005	0.0005	0.0007	0.0005	0.0005	0.0005	0.0005
0.0012	0.0012	0.0012	0.0012	0.0011	0.0011	0.0011
0.0017	0.0019	0.0019	0.0019	0.0018	0.0017	0.0018
0.0025	0.0027	0.0027	0.0027	0.0025	0.0025	0.0025
0.0031	0.0031	0.0031	0.0031	0.0030	0.0029	0.0030
0.0038	0.0037	0.0038	0.0037	0.0036	0.0035	0.0035
0.0044	0.0040	0.0042	0.0040	0.0039	0.0038	0.0039
0.0051	0.0043	0.0046	0.0043	0.0042	0.0041	0.0042

0.0065	0.0049	0.0056	0.0049	0.0049	0.0047	0.0048
0.0078	0.0059	0.0074	0.0059	0.0062	0.0059	0.0060
323 K						
Octatrimethylsiloxy POSS Mole Fractions						
Experimental	**Chrastil**	**C-W**	**d-A**	**K-J**	**MST**	**Bartle**
0.0005	0.0007	0.0008	0.0007	0.0007	0.0008	0.0008
0.0013	0.0013	0.0013	0.0013	0.0013	0.0013	0.0013
0.0017	0.0017	0.0017	0.0017	0.0017	0.0017	0.0017
0.0025	0.0023	0.0023	0.0023	0.0023	0.0023	0.0023
0.0031	0.0034	0.0034	0.0034	0.0034	0.0033	0.0034
0.0038	0.0035	0.0036	0.0035	0.0035	0.0035	0.0035
0.0044	0.0038	0.0040	0.0038	0.0039	0.0037	0.0038
0.0050	0.0040	0.0043	0.0040	0.0041	0.0040	0.0040
0.0063	0.0045	0.0049	0.0045	0.0046	0.0044	0.0046
0.0077	0.0048	0.0053	0.0048	0.0050	0.0047	0.0049
328 K						
Octatrimethylsiloxy POSS Mole Fractions						
Experimental	**Chrastil**	**C-W**	**d-A**	**K-J**	**MST**	**Bartle**
0.0005	0.0013	0.0012	0.0013	0.0015	0.0015	0.0015
0.0014	0.0019	0.0018	0.0019	0.0021	0.0021	0.0021
0.0019	0.0029	0.0025	0.0028	0.0030	0.0030	0.0030
0.0027	0.0033	0.0030	0.0033	0.0034	0.0035	0.0035
0.0034	0.0035	0.0033	0.0035	0.0037	0.0037	0.0037
0.0041	0.0039	0.0037	0.0039	0.0041	0.0041	0.0041
0.0048	0.0042	0.0040	0.0042	0.0044	0.0043	0.0044
0.0054	0.0049	0.0049	0.0049	0.0052	0.0051	0.0052
0.0068	0.0057	0.0060	0.0057	0.0061	0.0059	0.0060
0.0083	0.0065	0.0072	0.0065	0.0071	0.0067	0.0069

The empirical parameters of each model are determined with MATLAB where the AARD (absolute average relative deviation) as the objective function was minimized. The parameters obtained in each model with the calculated AARD values are given in Table 4.7. Among all the models C-W model gives the lowest AARD value.

The AARD values of all the correlations, which represent the ability of each model to fit the experimental data, are in the range of 22-25%. This shows that the employed models satisfactorily approximate the trends in the presented data. This is especially evident in the lower concentration region in Figure 4.25.

Table 4.7. The empirical parameters of the density-based models and the AARD (%) values obtained for the SPOSS solubility in $scCO_2$.

Model	***AARD (%)***	***a***	***b***	***c***	***d***
Chrastil	22.54	9.74	-7278.09	-35.38	
C-W	22.16	-98.15	13560.07	0.01	9.90
d-A	22.56	9.71	-7264.36	7984.76	-35.28
K-J	24.08	11.47	-8504.29	0.02	
MST	25.70	-13501.67	5.32	29.19	
Bartle	24.45	33.93	-10545.00	0.02	

4.7.2. Trifluoropropyl POSS Solubility Modelling

The solubility data of trifluoropropyl POSS in $scCO_2$ at 318 and 328 K have been correlated by various density-based semi-empirical models which are Chrastil [43], Chrastil modified by Wang (C-W) [38], del Valle and Aguilerra (d-A) [44], Kumar and Johnston (K-J) [45], Mendez-Santiago and Teja (MST) [46] ,and Bartle models [47].The solubility values obtained with the correlations are listed in Table 4.8. The

calculated and the experimental mole fractions plotted against the experimental solvent density data at each temperature are given in Figure 4.26.

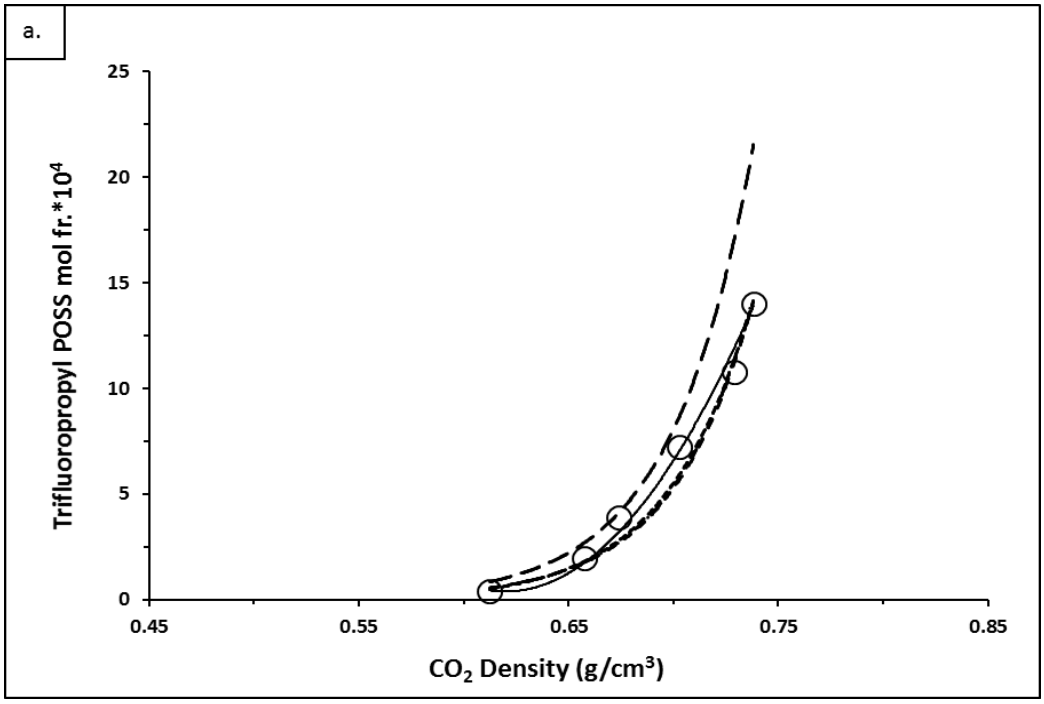

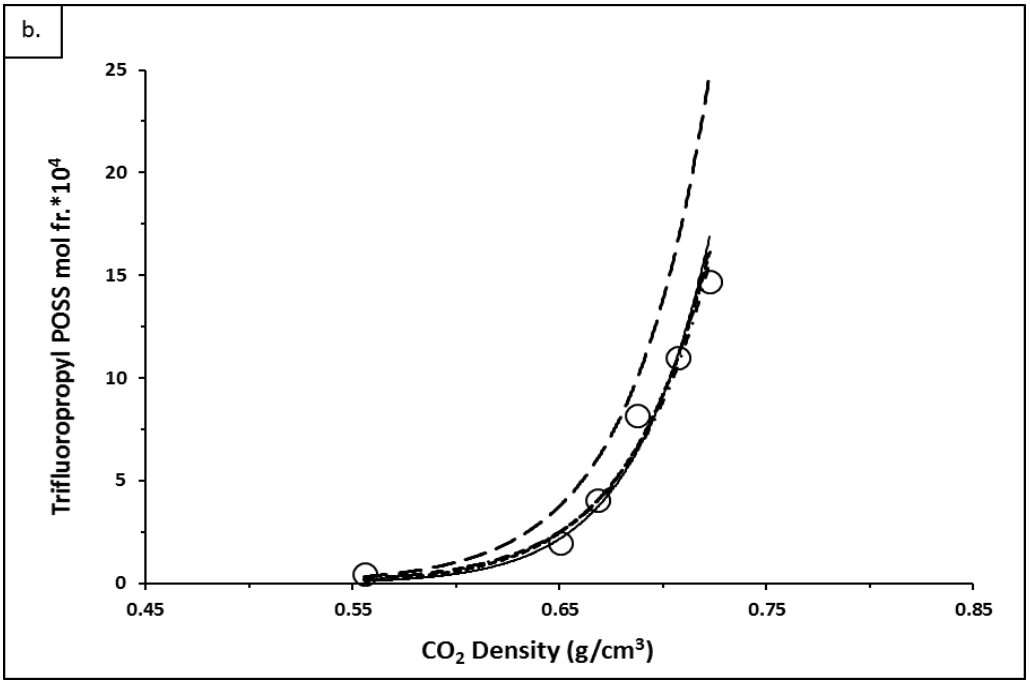

Figure 4.26. The density based correlations, (——) C-W, (·····) Chrastil, (– – –) D-A, (- - -) K-J, (– · –) MST, (— —) Bartle, and the experimental solubility data of TFPOSS in $scCO_2$ (○) plotted against the CO_2 densities at the cloud points at a) 318 K, and b) 328 K.

Table 4.8. The estimated solubility mol fractions of TFPOSS-CO_2 binary systems.

318 K						
Trifluoropropyl POSS Mole Fractions						
Experimental	**Chrastil**	**C-W**	**d-A**	**K-J**	**MST**	**Bartle**
0.00004	0.00005	0.00004	0.00005	0.00005	0.00005	0.00008
0.00019	0.00018	0.00019	0.00018	0.00017	0.00018	0.00027
0.00039	0.00028	0.00031	0.00028	0.00027	0.00027	0.00041
0.00072	0.00062	0.00070	0.00062	0.00059	0.00061	0.00091
0.00108	0.00111	0.00117	0.00111	0.00110	0.00111	0.00166
0.00140	0.00140	0.00140	0.00140	0.00140	0.00140	0.00210

328 K						
Trifluoropropyl POSS Mole Fractions						
Experimental	**Chrastil**	**C-W**	**d-A**	**K-J**	**MST**	**Bartle**
0.00005	0.00002	0.00001	0.00002	0.00002	0.00002	0.00003
0.00020	0.00025	0.00024	0.00025	0.00025	0.00025	0.00038
0.00040	0.00040	0.00040	0.00040	0.00040	0.00040	0.00061
0.00082	0.00068	0.00068	0.00068	0.00067	0.00066	0.00102
0.00110	0.00110	0.00107	0.00110	0.00110	0.00105	0.00165
0.00147	0.00161	0.00147	0.00161	0.00163	0.00152	0.00241

The parameters obtained in each model with the calculated AARD values are given in Table 4.9. Like for octatrimethlysiloxy POSS, C-W Model gives the lowest AARD value. The AARD values of the correlations are in the range of 13-17%, which less than that is obtained for the octatrimethlysiloxy POSS. Overall, the semi-emprical density-based solubility models give a better performance in estimating the experimental solubility data of trifluoropropyl POSS than that of octatrimethlysiloxy POSS.

Table 4.9. The empirical parameters of the density-based models and the AARD (%) values obtained for the TFPOSS solubility in $scCO_2$.

Model	***AARD (%)***	***a***	***b***	***c***	***d***
Chrastil	16.41	18.80	-5395.63	-103.46	
C-W	12.79	96.22	-28819.24	0.05	-9.93
d-A	16.41	18.80	-5355.81	-6430.00	-103.52
K-J	17.06	-7.44	-5796.17	0.03	
MST	16.48	-13962.04	8.97	19.22	
Bartle	16.68	23.06	-8178.57	0.03	

4.7.3. Octaisobutyl POSS Solubility Modelling

The solubility data of octaisobutyl POSS in $scCO_2$ at 318 and 328 K have been correlated by various density-based semi-empirical models which are Chrastil [43], Chrastil modified by Wang (C-W) [38], del Valle and Aguilerra (d-A) [44], Kumar and Johnston (K-J) [45], Mendez-Santiago and Teja (MST) [46] ,and Bartle models [47]. The solubility values obtained with the correlations are listed in Table 4.10. The calculated and the experimental mole fractions plotted against the experimental solvent density data at each temperature are given in Figure 4.27.

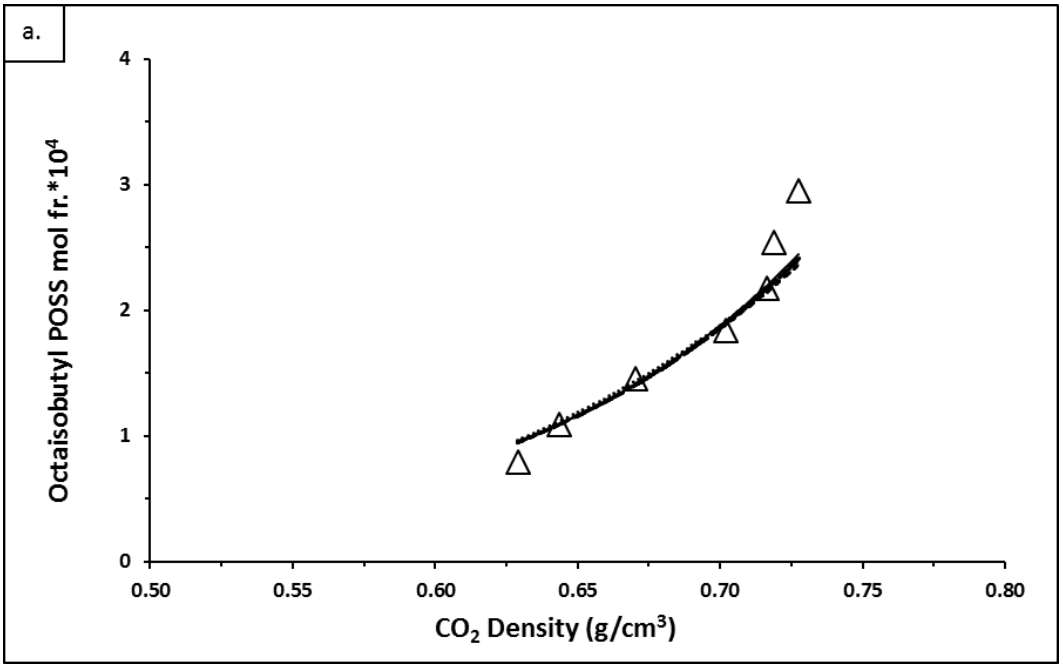

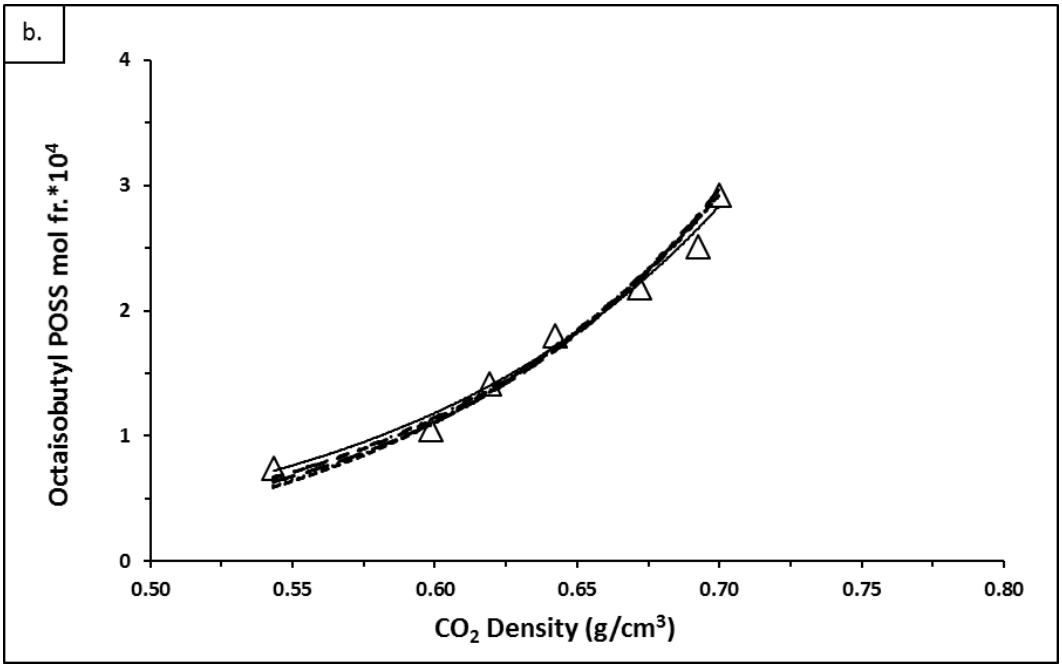

Figure 4.27. The density based correlations, (——) C-W, (·····) Chrastil, (– – –) D-A, (- - -) K-J, (– · –) MST, (— —) Bartle, and the experimental solubility data of OIPOSS in $scCO_2$ (□) plotted against the CO_2 densities at the cloud points at a) 318 K, and b) 328 K.

Table 4.10. The estimated solubility mol fractions of OIPOSS-CO_2 binary systems.

318 K						
Octaisobutyl POSS Mole Fractions						
Experimental	**Chrastil**	**C-W**	**d-A**	**K-J**	**MST**	**Bartle**
0.00008	0.00010	0.00010	0.00009	0.00010	0.00009	0.00009
0.00011	0.00011	0.00011	0.00011	0.00011	0.00011	0.00011
0.00015	0.00014	0.00014	0.00014	0.00014	0.00014	0.00014
0.00018	0.00019	0.00019	0.00019	0.00019	0.00019	0.00019
0.00022	0.00022	0.00022	0.00021	0.00022	0.00022	0.00022
0.00025	0.00022	0.00023	0.00022	0.00022	0.00022	0.00022
0.00029	0.00024	0.00025	0.00024	0.00024	0.00024	0.00024

328 K						
Octaisobutyl POSS Mole Fractions						
Experimental	**Chrastil**	**C-W**	**d-A**	**K-J**	**MST**	**Bartle**
0.00007	0.00006	0.00007	0.00006	0.00007	0.00007	0.00006
0.00011	0.00011	0.00011	0.00011	0.00011	0.00011	0.00011
0.00014	0.00014	0.00014	0.00013	0.00014	0.00014	0.00014
0.00018	0.00017	0.00017	0.00017	0.00017	0.00017	0.00017
0.00022	0.00023	0.00022	0.00023	0.00022	0.00023	0.00023
0.00025	0.00027	0.00027	0.00027	0.00027	0.00027	0.00027
0.00029	0.00029	0.00029	0.00029	0.00029	0.00029	0.00029

The parameters obtained in each model with the calculated AARD values are given in Table 4.11. C-W Model gives the lowest AARD value while the AARD values of all the correlations are in the range of 6-7.5% which is less than those of trifluoropropyl and octatrimethlysiloxy POSS, indicating that the density based semi-empirical equations give a better correlation performance for the alkyl functionalized POSS than for the alkylsiloxy and fluoroalkyl functionalized POSS.

Table 4.11. The empirical parameters of the density-based models and the AARD (%) values obtained for the OIPOSS solubility in $scCO_2$.

Model	***AARD (%)***	***a***	***b***	***c***	***D***
Chrastil	7.51	7.22	-4603.43	-31.88	
C-W	6.03	-23.95	537.80	0.01	2.12
d-A	7.49	7.30	-4770.79	2144.15	-31.92
K-J	6.71	-0.32	-4729.37	0.01	
MST	6.73	-9777.29	3.74	16.52	
Bartle	7.05	18.83	-7163.42	0.01	

4.7.4. Methacryl POSS Solubility Modelling

The solubility data of methacryl POSS in $scCO_2$ at 318 and 328 K have been correlated by various density-based semi-empirical models which are Chrastil [43], Chrastil modified by Wang (C-W) [38], del Valle and Aguilerra (d-A) [44], Kumar and Johnston (K-J) [45], Mendez-Santiago and Teja (MST) [46] ,and Bartle models [47]. The solubility values obtained with the correlations are listed in Table 4.12. The calculated and the experimental mole fractions plotted against the experimental solvent density data at each temperature are given in Figure 4.28.

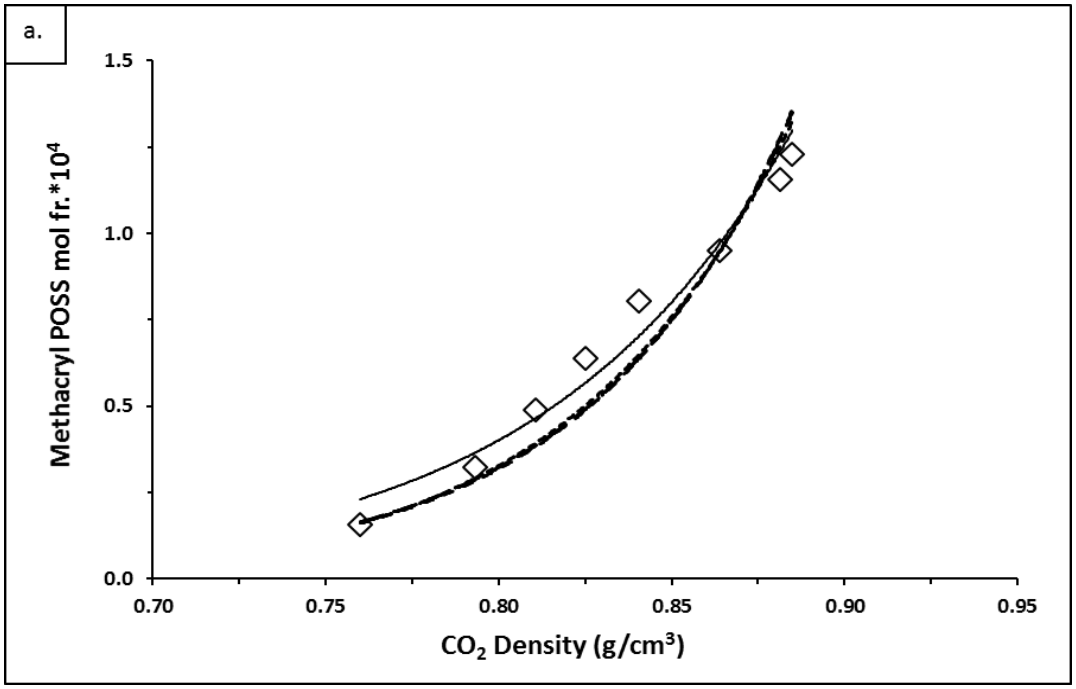

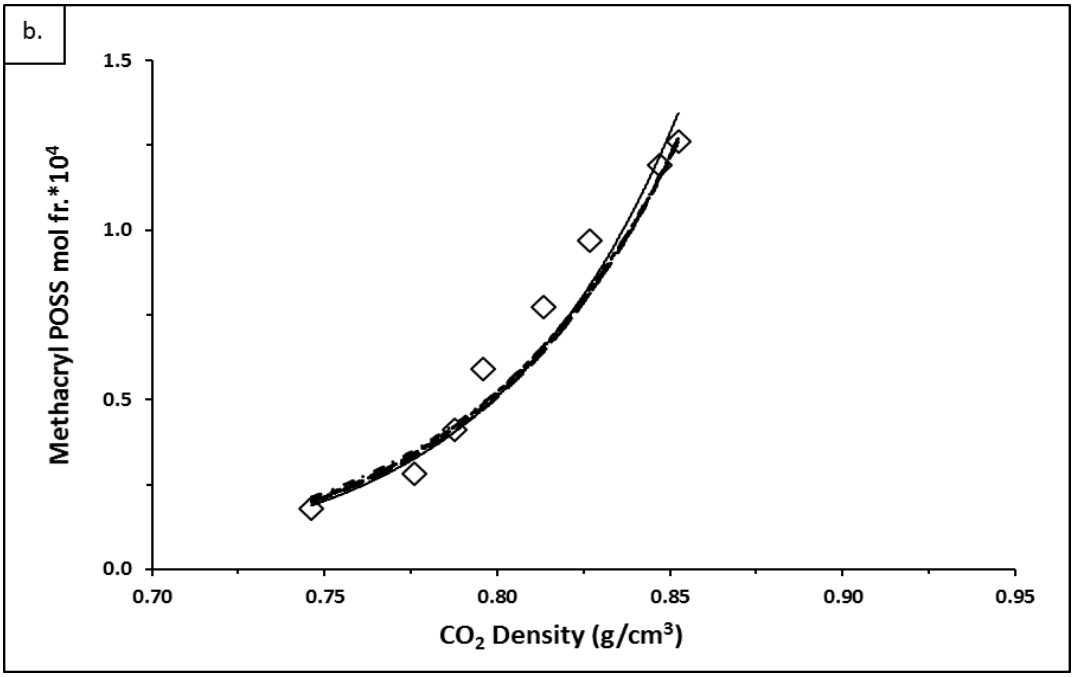

Figure 4.28. The density based correlations, (——) C-W, (·····) Chrastil, (– – –) D-A, (- - -) K-J, (– · –) MST, (— —) Bartle, and the experimental solubility data of MPOSS in $scCO_2$ (□) plotted against the CO_2 densities at the cloud points at a) 318 K, and b) 328 K.

Table 4.12. The estimated solubility mol fractions of MPOSS-CO_2 binary systems.

318 K						
Methacryl POSS Mole Fractions						
Experimental	**Chrastil**	**C-W**	**d-A**	**K-J**	**MST**	**Bartle**
0.00002	0.00002	0.00002	0.00002	0.00002	0.00002	0.00002
0.00003	0.00003	0.00004	0.00003	0.00003	0.00003	0.00003
0.00005	0.00004	0.00005	0.00004	0.00004	0.00004	0.00004
0.00006	0.00005	0.00006	0.00005	0.00005	0.00005	0.00005
0.00008	0.00006	0.00008	0.00006	0.00006	0.00006	0.00006
0.00010	0.00010	0.00010	0.00010	0.00010	0.00010	0.00010

0.00012	0.00013	0.00011	0.00013	0.00013	0.00013	0.00013
0.00012	0.00013	0.00012	0.00013	0.00014	0.00013	0.00013
328 K						
Methacryl POSS Mole Fractions						
Experimental	**Chrastil**	**C-W**	**d-A**	**K-J**	**MST**	**Bartle**
0.00002	0.00002	0.00002	0.00002	0.00002	0.00002	0.00002
0.00003	0.00003	0.00003	0.00003	0.00003	0.00004	0.00003
0.00004	0.00004	0.00004	0.00004	0.00004	0.00004	0.00004
0.00006	0.00005	0.00005	0.00005	0.00005	0.00005	0.00005
0.00008	0.00007	0.00007	0.00007	0.00006	0.00007	0.00006
0.00010	0.00008	0.00009	0.00008	0.00008	0.00008	0.00008
0.00012	0.00012	0.00012	0.00012	0.00012	0.00012	0.00012
0.00013	0.00013	0.00013	0.00013	0.00013	0.00013	0.00013

The parameters obtained in each model with the calculated AARD values are given in Table 4.13. C-W Model gave the best fits when compared with others. The AARD values of the correlations are in the range of 8-12%.

Table 4.13. The empirical parameters of the density-based models and the AARD (%) values obtained for the MPOSS solubility in $scCO_2$.

Model	***AARD (%)***	***a***	***b***	***c***	***d***
Chrastil	10.81	14.87	-4908.28	-84.15	
C-W	8.03	55.57	-21121.69	0.05	-7.60
d-A	10.81	14.87	-4836.08	-11726.66	-84.26
K-J	12.01	-8.25	-5022.88	0.02	
MST	11.60	-13109.63	6.92	16.42	
Bartle	10.88	15.41	-7213.35	0.02	

4.7.5. Isooctyl POSS Solubility Modelling

The solubility data of isooctyl POSS in $scCO_2$ at 318 and 328 K have been correlated by various density-based semi-empirical models which are Chrastil [43], Chrastil modified by Wang (C-W) [38], del Valle and Aguilerra (d-A) [44], Kumar and Johnston (K-J) [45], Mendez-Santiago and Teja (MST) [46] ,and Bartle models [47]. The solubility values obtained with the correlations are listed in Table 4.14. Predicted and experimental mole fractions are plotted with the experimental solvent density data at each temperature in Figure 4.29.

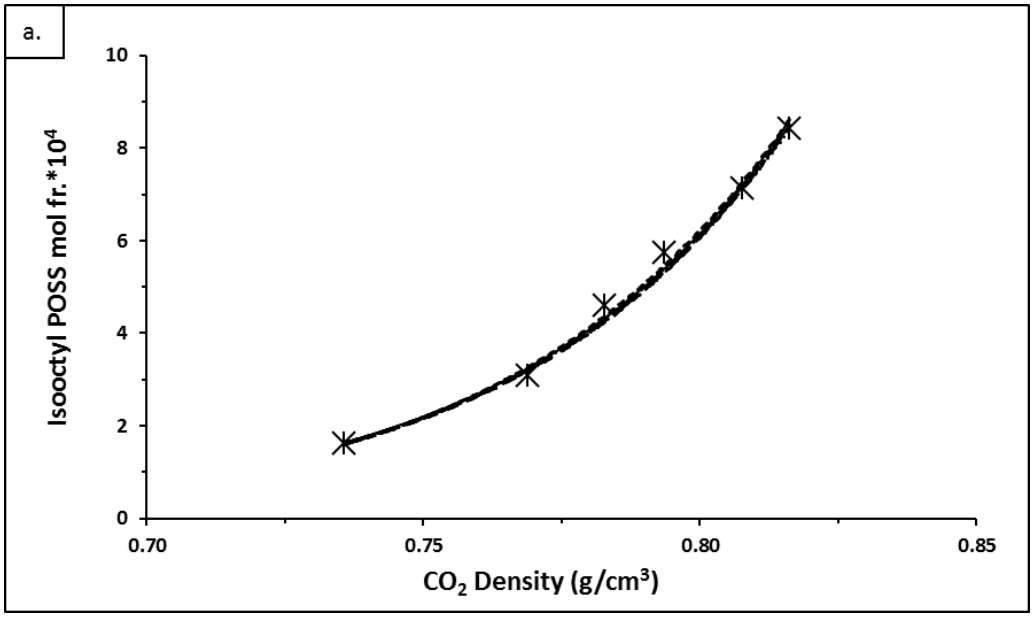

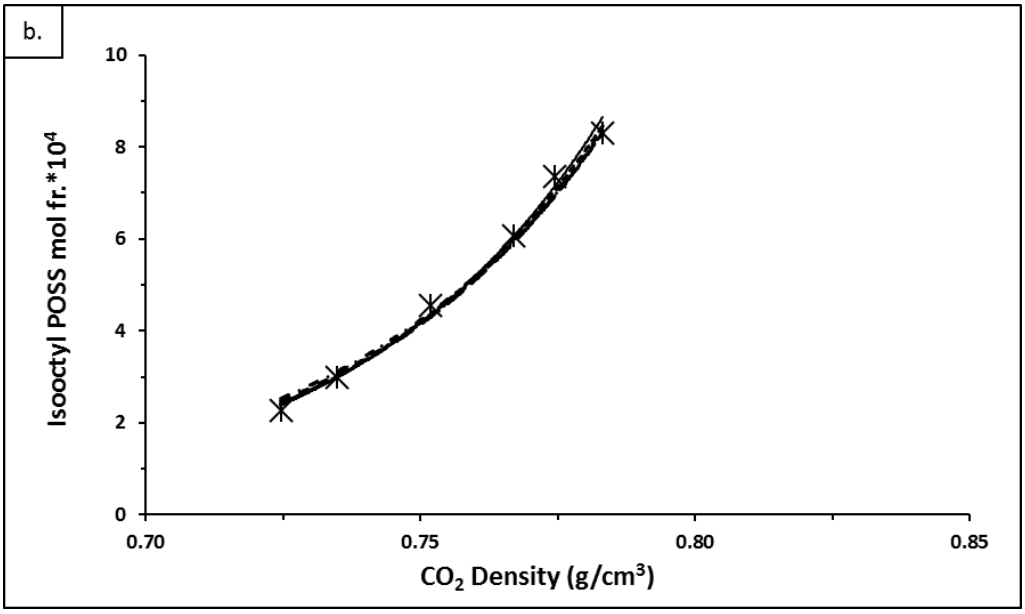

Figure 4.29. The density based correlations, (——) C-W, (·····) Chrastil, (– – –) D-A, (- - -) K-J, (– · –) MST, (— —) Bartle, and the experimental solubility data of IOPOSS in $scCO_2$ (□) plotted against the CO_2 densities at the cloud points at a) 318 K, and b) 328 K.

Table 4.14. The estimated solubility mol fractions of IOPOSS-CO_2 binary systems.

318 K						
Isooctyl POSS Mole Fractions						
Experimental	**Chrastil**	**C-W**	**d-A**	**K-J**	**MST**	**Bartle**
0.00016	0.00016	0.00016	0.00016	0.00016	0.00016	0.00016
0.00031	0.00032	0.00033	0.00033	0.00032	0.00032	0.00032
0.00046	0.00043	0.00044	0.00044	0.00042	0.00043	0.00043
0.00058	0.00054	0.00055	0.00055	0.00053	0.00053	0.00053
0.00071	0.00071	0.00072	0.00073	0.00071	0.00071	0.00071
0.00084	0.00084	0.00084	0.00086	0.00085	0.00084	0.00084
328 K						

Isooctyl POSS Mole Fractions						
Experimental	**Chrastil**	**C-W**	**d-A**	**K-J**	**MST**	**Bartle**
0.00023	0.00024	0.00024	0.00024	0.00025	0.00025	0.00024
0.00030	0.00030	0.00030	0.00030	0.00030	0.00031	0.00030
0.00046	0.00043	0.00044	0.00044	0.00043	0.00044	0.00043
0.00061	0.00060	0.00061	0.00060	0.00059	0.00060	0.00059
0.00073	0.00070	0.00072	0.00071	0.00069	0.00070	0.00069
0.00083	0.00083	0.00086	0.00085	0.00083	0.00083	0.00083

The parameters obtained in each model with the calculated AARD values are given in Table 4.15. C-W Model gave the best fits for isooctyl POSS among all the models, as it did for all the other POSS's. The AARD values of the correlations are in the range of 2.5-3.5% which is the best AARD range that has been obtained in this study.

Table 4.15. The empirical parameters of the density-based models and the AARD (%) values obtained for the IOPOSS solubility in $scCO_2$.

Model	***AARD (%)***	***a***	***b***	***c***	***d***
Chrastil	2.96	16.97	-6757.54	-89.53	
C-W	2.54	27.93	-14510.05	0.03	-3.07
d-A	3.07	17.26	-6762.81	-6384.64	-91.32
K-J	3.47	-2.25	-6908.21	0.02	
MST	3.47	-15438.32	7.85	24.34	
Bartle	3.11	24.60	-9295.04	0.02	

CHAPTER 5

CONCLUSIONS

In this research, the solubilities of five different POSS's which are trifluoropropyl (TFPOSS), methacryl (MPOSS), isooctyl (IOPOSS), octaisobutyl (IBPOSS) and octatrimethlysiloxy (SPOSS) POSS in supercritical carbon dioxide have been studied. SPOSS solubility in supercritical carbon dioxide has been studied for the first time in literature which was carried out at 308–328 K temperature range up to 14 MPa. Solubilities of other POSS's were studied at 308 and 323 K up to 30 MPa in previous studies [1,2] while in this study, to develop further information on phase equilibrium behavior of POSS-CO_2 binary systems, the solubilities of TFPOSS, MPOSS, IOPOSS, IBPOSS in supercritical carbon dioxide have been investigated at 318 and 328 K until 30 MPa. Solid-vapor equilibrium curves were plotted for TFPOSS, SPOSS and IBPOSS while liquid-vapor equilibrium curves were plotted for MPOSS and IOPOSS as mole fr. vs cloud or dew point pressures at the studied temperatures. At these temperatures all the studied POSSs were found to have significant solubilities in supercritical carbon dioxide and solubility dependency on temperature and pressure as in the previous studies conducted at 308 and 323 K. While SPOSS has been found to exhibit the highest solubility, MPOSS exhibit the lowest solubility. Solubility of POSS at constant temperature is increasing with pressure due to increasing solvent density, which is also the power of solvation. On the other hand, at constant pressure, solubilities of POSS decrease with temperature due to the decrease in solvent density. On the other hand, at constant solvent density, their solubilities increase with temperature due to the increase in the solute vapor pressure. While these trends are similar for each studied POSS, the extent of dependency varies with their molecular structures. It has been observed that in the

studied ranges of temperature, pressure and concentration, the changes in the solvent density is more dominant on solubility than the vapor pressure.

Chrastil, Chrastil modified by Wang, Del Valle and Aguilera, Kumar and Johnston, Mendez-Santiago and Teja, and Bartle semi-empirical density-based models have been used to correlate the POSS's solubility data at studied temperature and pressure ranges. Chrastil modified by Wang model gave the best fits for all the POSS types to their empirical data and the lowest absolute average relative deviation (AARD %) value. Among all the POSSs, best solubility correlation performance was obtained for IOPOSS, which is functionalized with long branched alkyl groups, with a minimum AARD% range as 2.5-3.5% while SPOSS, TFPOSS, IBPOSS and MPOSS values are in the 22-25%, 13-17%, 6-7.5% ,8-12 % ranges, respectively.

REFERENCES

[1] G. Li, L. Wang, H. Ni, C.U. Pittman Jr., Polyhedral oligomeric silsesquioxane (POSS) polymers and copolymers: a review, J. Inorg. Organomet. Polym. Mater. 11 (2001) 123–154, https://doi.org/10.1023/A:1015287910502.

[2] C. Dilek, Supercritical carbon dioxide-soluble polyhedral oligomeric silsesquioxane (POSS) nanocages and polymer surface modification, J. Supercrit. Fluids 73 (2013) 171–177, https://doi.org/10.1016/j.supflu.2012.10.012.

[3] B. Kanya, C. Dilek, Effects of functional groups on the solubilities of polyhedral oligomeric silsesquioxanes (POSS) in supercritical carbon dioxide, J. Supercrit. Fluids 102 (2015) 17–23, https://doi.org/10.1016/j.supflu.2015.03.024.

[4] I. Tezsevin, C. Demirtas, I. Onal, C. Dilek, Density functional theory study of interactions between carbon dioxide and functionalized polyhedral oligomeric silsesquioxanes, Int. J. Quantum Chem. 117 (2017) e25397, https://doi.org/10.1002/qua.25397.

[5] C. Demirtas, C. Dilek, Enhanced solubility of siloxy-modified polyhedral oligomeric silsesquioxanes in supercritical carbon dioxide, J. Supercrit. Fluids 143 (2019) 358–364 https://doi.org/10.1016/j.supflu.2018.09.015

[6] J. Wu, P.T. Mather, POSS polymers: physical properties and biomaterials applications, Polym. Rev. 49 (2009) 25–63, https://doi.org/10.1080/15583720802656237.

[7] M. Joshi, B.S. Butola, Polymeric nanocomposites-polyhedral oligomericsilsesquioxanes (POSS) as hybrid nanofiller, J. Macromol. Sci. C: Polym. Rev. 44 (2004) 389–410, https://doi.org/10.1081/MC-200033687.

[8] E. Ayandele, B. Sarkar, P. Alexandridis, Polyhedral oligomeric silsesquioxane (POSS)-containing polymer nanocomposites, Nanomaterials 2 (2012) 445–475, https://doi.org/10.3390/nano2040445.

[9] S.-W. Kuo, F.-C. Chang, POSS related polymer nanocomposites, Prog. Polym. Sci. 36 (2011) 1649–1696, https://doi.org/10.1016/j.progpolymsci.2011.05.002.

[10] W. Zhang, A.H.E. Müller, Progress in polymer science architecture, self-assembly and properties of well-defined hybrid polymers based on polyhedral oligomeric, Prog. Polym. Sci. 38 (2013) 1121–1162, https://doi.org/10.1016/j.progpolymsci.2013.03.002.

[11] H. Hussain, S.M. Shah, Recent developments in nanostructured polyhedral oligomeric silsesquioxane-based materials via “controlled” radical polymerization, Polym. Int. 63 (2014) 835–847, https://doi.org/10.1002/pi.4692.

[12] X. Liao, H. Zhang, T. He, Preparation of porous biodegradable polymer and its nanocomposites by supercritical CO2foaming for tissue engineering, J. Nano-materials 2012 (2012) 1–12, http://dx.doi.org/10.1155/2012/836394S

[13] Y.-P. Sun, Supercritical Fluid Technology in Materials Science and Engineering Synthesis, Properties, and Applications, Marcel Dekker, Inc., 2002.

[14] K. P. Johnston ,C. Haynes, Extreme solvent effects on reaction rate constants at supercritical fluid conditions, AIChE J., 33(12), 2017-2026. https://doi.org/10.1002/aic.690331212

[15] R.B. Gupta, J.-J. Shim, Solubility in Supercritical Carbon Dioxide, 1st Edition, CRC Press, 2006.

[16] M.A. Mchugh, V.J. Krukonis, Supercritical FIuid Extraction, 2nd Edition, Butterworth-Heinemann, 1994.

[17] L.T. Taylor, Supercritical Fluid Extraction, John Wiley, New York, 1996.

[18] Amooey, A. (2014). A simple correlation to predict drug solubility in supercritical carbon dioxide. Fluid Phase Equilibria, 375, 332-339. http://dx.doi.org/10.1016/j.fluid.2014.05.025

[19] Zhang, X., Heinonen, S., & Levänen, E. (2014). Applications of supercritical carbon dioxide in materials processing and synthesis. RSC Adv., 4(105), 61137-61152. http://dx.doi.org/10.1039/c4ra10662h

[20] García-González, C., Concheiro, A., & Alvarez-Lorenzo, C. (2015). Processing of Materials for Regenerative Medicine Using Supercritical Fluid Technology. Bioconjugate Chem., 26(7), 1159-1171. http://dx.doi.org/10.1021/bc5005922

[21] S. Kazarian, Polymer Processing with Supercritical Fluids, Polymer Science, Ser. C. 42 (2000) 78–101.

[22] Duarte, A., Santo, V., Alves, A., Silva, S., Moreira-Silva, J., & Silva, T. et al. (2013). Unleashing the potential of supercritical fluids for polymer processing in tissue engineering and regenerative medicine. J. Supercritical Fluids, 79, 177-185. http://dx.doi.org/10.1016/j.supflu.2013.01.004

[23] Duarte, A., Mano, J., & Reis, R. (2009). Supercritical fluids in biomedical and tissue engineering applications: a review. International Materials Reviews, 54(4), 214-222. http://dx.doi.org/10.1179/174328009x411181

[24] H. Peker, M. Srinivasan, J. Smith, B. McCoy, Caffeine Extraction Rates from Coffee Beans with Supercritical Carbon Dioxide, AIChE Journal. 38 (1992) 761–770. doi:10.1002/aic.690380513.

[25] H. Machida, M. Takesue, R.L. Smith, Green Chemical Processes with Supercritical Fluids: Properties, Materials, Separations and Energy, Journal of Supercritical Fluids. 60 (2011) 2–15. doi:10.1016/j.supflu.2011.04.016.

[26] D. Gnanasekaran, K. Madhavan, B.S.R. Reddy, Developments of Polyhedral Oligomeric Silsesquioxanes (POSS), POSS Nanocomposites and Their Applications: A Review, Journal of Scientific & Industrial Research. 68 (2009) 437–464.

[27] Y. Arai, T. Sako, Y. Takebayashi, Supercritical Fluids Molecular Interactions, Physical Properties, and New Applications, Springer, Berlin

[28] N. Novendra, N. Hasirci, C. Dilek, Supercritical processing of CO2-philic polyhedral oligomeric silsesquioxane (POSS)-poly(L-lactic acid) composites, J. Supercrit. Fluids 117 (2016) 230–242, http://doi.org/10.1016/j.supflu.2016.06.022.

[29] B. Bhargava, M. Saharay, S. Balasubramanian, B. Mater. Sci. 2008, 31, 327.

[30] C. Kirby, M. McHugh, Chem. Rev. 1999, 99, 565.

[31] J. Meredith, K. Johnston, J. Seminario, S. Kazarian, C. Eckert, J. Phys. Chem. 1996, 100, 10837.

[32] W.H. Teoh, R. Mammucari, N.R. Foster, Solubility of Organometallic Complexes in Supercritical Carbon Dioxide: A Review, Journal of Organometallic Chemistry. 724 (2013) 102–116. http://doi:10.1016/j.jorganchem.2012.10.005.

[33] K.P. Johnston, C.A. Eckert, An analytical Carnahan-Starling-van der Waals model for solubility of hydrocarbon solids in supercritical fluids, AIChE J. 27 (1981) 773–779, https://doi.org/10.1002/aic.690270511.

[34] Anitescu, G. and Tavlarides, L. L., J. Supercrit. Fluids, 10(3), 175–189, 1997.).

[35] H. Sim Yeoh, G. Hean Chong, N. Mohd Azahan, R. Abdul Rahman, T.S. Yaw Choong, Solubility Measurement Method and Mathematical Modeling in Supercritical Fluids, Engineering Journal. 17 (2013) 67–78. doi:10.4186/ej.2013.17.3.67.

[36] L. Nasri, S. Bensaad, Z. Bensetiti, Modeling the Solubility of Dihydroxybenzoic Acid and Methylbenzoic Acid Isomers in Supercritical Carbon Dioxide, International Journal of Thermodynamics. 17 (2014) 81–85. doi:10.5541/ijot.513.

[37] M. Sauceau, J.J. Letourneau, D. Richon, J. Fages, Enhanced Density-based Models for Solid Compound Solubilities in Supercritical Carbon Dioxide with Cosolvents, Fluid Phase Equilibria. 208 (2003) 99–113. doi:10.1016/S0378-3812(03)00005-0.

[38] M. Skerget, Z. Knez, M. Knez-Hrncic, Solubility of solids in sub- and supercritical fluids: a review, J. Chem. Eng. Data 56 (2011) 694–719, https://doi.org/10.1021/ je1011373.

[39] Macnaughton, S., Kikic, I., Foster, N., Alessi, P., Cortesi, A., & Colombo, I. (1996). Solubility of Anti-Inflammatory Drugs in Supercritical Carbon Dioxide. J. Chemical & Engineering Data, 41(5), 1083-1086. http://dx.doi.org/10.1021/je960103q

[40] Zabihi, F., Vaziri, A., Akbarnejad, M., Ardjmand, M., Otadi, M., & Bozorgmanesh, A. (2010). A novel mathematical method for prediction of rapid expansion of supercritical solution (RESS) processed ibuprofen powder size distribution. Korean J. Chemical Engineering, 27(5), 1601-1605. http://dx.doi.org/10.1007/s11814-010-0265-9

[41] Z. Tang, J. Jin, Z. Zhang, H. Liu, New Experimental Data and Modeling of the Solubility of Compounds in Supercritical Carbon Dioxide, Industrial &

Engineering Chemistry Research. 51 (2012) 5515–5526. doi:10.1021/ie2016224.

[42] B. Hadi, H.-A. Ali, L. Nader, Thermodynamic Modeling of Solid Solubility in Supercritical Carbon Dioxide: Comparison Between Mixing Rules, Chemical Industry and Chemical Engineering Quarterly. 19 (2012) 74–74. doi:10.2298/CICEQ120203074B.

[43] J. Chrastil, Solubility of solids and liquids in supercritical gases, J. Phys. Chem. 86 (1982) 3016–3021, https://doi.org/10.1021/j100212a041.

[44] J.M. Del Valle, J.M. Aguilera, An improved equation for predicting the solubility of vegetable oils in supercritical carbon dioxide, Ind. Eng. Chem. Res. 27 (1988) 1551–1553, https://doi.org/10.1021/ie00080a036.

[45] S.K. Kumar, K.P. Johnston, Modelling the solubility of solids in supercritical fluids with density as the independent variable, J. Supercrit. Fluids 1 (1988) 15–22,https://doi.org/10.1016/0896-8446(88)90005-8.

[46] J. Mendez-Santiago, A.S. Teja, The solubility of solids in supercritical fluids, Fluid Phase Equilib. 158–160 (1999) 501–510, https://doi.org/10.1016/S0378-3812(99) 00154-5.

[47] K.D. Bartle, A.A. Clifford, S.A. Jafar, G.F. Shilstone, Solubilities of solids and liquids of low volatility in supercritical carbon dioxide, J. Phys. Chem. Ref. Data 20 (1991) 713–756, https://doi.org/10.1063/1.555893.

[48] T. A. Hoefling, R. M. Enick, E. J. Beckman, Microemulsions in near-critical and supercritical CO_2, J. Phys. Chem. 95 (1991) 7127–7129. https://doi.org/10.1021/j100172a006.

[49] T. A. Hoefling, D. A. Newman, R. M. Enick, E. J. Beckman, Effect of structure on the cloud-point curves of silicone-based amphiphiles in supercritical carbon dioxide, J. Supercrit. Fluids 6 (1993) 165–171. https://doi.org/10.1016/0896-8446(93)90015-P.

[50] Y. Xiong, E. Kiran, Miscibility, density and viscosity of poly(dimethylsiloxane) in supercritical carbon dioxide, Polymer 36 (1995) 4817-4826. https://doi.org/10.1016/0032-3861(95)99298-9.

[51] J. J. Lee, S. D. Cummings, E. J. Beckman, R. M. Enick, W. A.Burgess, M. D. Doherty, M. J.O'Brien, R. J. Perry, The solubility of low molecular weight Poly (Dimethyl siloxane) in dense CO_2 and its use as a CO_2-philic segment, J. Supercrit. Fluids 119 (2017) 17–25. http://dx.doi.org/10.1016/j.supflu.2016.08.003.

[52] D. Sanli, C. Erkey, Demixing pressures of hydroxy-terminated poly(dimethylsiloxane)–carbon dioxide binary mixtures at 313.2 K 323.2 Kand 333.2 K, J. Supercritical Fluids 92 (2014) 264–271. http://dx.doi.org/10.1016/j.supflu.2014.05.014.

[53] E. Vyhmeister, A. J. Muscat, D. Suleiman, L. A. Estévez, High-pressure phase equilibria for chlorosilane + carbon dioxide mixtures, Fluid Phase Equilibria 270 (2008) 121–128. https://doi.org/10.1016/j.fluid.2008.06.017.

[54] C. A. Garcia-Gonzalez, J. Fraile, A. Lopez-Periago, J. Saurina, C. Domingo, Measurements and Correlation of Octyltriethoxysilane Solubility in Supercritical CO_2 and Assembly of Functional Silane Monolayers on the Surface of Nanometric Particles 48 (2009) 9952–9960. https://doi.org/10.1021/ie900775z.

[55] A. Garg, E. Gulari, C. W. Manke, Thermodynamics of Polymer Melts Swollen with Supercritical Gases 27 (1994) 5643–5653. https://doi.org/10.1021/ma00098a019.

[56] M. J. O'Brien, R. J. Perry, M. D. Doherty, J. J. Lee, A. Dhuwe, E. J. Beckman, R. M. Enick, Anthraquinone Siloxanes as Thickening Agents for Supercritical CO_2,Energy & Fuels 30 (2016) 5990-5998. https://doi.org/10.1021/acs.energyfuels.6b00946.

[57] C. Dindar, E. Kiran, High-pressure viscosity and density of polymer solutions at the critical polymer concentration in near-critical and supercritical fluids, Ind. Eng. Chem. Res. 41 (2002) 6354–6362. https://doi.org/10.1021/ie0108999.

[58] Z. Bayraktar, E. Kiran, Miscibility, phase separation, and volumetric properties in solutions of poly (dimethylsiloxane) in supercritical, J. Applied Polymer Science 75 (2000) 1397–1403. https://doi.org/10.1002/(SICI)1097-4628(20000314)75:11<1397::AID-APP12>3.0.CO;2-F.

[59] R. Fink, D. Hancu, R. Valentine, E.J. Beckman, Toward the development of "CO_2-philic" hydrocarbons. 1. Use of side-chain functionalization to lower the miscibility pressure of polydimethylsiloxanes in CO_2, J. Physical Chemistry, B 103 (1999) 6441–6444. http://dx.doi.org/10.1021/jp990333m.

[60] R. Fink, E. J. Beckman, Phase behavior of siloxane-based amphiphiles in supercritical carbon dioxide, J. Supercrit. Fluids 18 (2000) 101–110. https://doi.org/10.1016/S0896-8446(00)00052-8.

[61] J. A. Dzielawa, A. V. Rubas, C. Lubbers, D. C. Stepinski, A. M. Scurto, R. E. Barrans Jr., M. L. Dietz, A. W. Herlinger, J. F. Brennecke, Carbon dioxide solubility enhancement through silicone functionalization: 'CO_2-philic' Oligo(dimethylsiloxane)-substituted diphosphonates, Sep. Sci. Technol. 43 (2008) 2520–2536. https://doi.org/10.1080/01496390802122063.

[62] A. Fina, D. Tabuani, A. Frache, G. Camino, Polypropylene-Polyhedral Oligomeric Silsesquioxanes (POSS) Nanocomposites, Polymer. 46 (2005) 7855–7866. https://doi:10.1016/j.polymer.2005.06.121.

[63] F. Baldi, F. Bignotti, A. Fina, D. Tabuani, T. Ricco, Mechanical Characterization of Polyhedral Oligomeric Silsesquioxane/Polypropylene Blends, Journal of Applied Polymer Science. 105 (2007) 935–943. https://doi:10.1002/app.

[64] H. Mahfuz, F. Powell, R. Granata, M. Hosur, M. Khan, Coating of Carbon Fiber with Polyhedral Oligomeric Silsesquioxane (POSS) to Enhance Mechanical Properties and Durability of Carbon/Vinyl Ester Composites, Materials. 4 (2011) 1619–1631. doi:10.3390/ma4091619.

[65] S.R. Jin, J.K. Lee, Isothermal Physical Aging of Poly(ethyl methacrylate)/Polyhedral Oligomeric Silsequioxanes Nanocomposite Thin Films, Advanced Materials Research. 287-290 (2011) 2234–2239. doi:10.4028/www.scientific.net/AMR.287-290.2234.

[66] G. Eris, D. Sanli, Z. Ulker, S.E. Bozbag, A. Jonás, A. Kiraz, C. Erkey, Three-dimensional optofluidic waveguides in hydrophobic silica aerogels via supercritical fluid processing, J. Supercrit. Fluids 73 (2013) 28–33, https://doi.org/10.1016/j.supflu. 2012.11.001.

[67] S. Costeux, L. Zhu, Low density thermoplastic nanofoams nucleated by nanoparticles, Polymer 54 (2013) 2785–2795, https://doi.org/10.1016/j.polymer.2013. 03.052.

[68] E.W. Lemmon, M.O. McLinden, D.G. Friend, Thermophysical properties of fluidsystems, in: P.J. Linstrom, W.G. Mallard (Eds.), NIST Chemistry WebBook, NIST Standard Reference Database Number 69, June National Institute of Standardsand Technology, Gaithersburg, MD, (n.d.). http://webbook.nist.gov

[69] C. Dilek, C.W. Manke, E. Gulari, Phase behavior of β-D-galactose pentaacetatecarbon dioxide binary system, Fluid Phase Equilib. 239 (2006) 172–177, https://doi.org/10.1016/j.fluid.2005.11.013.

[70] C. Dilek, L. Hong, R.M. Enick, E. Gulari, C.W. Manke, Sustainable debinding and recovery of CO2-soluble binders, Ind. Eng. Chem. Res. 51 (2012) 9101–9105,https://doi.org/10.1021/ie202608t.

[71] T. Chartier, M. Ferrato, J.F. Baumard, Supercritical debinding of injection molded ceramics, J. Am. Ceram. Soc. 78 (1995) 1787–1792, https://doi.org/10.1111/j.1151-2916.1995.tb08890.x.

[72] A. Royer, T. Barriere, Y. Bienvenu, Influence of supercritical debinding and processing parameters on final properties of injection-moulded Inconel 718, Powder Technol. 336 (2018) 311–317, https://doi.org/10.1016/j.powtec.2018.05.047.

[73] M. McHugh, M.E.Paulaitls, Solid Solubilities of Naphthalene and Biphenyl in Supercritical Carbon Dioxide, J. Chem. Eng. Data 1980, 25, 326-329, https://doi:10.1021/je60087a018